CONDUCTING THERMOSET POLYMERS

FINAL TECHNICAL REPORT

FOR THE PERIOD 30 SEPTEMBER 1992 THROUGH 29 SEPTEMBER 1995

AFOSR-TR-95

0786

Approved for public release; distribution unlimited

Prepared for

UNITED STATES AIR FORCE

Air Force Office of Scientific Research

Bolling Air Force Base, DC 20332

NOVEMBER 1995

REPORT DOCUMENTATION PAGE

Form Approved
OMB No. 0704-0188

1. AGENCY USE ONLY (Leave blank)	2. REPORT DATE	3. REPORT TYPE AND DATES COVERED
	30 November 1995	Final Technical 9/30/92-9/29/95

4. TITLE AND SUBTITLE

Conducting Thermoset Polymers

5. FUNDING NUMBERS

61102F 2303 CS

F49620-92-C-0074

6. AUTHOR(S)

I. M. Brown
D. J. Leopold
T. C. Sandreczki

7. PERFORMING ORGANIZATION NAME(S) AND ADDRESS(ES)

McDonnell Douglas Aerospace
P.O. Box 516
MC 1111041
St. Louis, MO 63166-0516

8. PERFORMING ORGANIZATION REPORT NUMBER

MDC 95P0082

9. SPONSORING/MONITORING AGENCY NAME(S) AND ADDRESS(ES)

AFOSR/NENL
Building 410
Bolling AFB, DC 20332-6448

Dr Lee

10. SPONSORING/MONITORING AGENCY REPORT NUMBER

11. SUPPLEMENTARY NOTES

12a. DISTRIBUTION/AVAILABILITY STATEMENT

Approved for public release;
distribution unlimited.

12b. DISTRIBUTION CODE

13. ABSTRACT (Maximum 200 words)

Efforts to develop electrically conducting thermoset polymers in which the pi-conjugation extends along the backbone and through the crosslink are described. Hot/melt processing of the monomers and oligomers was used to form the thermosets. Three different approaches were used to get the thermoset polymers conducting. The acetylene-terminated Schiff base and acetylene-terminated polythiophene monomers were first cured, then doped with iodine, whereas the acetylene-terminated polyaniline oligomers were first doped with protonic acids then cured. In the third method, an acetylene-terminated Schiff base thermoset was implanted with high energy argon ions using a commercial ion implanter. Electron spin resonance, photoluminescence, and photoabsorption data suggest that polarons can form in the doped and undoped forms of the acetylene-terminated Schiff base and polythiophene thermoset polymers. The spin susceptibilities and electron spin resonance lineshape parameters were measured in these thermosets as a function of iodine content. Two methods to synthesize the acetylene-terminated polyaniline oligomers were investigated. Several substituted derivatives of acetylene-terminated polyaniline were synthesized and doped with different acids such as tosylic acid, benzenedisulfonic acid, duodecylbenzenesulfonic acid, and camphorsulfonic acid. All conductivity values in the thermosets were less than 0.02 Siemens/cm.

14. SUBJECT TERMS	15. NUMBER OF PAGES
Conducting polymer, thermoset, acetylene-terminated Schiff base, acetylene-terminated polythiophene, acetylene-terminated polyaniline, iodine dopant, acid dopant	137
	16. PRICE CODE

17. SECURITY CLASSIFICATION OF REPORT	18. SECURITY CLASSIFICATION OF THIS PAGE	19. SECURITY CLASSIFICATION OF ABSTRACT	20. LIMITATION OF ABSTRACT
UNCLASSIFIED	UNCLASSIFIED	UNCLASSIFIED	

30 NOV 1995

GENERAL INSTRUCTIONS FOR COMPLETING SF 298

The Report Documentation Page (RDP) is used in announcing and cataloging reports. It is important that this information be consistent with the rest of the report, particularly the cover and title page. Instructions for filling in each block of the form follow. It is important to *stay within the lines* to meet *optical scanning requirements*.

Block 1. Agency Use Only *(Leave blank)*.

Block 2. Report Date. Full publication date including day, month, and year, if available (e.g. 1 Jan 88). Must cite at least the year.

Block 3. Type of Report and Dates Covered. State whether report is interim, final, etc. If applicable, enter inclusive report dates (e.g. 10 Jun 87 - 30 Jun 88).

Block 4. Title and Subtitle. A title is taken from the part of the report that provides the most meaningful and complete information. When a report is prepared in more than one volume, repeat the primary title, add volume number, and include subtitle for the specific volume. On classified documents enter the title classification in parentheses.

Block 5. Funding Numbers. To include contract and grant numbers; may include program element number(s), project number(s), task number(s), and work unit number(s). Use the following labels:

C	- Contract	PR	- Project
G	- Grant	TA	- Task
PE	- Program Element	WU	- Work Unit Accession No.

Block 6. Author(s). Name(s) of person(s) responsible for writing the report, performing the research, or credited with the content of the report. If editor or compiler, this should follow the name(s).

Block 7. Performing Organization Name(s) and Address(es). Self-explanatory.

Block 8. Performing Organization Report Number. Enter the unique alphanumeric report number(s) assigned by the organization performing the report.

Block 9. Sponsoring/Monitoring Agency Name(s) and Address(es). Self-explanatory.

Block 10. Sponsoring/Monitoring Agency Report Number. *(If known)*

Block 11. Supplementary Notes. Enter information not included elsewhere such as: Prepared in cooperation with...; Trans. of...; To be published in.... When a report is revised, include a statement whether the new report supersedes or supplements the older report.

Block 12a. Distribution/Availability Statement. Denotes public availability or limitations. Cite any availability to the public. Enter additional limitations or special markings in all capitals (e.g. NOFORN, REL, ITAR).

- DOD - See DoDD 5230.24, "Distribution Statements on Technical Documents."
- DOE - See authorities.
- NASA - See Handbook NHB 2200.2.
- NTIS - Leave blank.

Block 12b. Distribution Code.

- DOD - Leave blank.
- DOE - Enter DOE distribution categories from the Standard Distribution for Unclassified Scientific and Technical Reports.
- NASA - Leave blank.
- NTIS - Leave blank.

Block 13. Abstract. Include a brief *(Maximum 200 words)* factual summary of the most significant information contained in the report.

Block 14. Subject Terms. Keywords or phrases identifying major subjects in the report.

Block 15. Number of Pages. Enter the total number of pages.

Block 16. Price Code. Enter appropriate price code *(NTIS only)*.

Blocks 17. - 19. Security Classifications. Self-explanatory. Enter U.S. Security Classification in accordance with U.S. Security Regulations (i.e., UNCLASSIFIED). If form contains classified information, stamp classification on the top and bottom of the page.

Block 20. Limitation of Abstract. This block must be completed to assign a limitation to the abstract. Enter either UL (unlimited) or SAR (same as report). An entry in this block is necessary if the abstract is to be limited. If blank, the abstract is assumed to be unlimited.

TABLE OF CONTENTS

Section			Page
1.0	INTRODUCTION		1
2.0	RESEARCH OBJECTIVE AND APPROACH		2
3.0	RESULTS		3
	3.1	AT-Schiff Base and AT-Polythiophene Studies	3
		3.1.1 Electrical Measurements	3
		3.1.2 Monomer Synthesis and Sample Preparation	23
		3.1.3 ESR Measurements	33
		3.1.4 Optical and Infrared Measurements	57
	3.2	AT-Polyaniline Studies	79
		3.2.1 Oligomer Synthesis	79
		3.2.2 Characterization of Oligomers	88
		3.2.3 Conductivity Studies	106
		3.2.4 Additional Curing Studies	114
		3.2.5 Oxidation of Samples for Improved Conductivity	116
4.0	CONCLUSIONS		121
5.0	REFERENCES		128
6.0	EXECUTIVE SUMMARY		130
	6.1	Personnel	130
	6.2	Publications	130

LIST OF ILLUSTRATIONS

Figure		Page
1	Monomers studied: (a) acetylene-terminated Schiff base Thermcon 1000, (b) acetylene-terminated Schiff base Thermcon 2000, (c) vinyl-terminated Schiff base, (d) epoxy-terminated Schiff base, (e) cumyl-substituted acetylene-terminated Schiff base.	4
2	Surface resistivities for several thermosets as a function of iodine content.	5
3	Scanning Electron Micrographs of the cross sections of iodine-doped cured samples of Thermcon 1000: (a) illustrating the contrast shown between the iodine-doped layer and the undoped thermoset, and also the presence of microcracks in the undoped region, and (b) showing the microcracks in the conducting layer.	7
4	Scanning Electron Micrographs of iodine-doped cured samples of Thermcon 1000:(a) cross section of thin film (thickness = 400 microns) where only one surface was exposed to iodine vapor, and (b) surface of thick sample (thickness = 5mm).	8
5	Linescan profile of iodine concentration at different depths into a cured Thermcon 1000 sample using the EDX technique. An SEM of the same cross section with depth of iodine penetration *d* is shown for comparison.	9
6	Plots of iodine uptake versus exposure time to iodine vapor for samples with different crosslink densities.	10
7	Plots of (a) iodine penetration depth, (b) iodine concentration and (c) electrical conductivity versus iodine content for the thermosets.	12
8	The epoxy resin and amine-curing agents studied: (a) diglycidyl ether of bisphenol A, (DGEBA), (b) diethylenetriamine (DETA), and (c) N,N'-dimethyl-1,6-hexanediamine (DDH).	13
9	Surface resistivities for selected thermosets as a function of iodine content.	14
10	The acetylene-terminated polythiophenes studied.	15
11	DSC and TGA plots for 3T-2AcPh.	18

LIST OF ILLUSTRATIONS (continued)

Figure		Page
12	Plots of iodine uptake versus exposure time to iodine vapor for samples of 3T-2AcPh with different crosslink densities, i.e., with different postcure treatments.	19
13	Surface resistivities for selected thermosets as a function of iodine content.	20
14	Conductivity of cured samples of Thermcon 1000 as a function of ion fluence after ion implantation with 180 keV argon ions.	22
15	Scheme I which was used to synthesize acetylene-terminated Schiff bases.	23
16	Scheme II which was used to synthesize the 3-ethynylbenzaldehyde used in Scheme I.	24
17	Scheme III which was used to synthesize the AT-polythiophene T-Si-T-2Ac.	26
18	Scheme IV which was used to synthesize 3T-2Ac.	27
19	Scheme V which was used to synthesize 3T-2AcPh.	28
20	Scheme VI which was used to synthesize the phenylacetylene-terminated Schiff base.	30
21.	Scheme VII which was used to synthesize 3-phenylethynylaniline used in Scheme VI.	31
22	Normalized Spin Susceptibility versus cure time at 160°C for Thermcon 1000.	35
23	ESR Linewidth versus cure time at 160°C for Thermcon 1000.	36
24	Normalized Spin Susceptibility versus cure time at 220°C for epoxy-terminated Schiff base.	37
25	Normalized Spin Susceptibility versus cure time at 220°C for 3T-2AcPh.	39
26	Normalized Spin Susceptibility versus cure time at 90°C for 3T-2Ac.	40
27	(a) Definitions for ESR lineshape parameters and effective g-value, (b) ESR lineshape expected from a value of $(g_{\parallel} - g_{\perp}) \approx 0.015$ and (c) lineshape expected from a value of $(g_{\parallel} - g_{\perp}) \approx 0.005$.	42

LIST OF ILLUSTRATIONS (continued)

Figure		Page
28	The normalized Spin Susceptibility versus iodine content for cured samples of Thermcon 1000.	43
29	The equilibrium scheme used to explain the reversible changes in the ESR lineshape parameters measured on iodine-doping of the thermosets.	44
30	The <g> value versus iodine content for cured samples of Thermcon 1000.	46
31	The A/B value versus iodine content for cured samples of Thermcon 1000.	47
32	The Linewidth versus iodine content for cured samples of Thermcon 1000.	48
33	The normalized Spin Susceptibilty versus iodine content for cured samples of 3T-2AcPh.	51
34	The <g> value versus iodine content for cured samples of 3T-2AcPh.	52
35	The Linewidth versus iodine content for cured samples of 3T-2AcPh.	53
36	The A/B value versus iodine content for cured samples of 3T-2AcPh.	54
37	Infrared transmittance spectrum measured in a Thermcon 1000 film after curing at 160°C for 2 hours.	59
38	Infrared transmittance spectrum measured in a Thermcon 1000 film after curing at 160°C for 5.5 hours.	60
39	Infrared transmittance spectrum measured in a Thermcon 1000 after curing at 160°C for 22.5 hours.	61
40	Infrared absorbance spectra measured near the region of the 3295 cm^{-1} acetylenic end-group absorption band in the polythiophene monomer, 3T-2Ac, showing the difference in peak height for the uncured state and after a cure at 95°C for 19 hours.	62
41	Infrared absorbance spectra measured near the region of the 2108 cm^{-1} acetylene end-group absorption band in a polythiophene monomer, 3T-2Ac, showing the difference in peak height for the uncured state and after a cure at 95°C for 19 hours.	63

LIST OF ILLUSTRATIONS (continued)

Figure		Page
42	Infrared absorbance spectra measured near the region of the 2108 cm^{-1} acetylene end group absorption band showing the changes in peak height for different lengths of cure time in the polythiophene monomer T-Si-T-2Ac.	64
43	Optical absorption edge measured in a thin film of Thermcon 1000 after curing for different times	66
44	Optical absorption edge measured in a Thermcon 1000 film after doping with iodine vapor.	69
45	Optical absorption edge measured in a Thermcon 2000 film after doping with iodine vapor.	70
46	Optical absorption edge measured in a 3T-2AcPh film after doping with iodine vapor.	71
47	Photoluminescence spectrum measured in a partially cured Thermcon 1000 film.	72
48	Time dependent decay of the photoluminescence intensity measured in a Thermcon 1000 film.	73
49	Time dependent decay and partial dark recovery of the photoluminescence intensity measured in a Thermcon 1000 film.	74
50	Photoluminescence spectra measured in a Thermcon 1000 film before and after doping with iodine vapor and waiting for the periods of time indicated.	76
51	Optical absorption edge measured in a Thermcon 1000 film before and after doping with iodine vapor and waiting for the periods of time indicated.	77
52	Structures (leuco forms) of polyaniline-type oligomers and polymers investigated in this work.	80
53	Scheme VIII: Procedure used to synthesize 2,5-dioxo-1,4-cyclohexanedicarboxylic acid (DCCA).	81
54	Scheme IX: Procedure of Wudl et al., used to synthesize polyaniline oligomers.	82

LIST OF ILLUSTRATIONS (continued)

Figure		Page
55	Scheme X: Our adaptation of the procedure of Manassen and Khalif used to synthesize polyaniline oligomers.	84
56	Schematic of a typical polyaniline-type material in various oxidation states: (a) Leucoemeraldine, (b) emeraldine, and (c) pernigraniline.	85
57	UV-VIS spectrum from phenyl-capped aniline oligomers (COA) prepared using MK approach.	86
58	IR spectra recorded from acetylene-terminated polyaniline oligomers: (a) ATPA-7 synthesized using the MHW approach.	89
59	UV-VIS spectra recorded from acetylene-terminated polyaniline oligomers: (a) ATPA-9 synthesized using the MHW approach. b) ATPA-7 synthesized using the MK approach.	90
60	UV-VIS spectra of polyaniline: (a) prepared by chemical oxidation of aniline using ammonium persulfate and (b) prepared using MHW approach.	91
61	UV-VIS spectra of ATPA-7(MK): (a) As-synthesized, (b) Following oxidation with O_2, and (c) Following reduction with phenylhydrazine.	93
62	TGA (derivative) and mass-spectrum total ion current from ATPA prepared using MHW approach.	94
63	Fragments contributing to mass-spectrum total ion current from ATPA prepared using MHW approach.	95
64	TGA from ATPA-7 prepared using MK approach.	96
65	IR spectrum from phenyl-capped aniline oligomers (COA) prepared using MK approach.	97
66	IR spectrum from fully oxidized polyaniline (i.e., pernigraniline state), with equal numbers of quinoid (Q) and benzenoid (B) rings in the sample.	98
67	ESR spectra from undoped and HCl-doped ATPA prepared using MHW approach.	99

LIST OF ILLUSTRATIONS (continued)

Figure		Page
68	ESR spectra from undoped and HCl-doped ATPA prepared using MK approach.	100
69	Electrochemical cell potential as a function of fraction of repeat units reduced for (a) Conventional polyaniline, and (b) typical as-synthesized ATPA-7(MK).	101
70	^{1}H NMR spectra of ATPA-7(MK) and COA(MK), both following the reduction with phenylhydrazine. (a) COA(MK) and (b) ATPA-7(MK).	102
71	GPC chromatograms for ATPA-7(MK) prior to and following reduction using phenylhydrazine: (a) Before reduction, and (b) After reduction.	104
72	GPC chromatogram for ATPA-7(MK) in 5% DNBA/THF.	105
73	Conductivity (4-point probe) of tosylic acid-doped ATPA-3(MK) measured as a function of time at 150°C.	111
74	Conductivity of BDSA-doped polyaniline and BDSA-doped ATPA-7(MK) as a function of time at 150°C.	113
75	Curing of ATPA-7 (MK) at 150°C, as monitored by the ratio of the 3290 cm^{-1} (acetylene peak) to the 830 cm^{-1} IR peaks.	115
76	UV-VIS spectra of COA (MK)exposed to different treatments.	118
77	Possible structures of crosslinks in thermosets formed from acetylene-terminated monomers and oligomers: (a) the polyene, (b) the substituted benzene, (c) the enyne, (d) the substituted naphthalene, and (e) the non-conjugated linkage.	122

LIST OF TABLES

Table		Page
1	The Maximum Spin Concentrations Measured in Thermosets with Different Doping Conditions.	38
2	Temperature Dependence of ESR Lineshape Parameters.	56

LIST OF TABLES (continued)

Table		Page
3	ESR Parameters for Uncured Aniline Oligomers.	100
4	Conductivity of Doped Polyaniline Derivatives and Uncured Oligomers.	107
5	Doping and Conductivity of Polyaniline Derivatives and Uncured Oligomers.	109
6	Conductivity of ATPA-7 Doped with 0.2 M Camphorsulfonic Acid versus Cure Time.	112
7	Effect of Oxidation with O_2 On Conductivity of Uncured Oligomers.	117

LIST OF PAGES

Title Page

Report Documentation Page

i-vii

1-130

1.0 INTRODUCTION

From the vast amount of research that has been performed on conducting polymers since the discovery of highly conducting polyacetylene [1-5], several factors necessary for high conductivity (i.e., > 1 S/cm) have emerged. For example, it is now well established that for high conductivity in polymers containing redox dopants the polymer must have extended conjugation. Moreover, the data suggest that the conductivity is limited by the charge transport and not by the charge carrier concentration.

Almost all conducting polymers are thermoplastics with a heterogeneous crystalline morphology consisting of conducting islands [5] (sometimes referred to as "particles" or "domains"). The conductivity is then determined by three types of charge-transport, viz., (a) the intrachain charge transport along the conjugated chain, (b) the interchain charge transport for hopping between chains in the same conducting island, and (c) the inter-island charge transport for hopping from a chain in one island to a neighboring chain in a contiguous island. The intrachain transport usually involves polaron or bipolaron transport which is governed by the effective mass of the combined charge carrier and the associated lattice distortion, along with scattering by impurities or chain defects and structural disorder. The interchain transport depends on the coupling strength between the quasi-one dimensional polymer chains and can often be identified with some form of hopping process. The inter-island transport usually involves larger hopping barriers because of chain misalignment and the relatively larger inter-island distances.

All three charge transport terms determine the macroscopic conductivity to some degree but usually the interchain and inter-island terms are the limiting factors. Therefore, to increase the macroscopic conductivity in a polymer system, it is necessary to increase the interchain and inter-island jump rates by lowering the hopping barriers. One possible way is in the use of conducting

thermoset polymers, which have a conjugated network extending throughout the sample. For this conjugated network to be "one giant molecule" the π-conjugation has to extend along the backbone and through the crosslinks formed after polymerization. We investigated this idea by studying several types of conjugated monomers which have acetylene-terminated end-groups, since it has been established that conjugated crosslinks are formed when acetylene-terminated (AT)-oligomers polymerize [6-12].

This report summarizes the results and conclusions of these investigations carried out from 1 October 1992 to 31 September 1995.

2.0 RESEARCH OBJECTIVE AND APPROACH

Our objective was a feasibility study of using acetylene-termination chemistry to provide the processing, mechanical properties, and electrical conductivity necessary to realize a single-component conductive thermosetting material.

Our approach has been to synthesize selected monomers, hot-melt these monomers into thermosets and use different methods to get them conducting. Three classes of monomers (or oligomers) were studied, viz., AT-Schiff bases, AT-polythiophenes, and AT-polyanilines. In the case of the AT-Schiff bases and AT-polythiophenes, the monomers were cured first then doped with iodine. On the other hand, for the AT-polyanilines the oligomers were doped first with protonic acids then cured. Ion implantation studies were also carried out on one of the AT-Schiff bases.

3.0 RESULTS

3.1 AT-Schiff Base and AT-Polythiophene Studies

3.1.1 Electrical Measurements

Surface resistivity measurements were made on the iodine-doped cured samples in the form of discs having 16mm diameters. Over the range 10^5 to 10^{11} ohms/square measurements were made with a two-point probe and a Hiresta model electrometer (Mitsubishi); whereas from 10^4 to 10^7 ohms/square a four-point probe and a Loresta model electrometer (Mitsubishi) were used. In the intermediate region (10^5 to 10^7 ohms/square) the two methods usually gave consistent results.

We completed a comparative study of the conductivity values of AT-Schiff base thermosets with those measured in Schiff base thermosets that have nonconjugated crosslinks. The latter were chosen as the vinyl and epoxy-terminated counterparts. The structures of these monomers are shown in Figure 1. The AT-Schiff bases include the para- and meta-substituted Schiff bases shown in Figures 1(a) and 1(b) (i.e., Thermcon 1000 and Thermcon 2000) as well as the cumyl-substituted Schiff base shown in Figure 1(e). Thermcon 1000 is the meta-substituted AT-counterpart of the VT- and ET-structures shown in Figures 1(c) and 1(d).

The surface resistivity data for the five thermosets prepared from the five Schiff bases are shown as a function of iodine content in Figure 2. As can be seen from Figure 2, the surface resistivities of cured Thermcon 1000 are approximately the same as those for Thermcon 2000 at all iodine concentrations. Secondly, at the same iodine contents the surface resistivities of the thermosets from CD-EB, ET- and VT- Schiff bases are all approximately ten times greater than the values measured in either Thermcon 1000 or Thermcon 2000. However, to draw any conclusions about the influence of the structure on the charge transport, it is the values of the bulk

a) 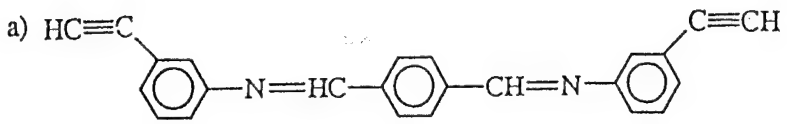

AT-SB

b) 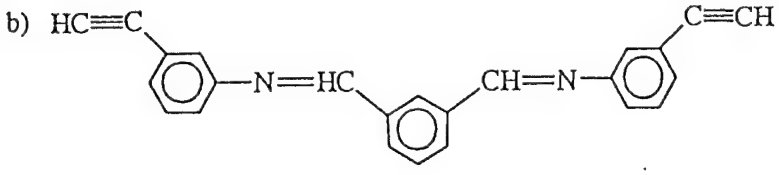

AT-SB

c) 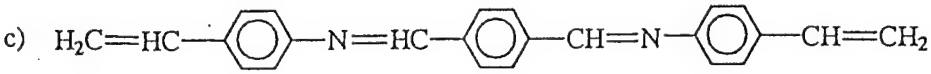

VT-SB

d) 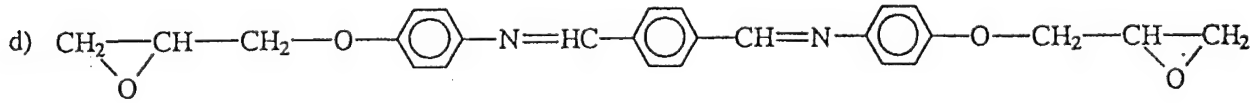

ET-SB

e) 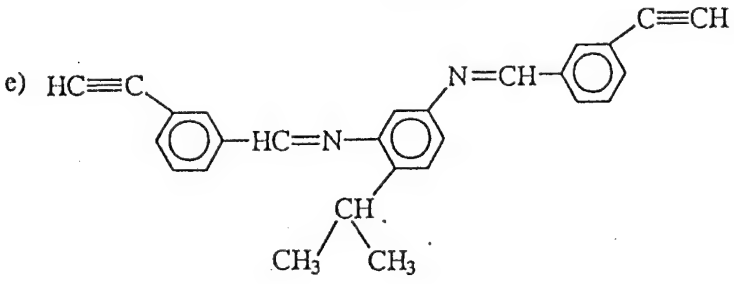

CD-EB

Figure 1. Monomers studied: (a) acetylene-terminated Schiff base Thermcon 1000, (b) acetylene-terminated Schiff base Thermcon 2000, (c) vinyl-terminated Schiff base, (d) epoxy-terminated Schiff base, (e) cumyl-substituted acetylene-terminated Schiff base.

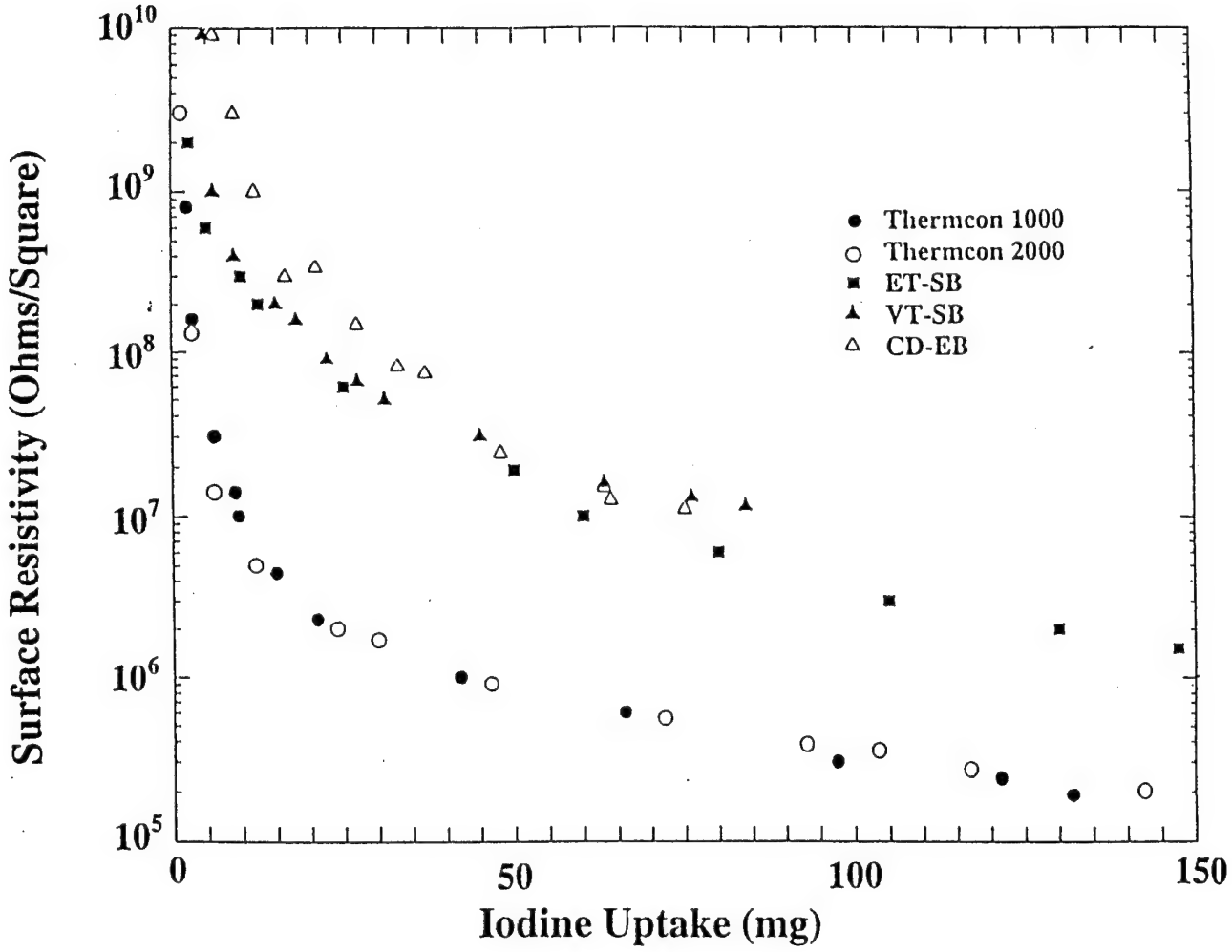

Figure 2. Surface resistivities for several thermosets as a function of iodine content.

conductivity that have to be compared. For a thin conducting layer the bulk conductivity (σ) is given by $\sigma = 1/\rho$, with $\rho = \rho_S\, d$, where ρ_S is the surface resistivity, ρ is the bulk resistivity and d is the thickness of the conducting layer (= the iodine penetration depth). Hence, to obtain values of the bulk conductivity one has to know the penetration depth of iodine into the thermoset.

Scanning electron micrographs (SEM) of sample cross sections clearly show the depth of penetration of the iodine. Figure 3(a) illustrates how distinct the contrast is between the iodine containing layer and the non-penetrated regions of the thermoset. Furthermore, SEM micrographs also show the presence of two types of microcracks in the sample cross sections. Thus, these microcracks occur either in nonconducting regions not penetrated by the iodine, as shown in Figure 3(a), or in the conducting layers, as shown in Figure 3(b). The former were usually observed in samples cured only at 160°C, whereas the latter were detected in samples which had an additional 40 h post-cure at 200°. Both types are the result of swelling stresses induced by the sorbed iodine. As the iodine uptake is increased these microcracks eventually lead to a mechanical failure of the sample. As is shown in Figure 4(a) , this swelling is also directly observable by SEM of thin films. Cracking was also observed on the surface of the disc samples when the samples were not post-cured. An example of this type of cracking is shown in Figure 4 (b).

We have also used Energy Dispersive X-Ray Spectroscopy (EDX) along with Scanning Electron Microscopy to probe the iodine concentration at different depths into the thermoset. In this technique, one monitors the characteristic x-rays emitted from the iodine following bombardment of a small area (approximately a few microns in diameter) of the sample cross section with the electron beam. The resulting linescan profile, such as the example shown in

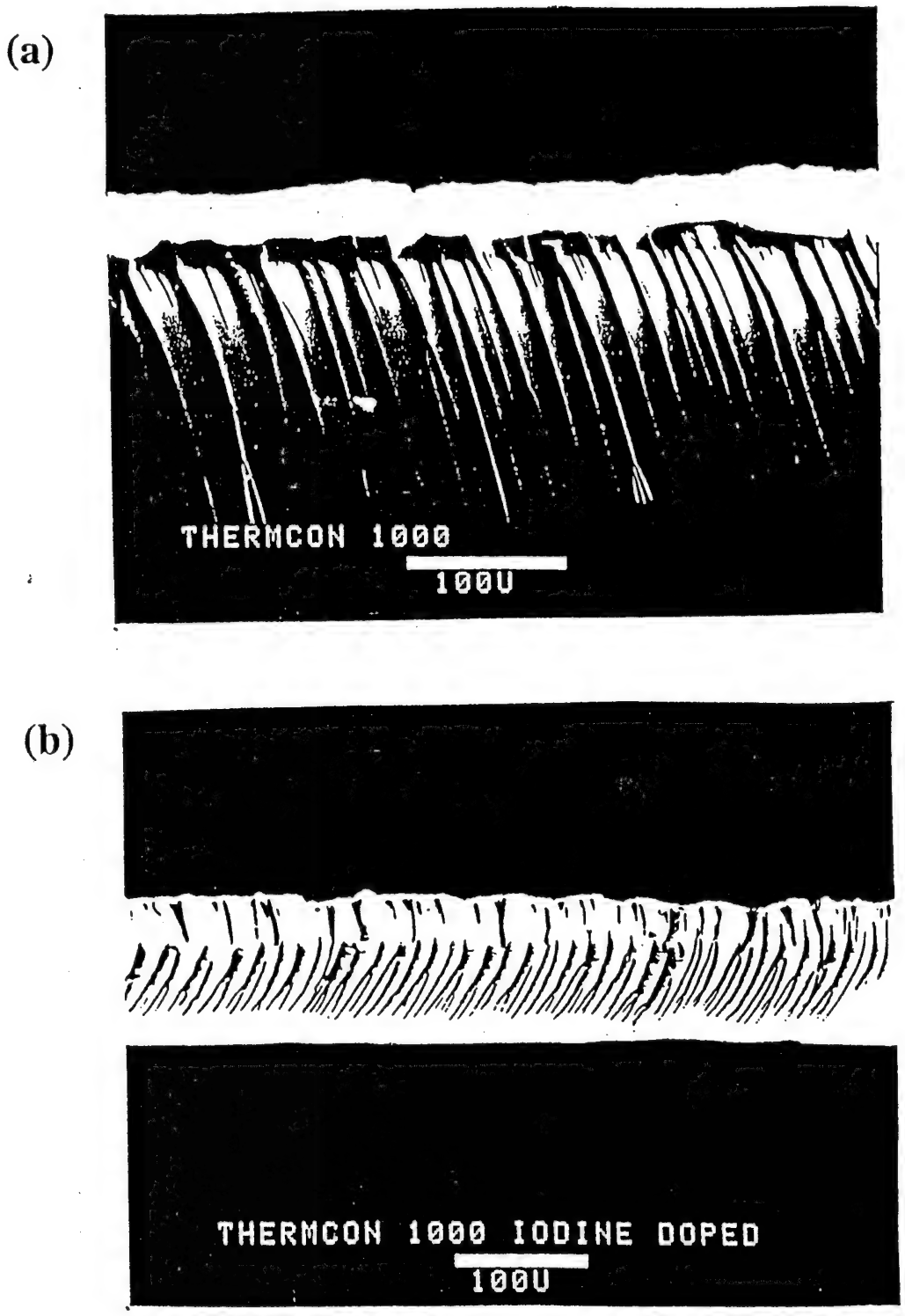

Figure 3. Scanning Electron Micrographs of the cross sections of iodine-doped cured samples of Thermcon 1000: (a) illustrating the contrast shown between the iodine-doped layer and the undoped thermoset, and also the presence of microcracks in the undoped region, and (b) showing the microcracks in the conducting layer.

(a)

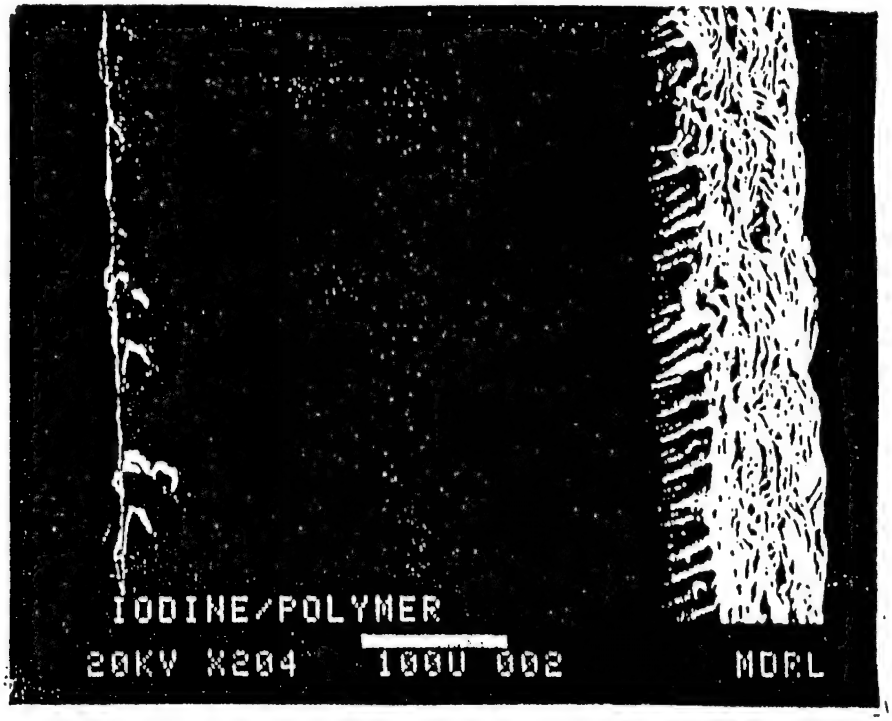

(b)

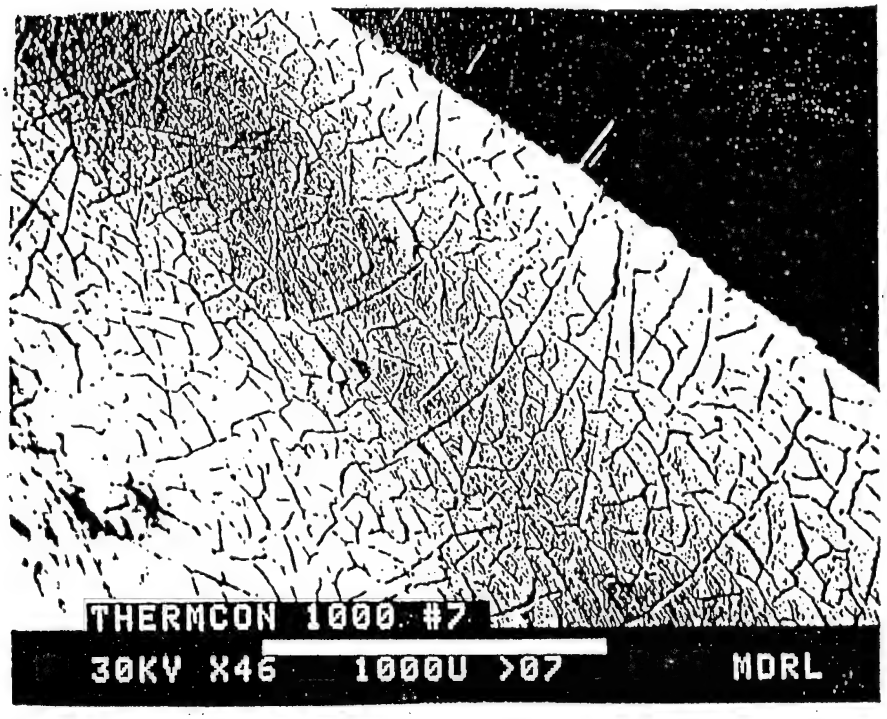

Figure 4. Scanning Electron Micrographs of iodine-doped cured samples of Thermcon 1000: (a) cross section of thin film (thickness = 400 microns) where only one surface was exposed to iodine vapor, and (b) surface of thick sample (thickness = 5mm).

Figure 5 along with the scanning electron micrograph of the same region, indicates that the iodine concentration is constant behind a steep front. This behavior is an example of non-Fickian, Case II type diffusion [13]. This type of diffusion has not yet been reported for dopant behavior in conducting polymers, but it is well known for penetrant behavior in thermosets [13]. It comes about because the iodine at the front plasticizes the polymer and, in so doing, increases the diffusion coefficient of the iodine coming behind so that it rapidly enters the polymer.

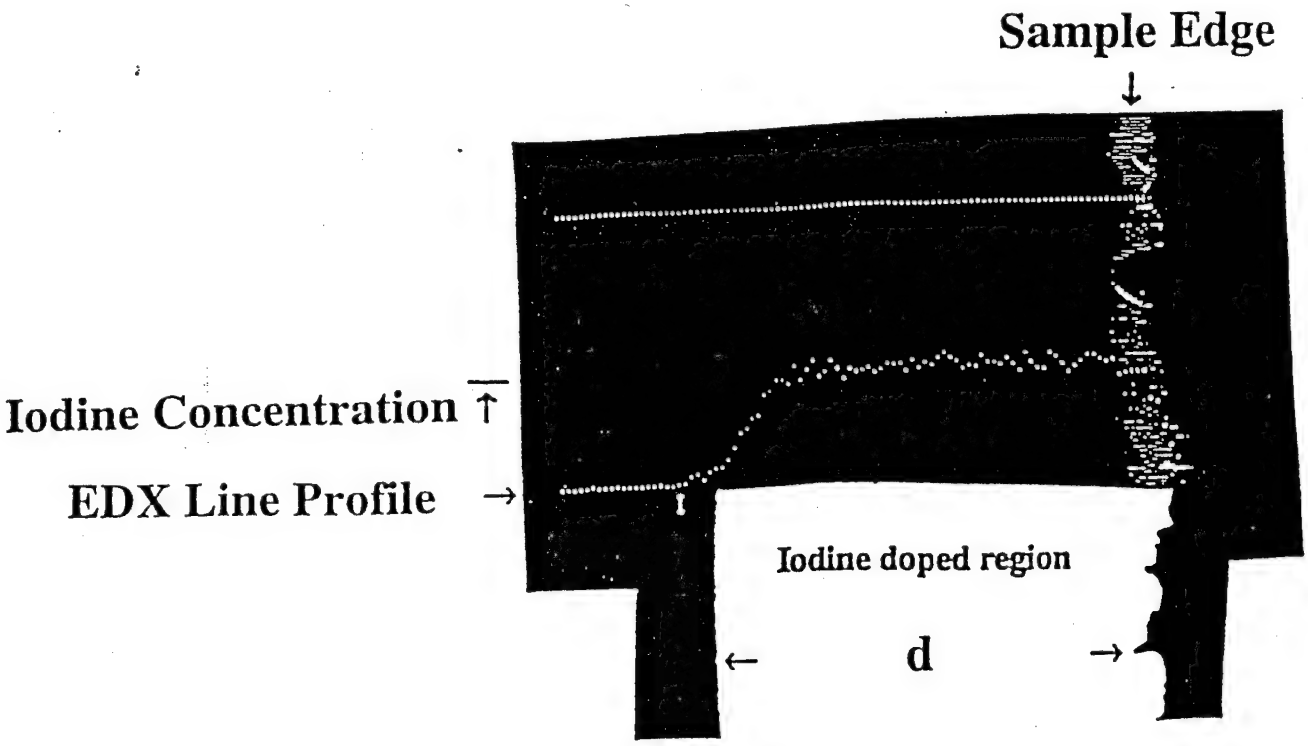

Figure 5. Linescan profile of iodine concentration at different depths into a cured Thermcon 1000 sample using the EDX technique. An SEM of the same cross section with depth of iodine penetration *d* is shown for comparison.

Additional evidence for this diffusion mechanism comes from the rate of iodine uptake by the thermoset. As is shown in Figure 6, the iodine uptake, as determined by the sample weight gain, depends linearly on the exposure time of the samples to the iodine vapor. If the diffusion had been Fickian, the iodine uptake would have been dependent on the square root of the exposure time[13]. Moreover, the data in Figure 6 also indicate that the rate of iodine uptake depends on the crosslink density of the sample.

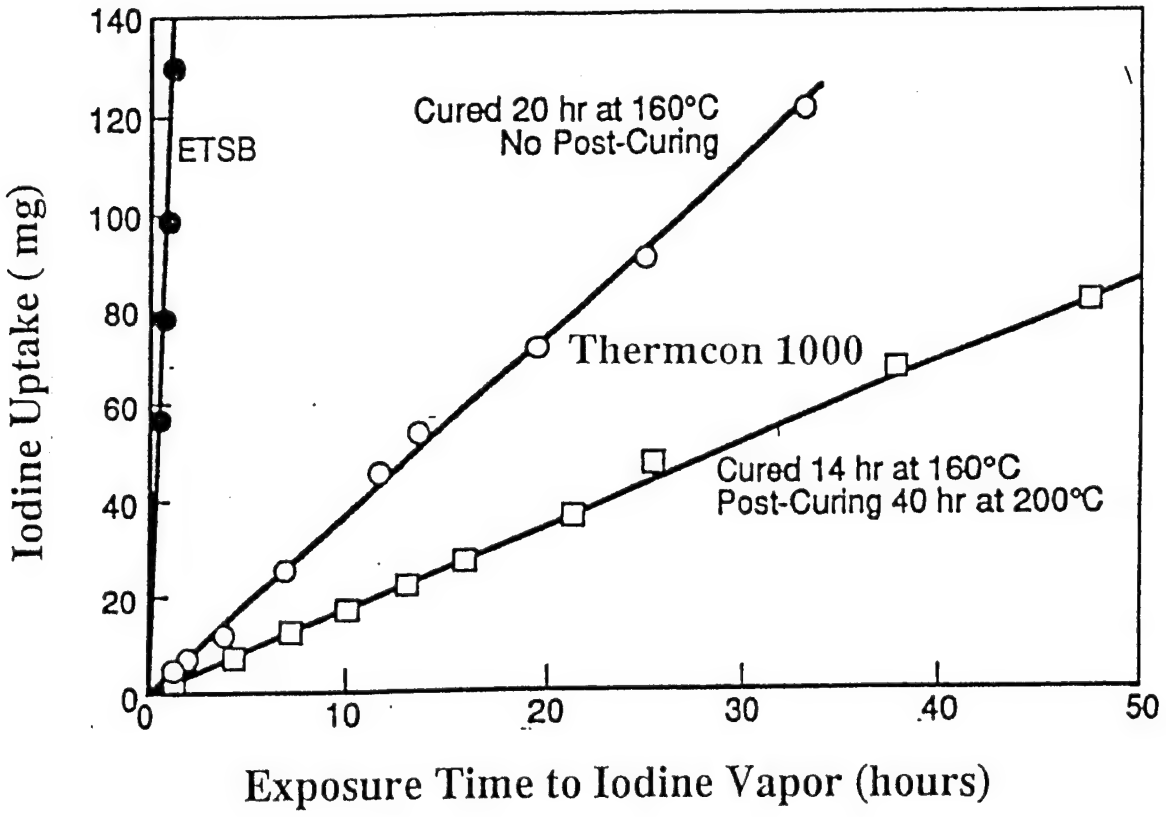

Figure 6. Plots of iodine uptake versus exposure time to iodine vapor for samples with different crosslink densities.

Knowing the iodine penetration depths allows us to calculate the iodine concentration as well as obtain a measure of the conductivity at different depths into the polymer samples. Both parameters are plotted in Figure 7 as a function of total iodine content for the three samples shown. The data show that (a) the penetration depth is linearly dependent on the iodine uptake, (b) the iodine concentration is constant at different depths into the polymer sample with an average value of approximately 2.75 g/cm^3 which is, in fact, a consequence of conclusion (a), (c) the conductivity values for the AT-Schiff base thermosets are constant with increasing depth, (d) the conductivity for the ET-Schiff base and the VT-Schiff base thermosets appears to increase over the depths measured, and (e) the conductivity for the AT-Schiff bases is approximately a factor of ten greater than the values in any of the CD-EB Schiff base, the ET-Schiff base or VT-Schiff base thermosets.

The same constant iodine concentration profile for different penetration depths in all three thermoset samples (viz., Thermcon 1000, ET-SB, and VT-SB) is a consequence of the non-Fickian Type II diffusion that governs the penetrant transport properties. Since this type of penetrant diffusion is characteristic of thermosets it can be expected to occur in all conducting thermosets.

If the bulk conductivity depends only on the iodine concentration one would expect it to be constant with increasing depth, as indeed was observed in the Thermcon 1000 thermoset. On the other hand, in the ET- and VT-Schiff base thermosets the increase in conductivity with increasing iodine content (i.e., increasing depth) is possibly the result of microcracking in or adjacent to the conducting layer of the types illustrated in Figure 3. Furthermore, it is reasonable

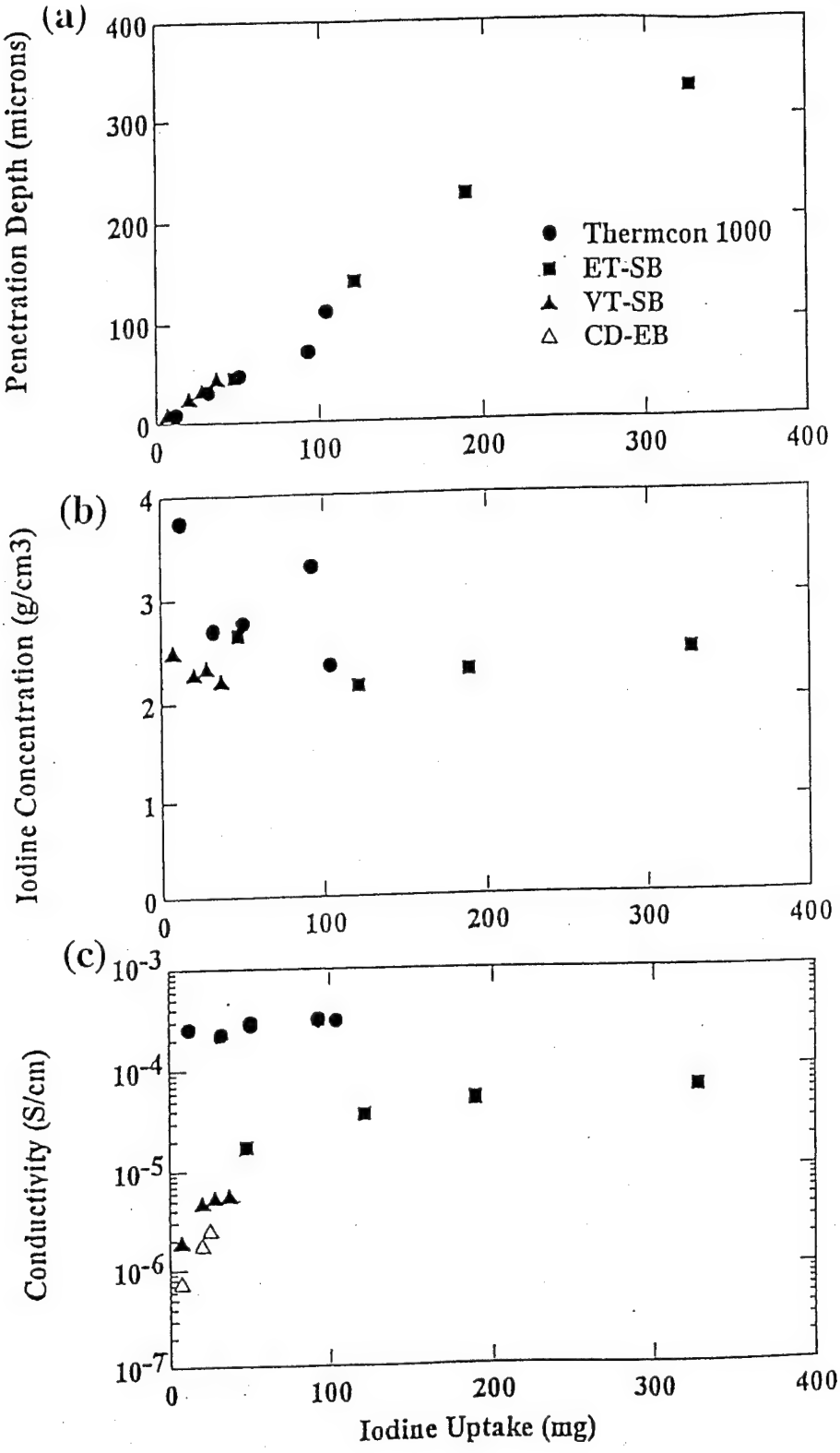

Figure 7. Plots of (a) iodine penetration depth, (b) iodine concentration, and (c) electrical conductivity versus iodine content for the thermosets.

to expect that such microcracking will play a more decisive role in increasing the resistance of the thinner layers.

The higher conductivity values for the Thermcon Schiff base thermosets following iodine doping suggests that the extended conjugation provided by the polyene crosslinks is responsible for the enhanced conductivity. Introduction of the bulky cumyl group as a sidechain in the CD-EB Schiff base thermoset also produces a lowering of the conductivity value over that exhibited by the Thermcon 1000 thermoset. Thus, we have been able to change the conductivity values of the Schiff base thermosets by changing the nature of either the crosslink or the backbone.

We have also obtained measurable conductivity in amine-cured epoxy thermosets which are non-conjugated. These included the diglycidyl ether of bisphenol A (DGEBA) cured with stoichiometric amounts of either 1,3-diethylenetriamine (DETA). The structures of these monomers are shown in Figure 8. Measured values of the surface resistivity versus iodine uptake

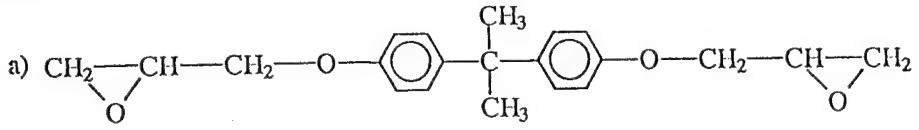

DGEBA

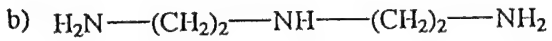

DETA

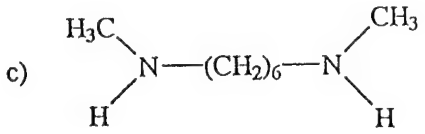

DDH

Figure 8. The epoxy resin and amine-curing agents studied: (a) diglycidyl ether of bisphenol A, (DGEBA), (b) diethylenetriamine (DETA), and (c) N,N'-dimethyl-1,6-hexanediamine (DDH).

are shown in Figure 9 along with measurements for the ET-Schiff base and Thermcon 1000 thermosets for comparison. The data show that at the same iodine contents the values for the DGEBA/DETA and the ET-Schiff base thermosets are, within experimental error, the same.

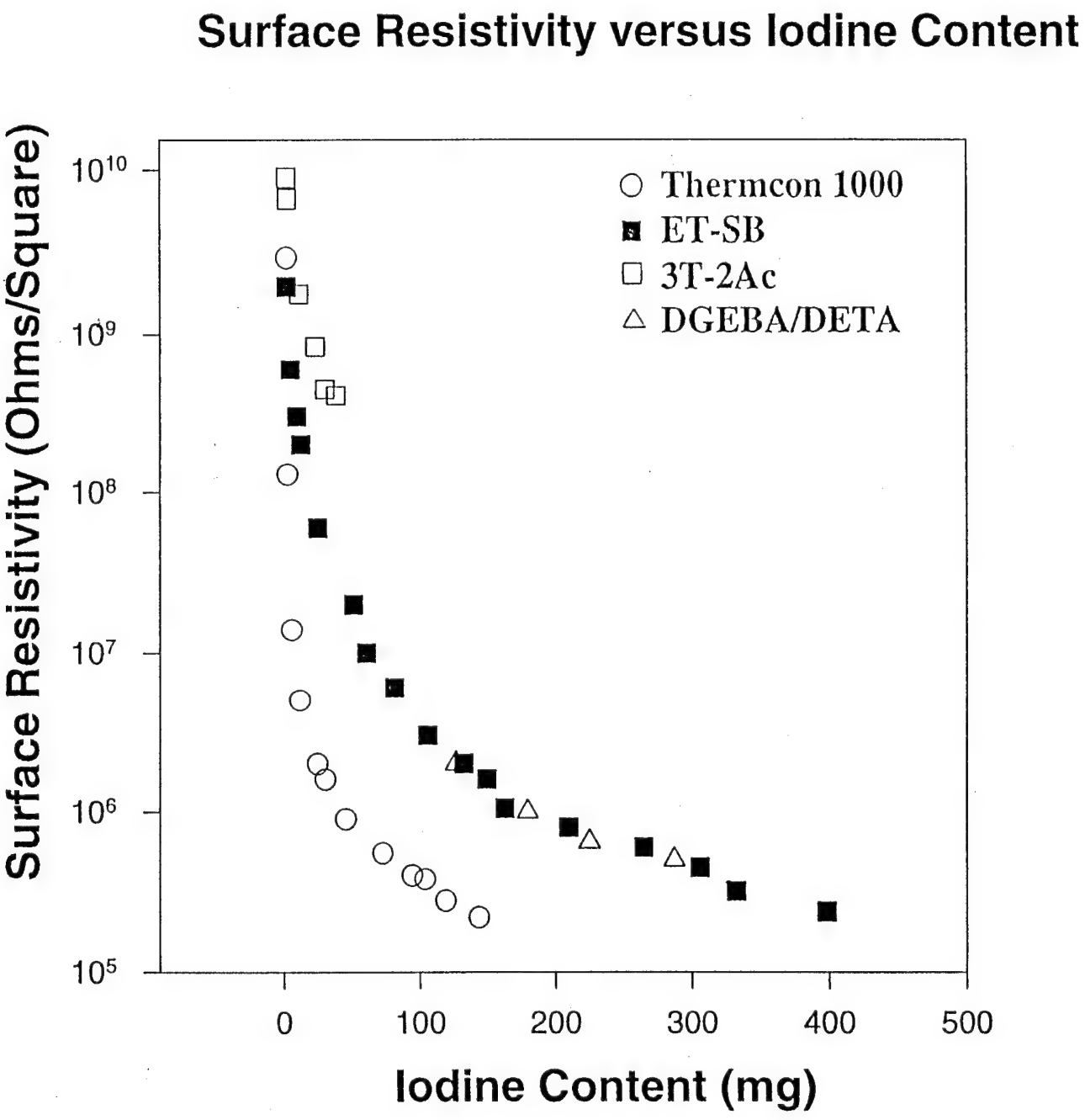

Figure 9. Surface resistivities for selected thermosets as a function of iodine content.

We have also extended our investigations to AT-polythiophenes. The structures of the three polythiophenes that were studied are shown in Figure 10.

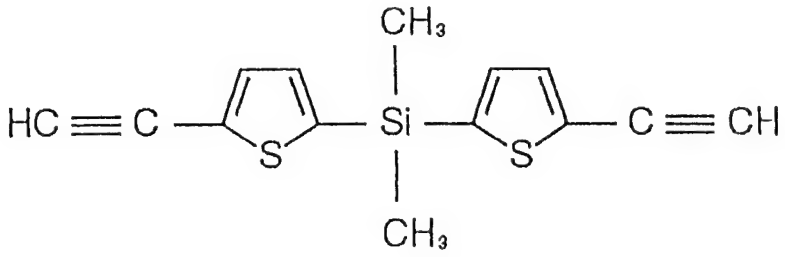

T-Si-T-2Ac

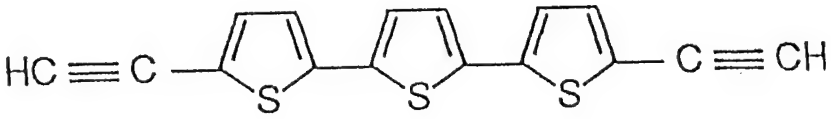

3T-2Ac

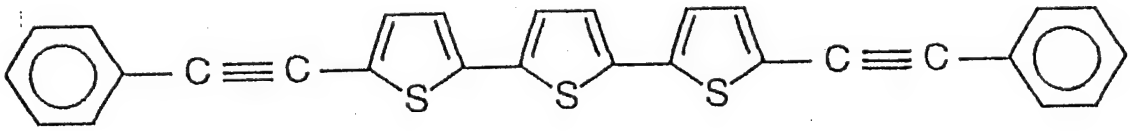

3T-2AcPh

Figure 10. The acetylene-terminated polythiophenes studied.

T-Si-T-2Ac is a volatile liquid which could not be cured into the form of thick films or discs for accurate electrical measurements. Thin films were cast between glass plates for the optical studies described below.

The DSC for 3T-2Ac showed an exotherm at 100°C but no endotherm associated with a melting. The TGA in air showed a weight increase up to 350°C (a maximum increase of 4%), probably due to an air oxidation. Curing at temperatures much above 125°C in air resulted in sample decomposition presumably because of thermal runaway. Pellets of the powder were therefore cured in vacuum oven at 95°C. The mechanical properties of these thermoset samples were poor and as a result only small amounts of iodine could be introduced into the pellet samples before they fell apart because of the swelling caused by the iodine. The maximum penetration depth was 30 microns, giving a maximum conductivity of only $3x10^{-6}$ S/cm. A high crosslink density, which is a consequence of the short length of the 3T-2Ac monomer, may be the reason for the poor mechanical properties. These results illustrate the importance of the mechanical properties in allowing the uptake of the dopant for low surface resistivity values in thermosets.

To investigate the consequences of high crosslink densities, we studied the electrical and magnetic properties of thermosets made from a monomer which was terminated with phenylacetylene group, i.e., 3T-2AcPh shown in Figure 10. These types of monomers have been reported to have excellent high temperature stability and good mechanical properties [14-16]. It is believed that the presence of the bulky phenyl group near the crosslink results in a lowering of the crosslink density, an increase in the free volume content of the cured thermoset, and hence a lowering of its brittle nature.

Our DSC measurements of 3T-2AcPh samples showed a wide window for cure. The DSC and TGA results shown in Figure 11 indicate a melting point at 199°C, a maximum in the exotherm at 255°C and good thermal stability up to 550°C (a 10% weight loss point at 560°C). Our initial samples were cured at 250°C for 6 hours then postcured at 295°C for 12 hours. These disc samples remained intact up to an iodine content of 150 mg and were as good as Thermcon 1000 samples whereupon they would usually fracture due to the swelling stresses arising from the iodine dopant. However, on reducing the cure temperature to 220°C (for 6 hours) and post-cure temperature to 245°C (for 12 hours), the samples sorbed a factor of three times more iodine (i.e., 500 mg) without ever undergoing fracture due to the swelling stresses. As is shown in Figure 12, the iodine uptake by the 3T-2AcPh thermoset was linearly dependent on the exposure time to the iodine vapor. The iodine transport can therefore be described in terms of a non-Fickian, Case II type diffusion, just as was observed in the Thermcon 1000 thermoset samples. Moreover, the data in Figure 12 showing the different rates of iodine uptake verify that the crosslink densities have been changed with the different cure procedures.

The results of measurements of the surface resistivity of the 3T-2AcPh samples as a function of iodine content are shown in Figure 13 along with the corresponding values for the Thermcon 1000 samples for comparison. As can be seen from Figure 13, within experimental error, the surface resistivities for the two samples are the same. Moreover, with our limited data, for a given iodine content the iodine penetration depths for both samples are the same. Hence, the bulk conductivity's for iodine-doped cured samples of Thermcon 1000 and 3T-2AcPh are the same, i.e., $\sigma = 2.75$ S/cm.

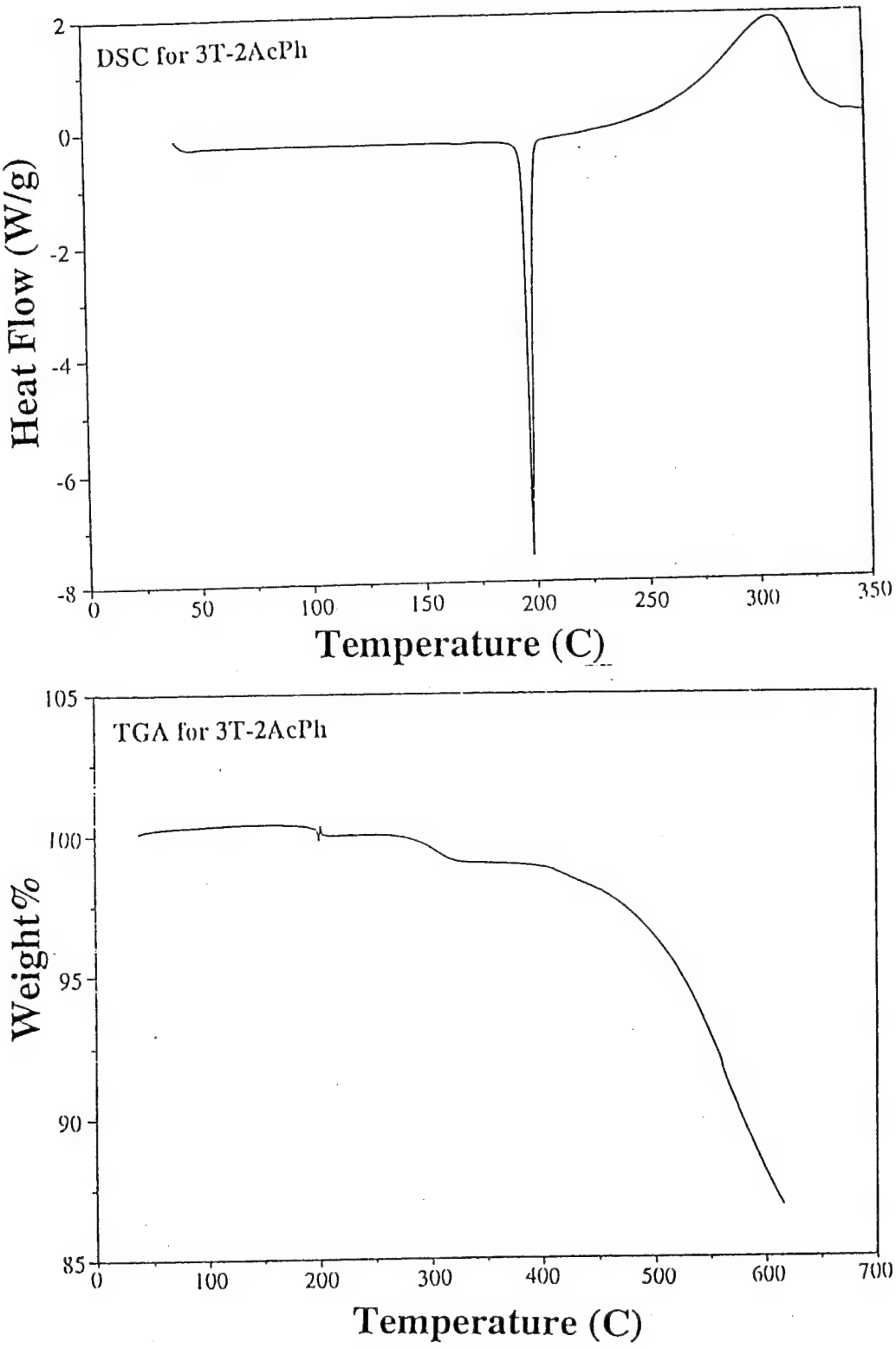

Figure 11. DSC and TGA plots for 3T-2AcPh.

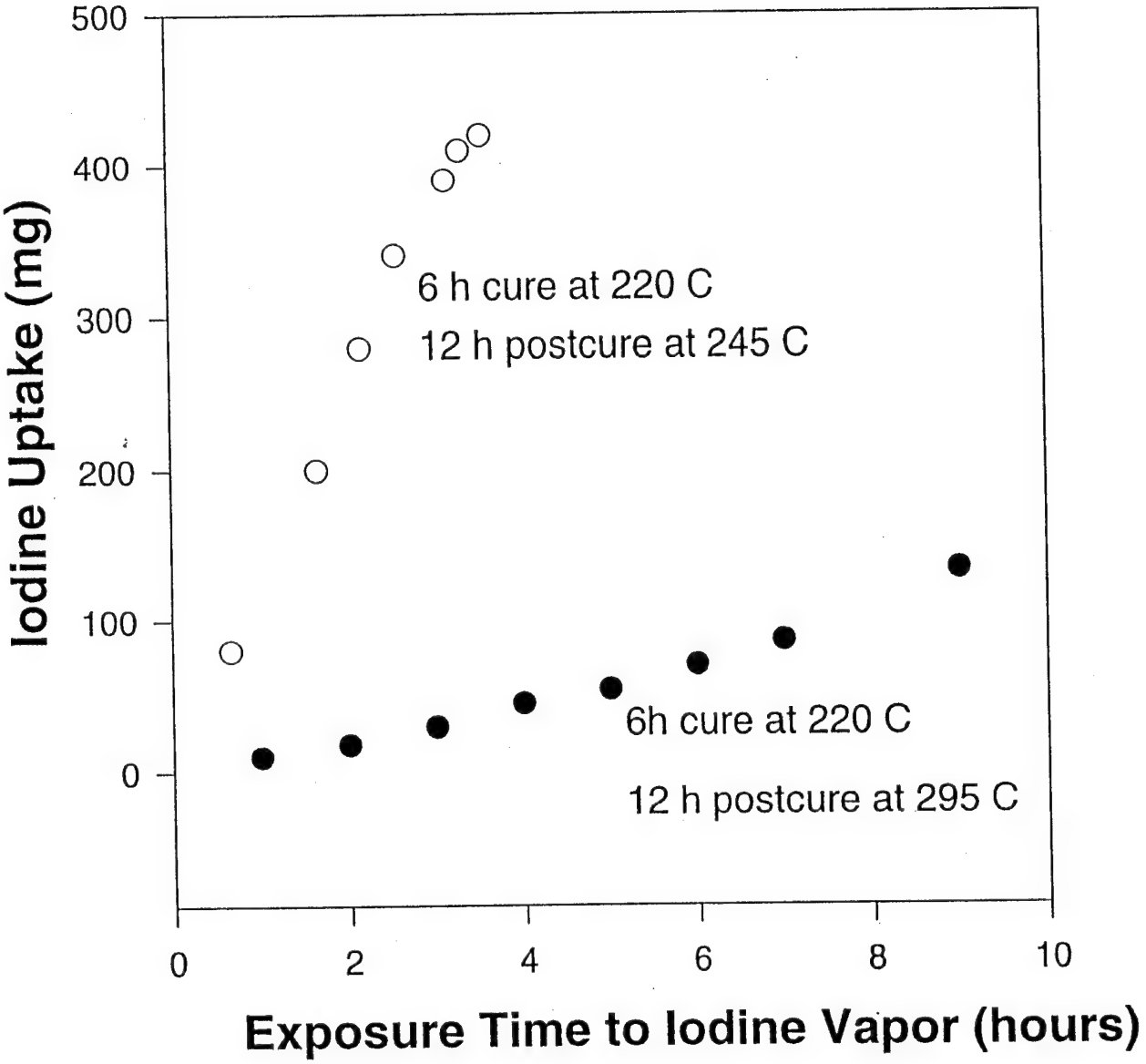

Figure 12. Plots of iodine uptake versus exposure time to iodine vapor for samples of 3T-2AcPh with different crosslink densities, i.e., with different postcure treatments.

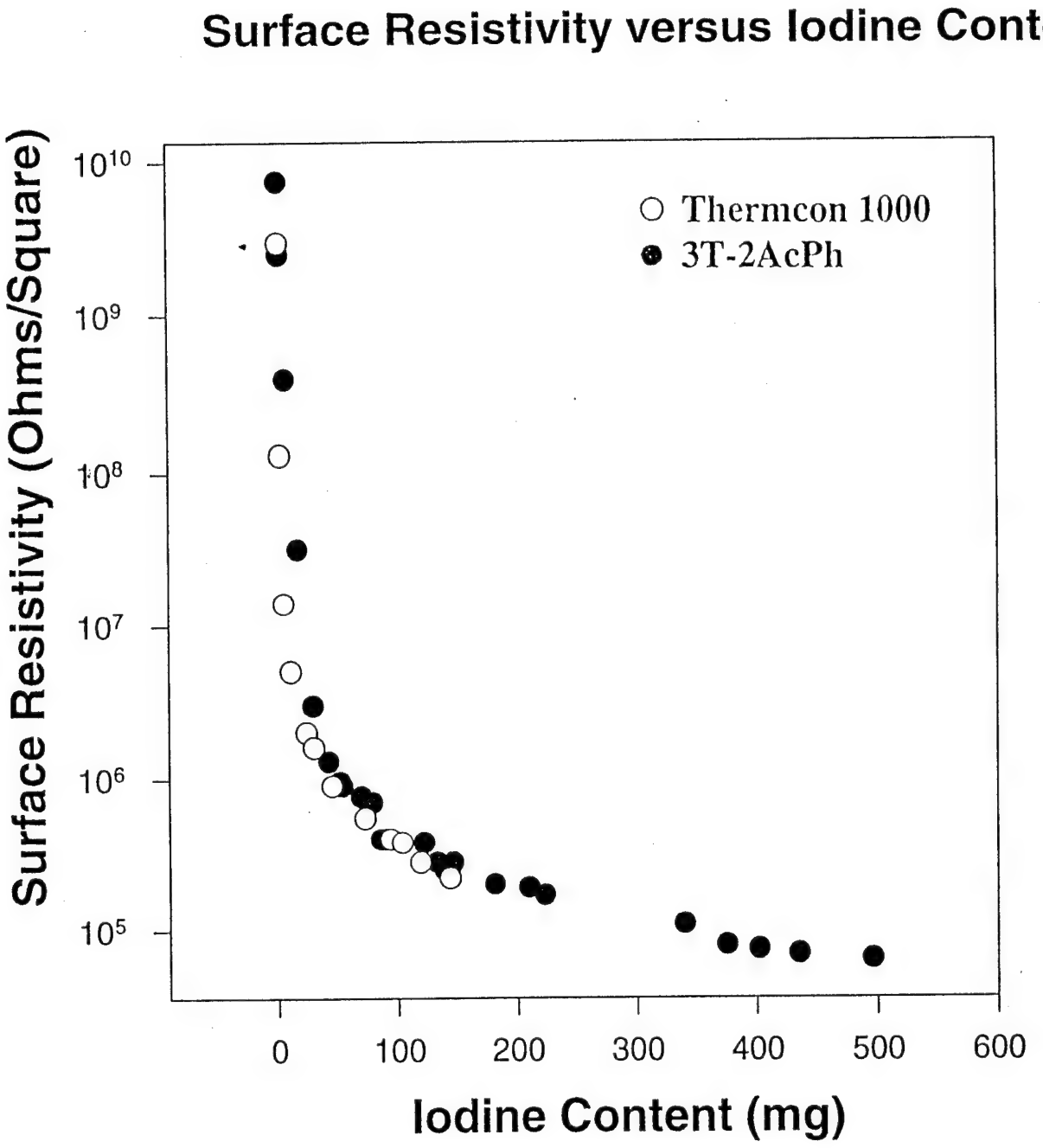

Figure 13. Surface resistivities for selected thermosets as a function of iodine content.

Samples of a phenylacetylene-terminated Schiff base were synthesized using the procedures already described [14]. However, DSC measurements showed no melting or exotherm below 350°C, in marked contradiction to the reported properties [14]. We suspect that, just as in the case of 3T-2Ac, polymerization had taken place before the compound was isolated. Further measurements on this material were not pursued.

We measured the conductivity in four samples of the Thermcon 1000 thermoset following ion implantation with 180 KeV argon ions. Thin films of Thermcon 1000 were formed on circular, stainless steel, sample holders by melting and curing (72 hours at 180°C). These sample holders were 10 cm in diameter and were compatible with the Eaton Model 3206 ion implanter used. Ion beam fluences were varied from $5x10^{15}$ to $1.5x10^{17}$ ions/cm^2. The values of the conductivity shown in Figure 14 were estimated from measurements of the surface resistivities assuming the thickness of the conducting layer was 0.75 microns (= argon ion penetration depth). As is shown in Figure 14 the maximum conductivity measured was $1.5x10^{-2}$ S/cm. The conductivity exhibited by ion implanted polymers has been attributed to charge carriers generated as a result of the radiation damaged caused by the energetic ion beam, rather than chemical doping [17-19]. In general, this radiation damage also involves chain scission, the formation of free radicals and vacancies, carbonization, crosslinking, as well as gas evolution. Although the maximum conductivity value of the ion implanted Thermcon 1000 thermoset is two orders of magnitude higher than that measured in the iodine-doped Thermcon 1000 thermoset, no meaningful comparison can be made between the two systems because the structure of the ion implanted layer differs greatly from that of the parent material as a result of this radiation damage.

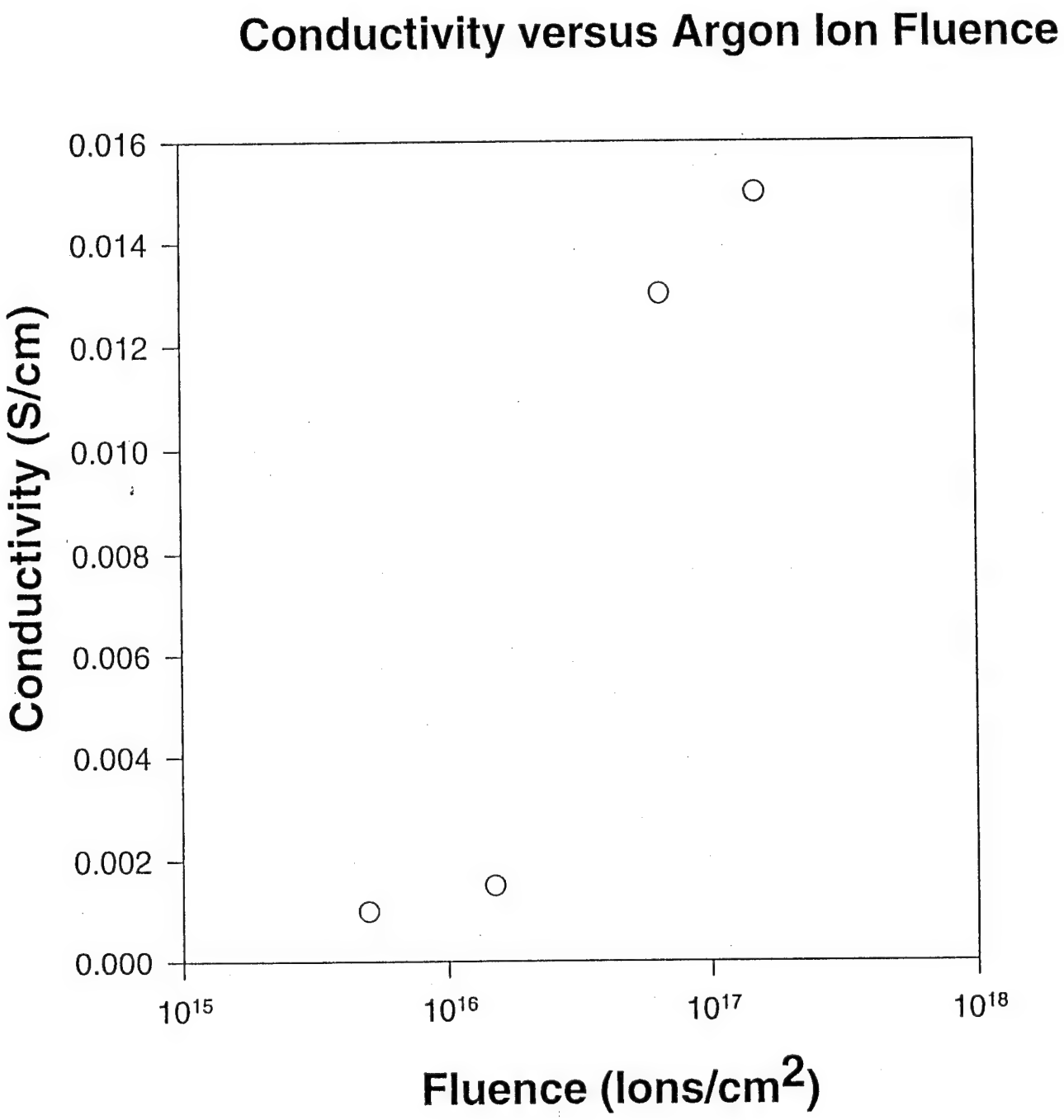

Figure 14. Conductivity of cured samples of Thermcon 1000 as a function of ion fluence after ion implantation with 180 keV argon ions.

However, the relatively high conductivity exhibited by the ion implanted thermosets warrants future studies of the use of this technique to other thermosets.

3.1.2 Monomer Synthesis and Sample Preparation

Monomer Synthesis: Thermcon 1000 and Thermcon 2000 (obtained as commercial resins from National Starch and Chemical Corporation, Bridgewater, New Jersey) were washed with methanol and then crystallized from a mixture of methylene chloride and hexane.

Acetylene-Terminated Schiff Bases: The AT-Schiff bases were synthesized by the reaction of two moles of 3-ethynylbenzaldehyde and one mole of the corresponding diamine as shown in Scheme I in Figure 15. The diamines were chosen so as to preserve the extensive

Scheme I

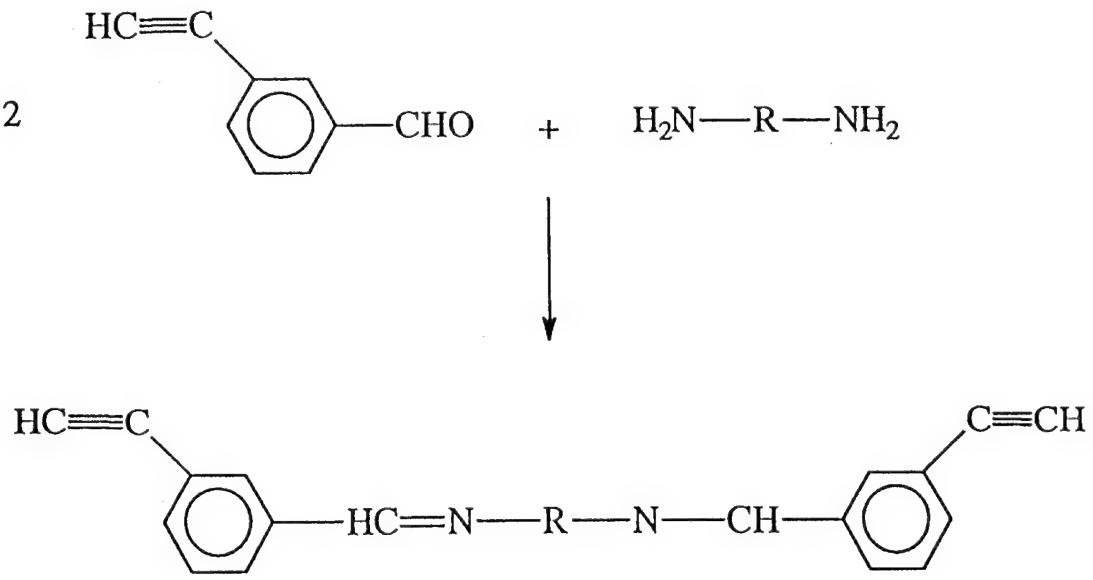

Figure 15. Scheme I which was used to synthesize acetylene-terminated Schiff bases.

conjugation in the final cured thermoset. For all the reactions methanol was used as the reaction medium. Sometimes it was necessary to add co-solvent such as ethylacetate to increase the solubility of the reactants. All reactions were carried out at room temperature for 20-24 hours. In a few cases heat was necessary to induce the reaction.

The starting material, 3-ethynylbenzaldehyde, was prepared using a method already reported in the literature [20]. The steps are shown in Scheme II in Figure 16. This method is expensive due to the high cost of ethynyltrimethylsilane but is justifiable because of the

Scheme II

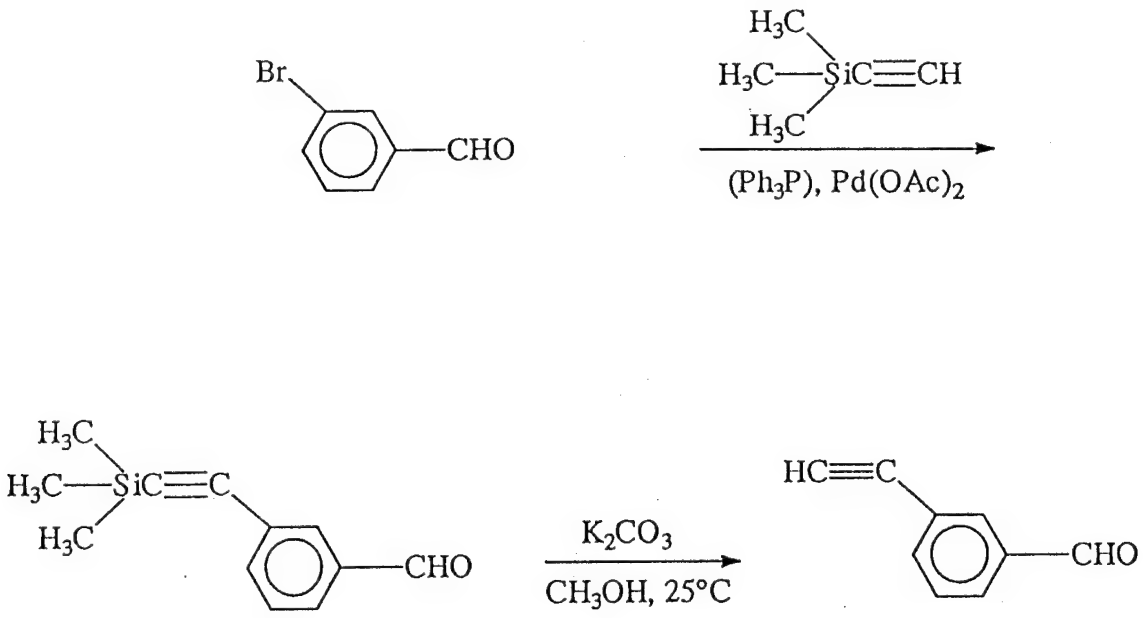

Figure 16. Scheme II which was used to synthesize the 3-ethynylbenzaldehyde used in Scheme I.

commercial availability of the materials, the high yields and the fact that the base sensitive aldehyde group is not affected by the reaction conditions. Ethynyltrimethylsilane was reacted with 3-bromobenzaldehyde in triethylamine solvent containing a small amount of palladium catalyst. In this procedure, triethylamine is used as the solvent and also as a scavenger for the hydrogen halide generated during the ethynylation reaction. The isolation of the insoluble amine salt provides a quantitative measure of the extent of the reaction.
3-(Trimethylsilyl)ethynylbenzaldehyde was purified by vacuum distillation and characterized by NMR, IR, and elemental analysis. The trimethylsilyl protecting group was removed under mild conditions by treatment with potassium carbonate. Extensive purification was needed at this stage. The final compound was purified by steam distillation, recrystallization, and column chromatography.

Vinyl-Terminated Schiff Base: The VT-Schiff base was prepared [21,22] by the reaction of two moles of p-aminostyrene with one mole of terephthalaldehyde in absolute ethanol under a nitrogen atmosphere at room temperature.

Epoxy-Terminated Schiff Base: The ET-Schiff base was synthesized [23] by first reacting terephthaldehyde with 4-aminophenol in a 1:2 mole ratio to obtain a dihydroxy Schiff base. A subsequent reaction with excess epichlorohydrin in the presence of a quaternary ammonium bromide as a catalyst yielded the ET-Schiff base. Epichlorohydrin was used as a reagent, the reaction medium and the recrystallization solvent.

Acetylene-Terminated Terthiophenes: The AT-Terthiophenes were synthesized using the procedures outlined in Schemes III, IV, and V, shown in Figures 17, 18, and 19 respectively. These were multistep preparations, and purification at each stage was necessary. All monomers

Scheme III

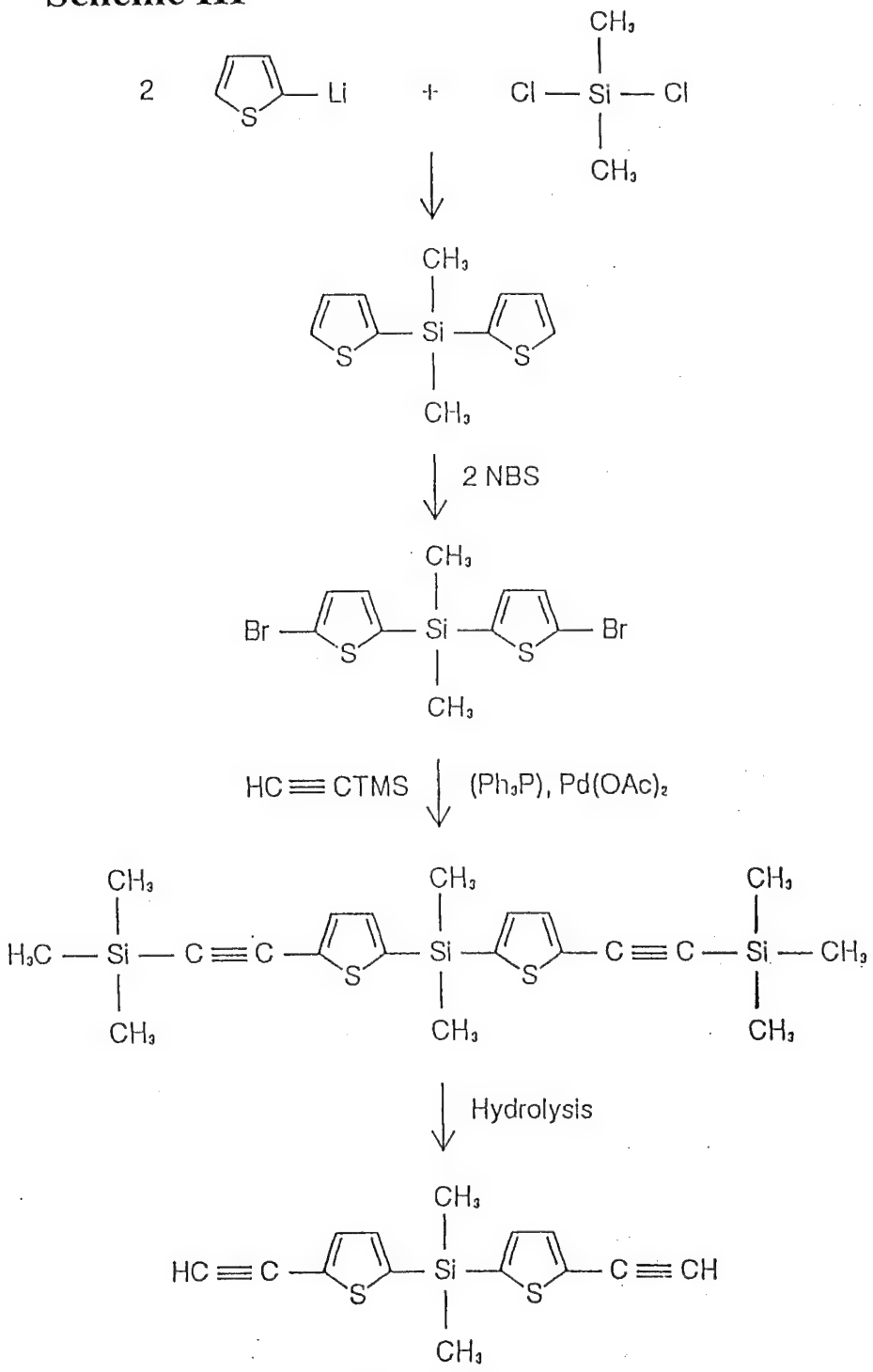

Figure 17. Scheme III which was used to synthesize the AT-polythiophene T-Si-T-2Ac.

Scheme IV

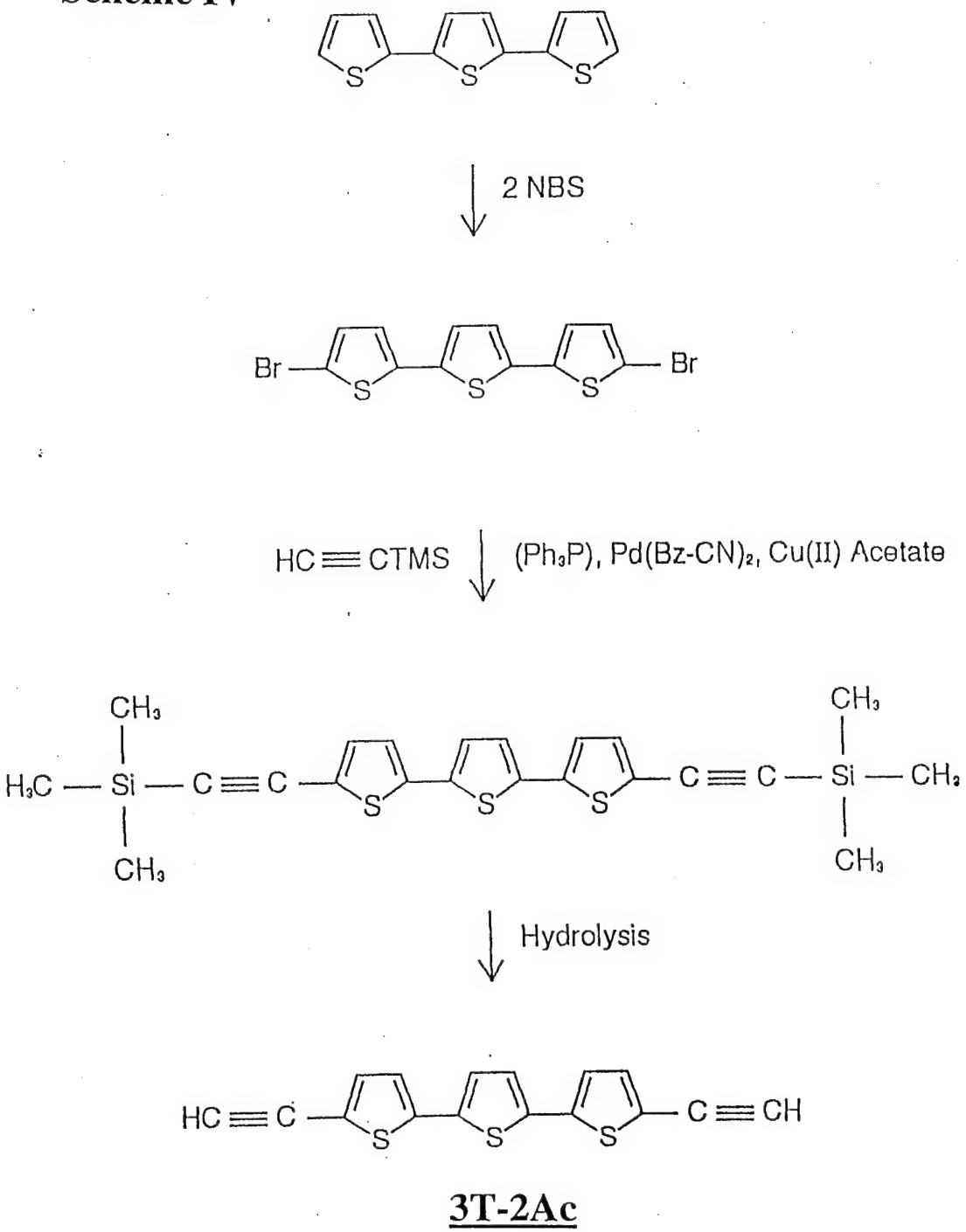

3T-2Ac

Figure 18. Scheme IV which was used to synthesize 3T-2Ac.

Scheme V

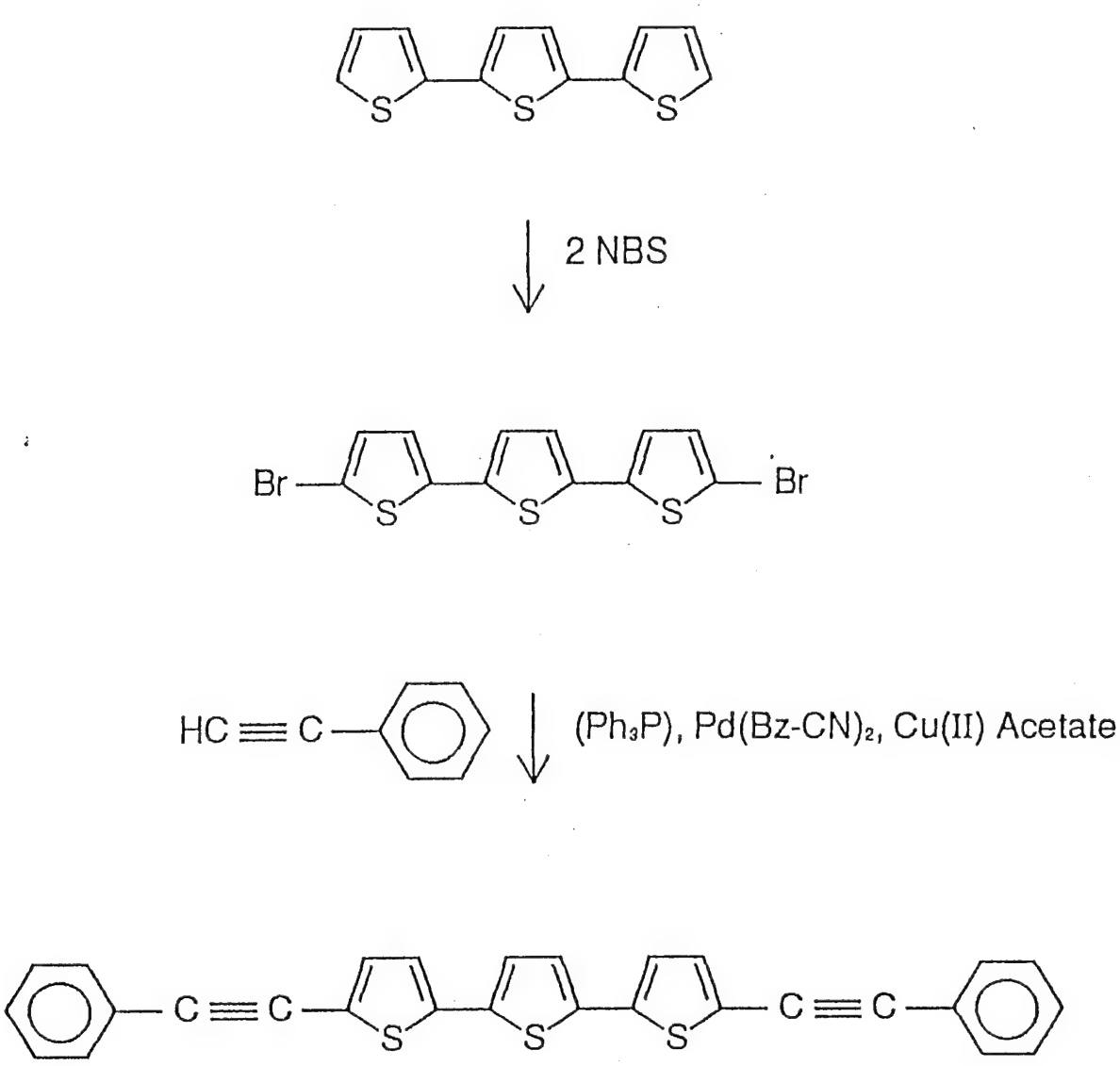

3T-2AcPh

Figure 19. Scheme V which was used to synthesize 3T-2AcPh.

were obtained in good yields from a sequence of lithiation, bromination, ethynylation and deprotection. The lithiation was achieved in hexane, and the condensation was carried out by slow addition of the required chlorosilane. A mild bromination agent such as N-bromosuccinimide was used for the bromination. Treatment of dibromo-compounds with trimethylsilyl (TMS) acetylene in the presence of palladium in amine solvents yielded TMS-ethynyl-substituted thiophenes. The TMS protecting groups were removed by hydrolysis with a mild base. All the compounds were characterized by IR and NMR spectroscopy as well as elemental analysis.

Phenylacetylene-Terminated Terthiophene: The terthiophene was brominated with N-bromosuccinimide in a chloroform/acetic (1:1 by volume) acid solution to yield the 5,5″-dibromo-2,2′:5′,2″-terthiophene. As is shown in Scheme V, treatment of this dibromo-compound with phenylacetylene in an diisopropylamine/pyridine (1:1 by volume) solvent containing a palladium catalysis yielded phenylacetylene-terminated terthiophene.

Phenylacetylene-Terminated Schiff Base: As shown in Scheme VI in Figure 20, the phenylacetylene-terminated Schiff base was synthesized by the reaction of two moles of 3-phenylethynylaniline with one mole of terphalaldehyde in an ethanol solution under an argon atmosphere[14]. The product, a yellow solid, was isolated by filtration washed with ethanol and methylene chloride and dried at 50°C under vacuum. Formation of the azomethine linkage was confirmed by IR (1624 cm^{-1}).

The 3-phenylethynylaniline was synthesized by way of the palladium-catalyzed coupling reaction of m-aminophenylacetylene with bromobenzene as shown in Scheme VII in Figure 21. In

Scheme VI

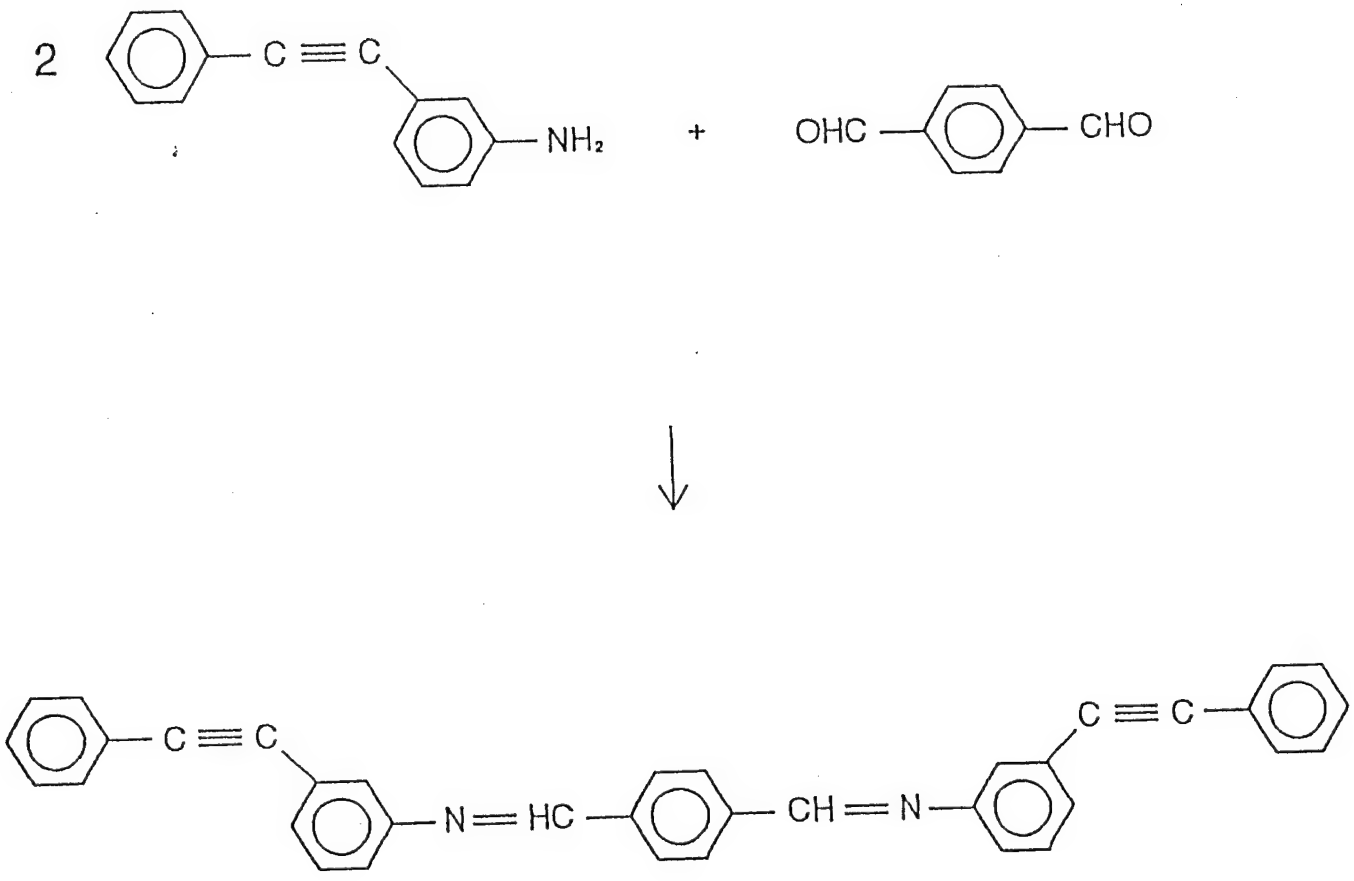

Figure 20. Scheme VI which was used to synthesize the phenylacetylene-terminated Schiff base.

Scheme VII

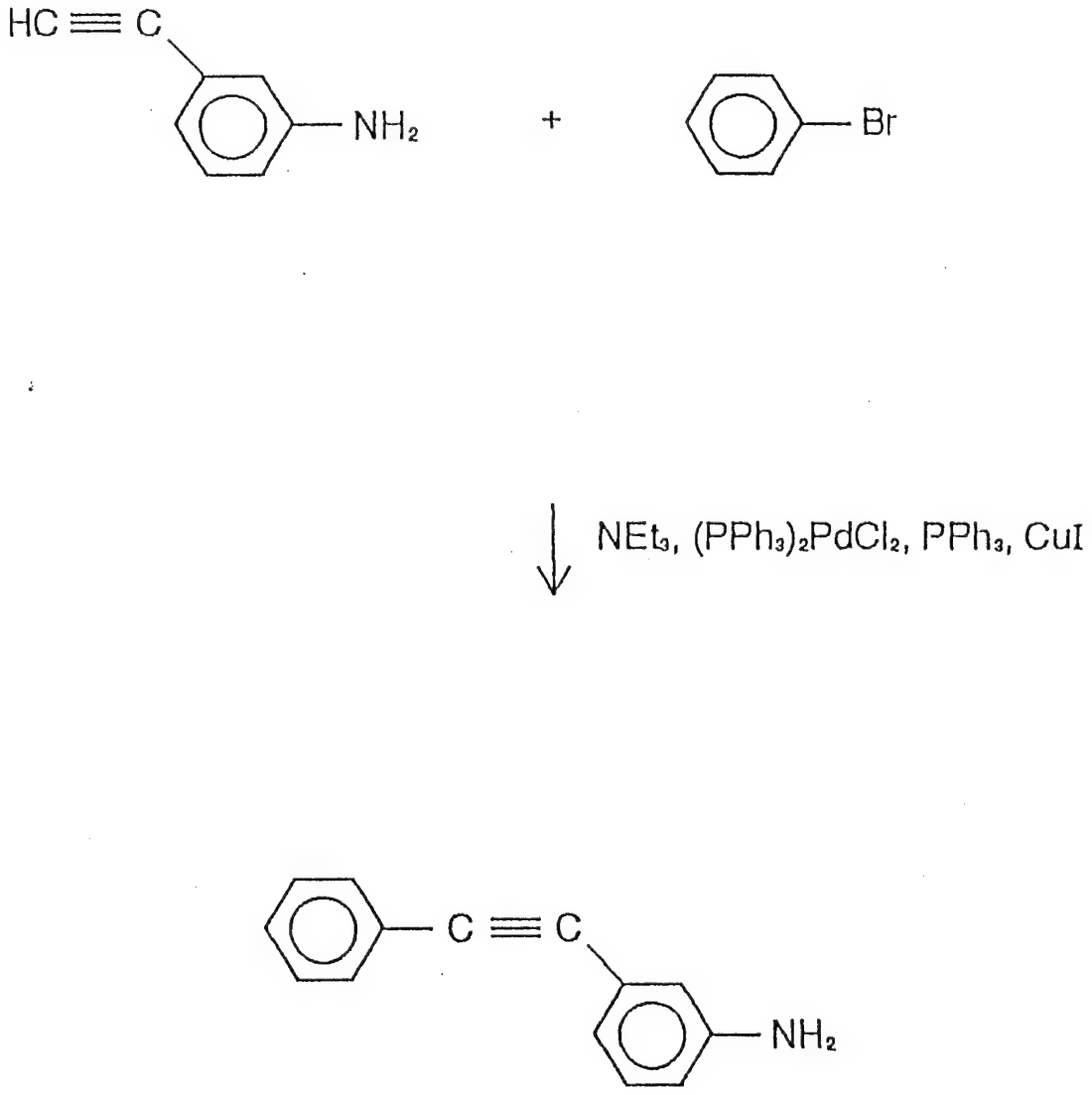

Figure 21. Scheme VII which was used to synthesize 3-phenylethynylaniline used in Scheme VI.

this procedure triethylamine was used as the solvent and also as the scavenger for the hydrogen halide generated during the reaction.

Preparation of Thermoset Samples: Hot-melt processing techniques of the corresponding monomers were used to form the thermosets. Initially, the two processing criteria used to select the monomers were: (1) an adequate processing window between the melting endotherm and the cure exotherm, and (2) the decomposition temperature of the thermosets (i.e., defined at a 10% weight loss and indicative of the thermal stability) had to be higher than the processing cure temperature. Differential Scanning Calorimetry (DSC) and Thermal Gravimetric Analysis (TGA) data were used to evaluate these criteria for each monomer. However, in some cases these criteria were not realizable. For example, in the case of the VT-Schiff base, the melting endotherm could not be distinguished from the cure exotherm, presumably because polymerization occurred instantly on melting. The cumyl-substituted AT-Schiff base monomer CD-EB, also showed no melting endotherm, but this was a consequence of the monomer being a glassy solid rather than a crystalline solid below 55°C. Thermo Mechanical Analysis (TMA) of this sample showed a softening temperature at 55°C. The instrumentation used for the DSC, TGA, and TMA measurements were TA Instruments Models TA 910, TA 951 and a TA 943, respectively.

The fabrication procedure used to obtain thermoset samples with the best mechanical properties was the following: The powdered monomer samples were mechanically squeezed into 16 mm diameter discs with a thickness of approximately 3 mm. These discs were then fitted into silicone molds which contained 16 mm diameter holes. All the AT-Schiff base monomers were cured at 160°C for times up to 24 hours; some were post-cured at 200°C for times up to 40

hours. The ET- and VT-Schiff bases were cured at 225°C for up to 24 hours, some samples were post-cured at 235°C for up to 12 hours.

Doping of AT-Schiff Base and AT-Polythiophene Thermoset Samples: The thermosets were made conducting by p-type doping with iodine. The iodine was introduced into the polymers in the vapor phase at a vapor pressure determined by the oven temperature. Most samples were doped at 90°C. The amount of iodine uptake by the polymer was measured from the increase in sample weight. The iodine was removed from the polymer using a vacuum oven.

3.1.3 ESR Measurements

The ESR spectra were obtained as first derivatives of the absorption by use of an X-band spectrometer (Bruker Model 380 and a Varian E-12) interfaced to a computer (Bruker 1600 and an IBM type 486). The software in both computer systems allowed signal averaging, spectral subtraction and spectral integration. The integrated ESR absorption intensities that were used as a measure of the spin susceptibilities were obtained from a double integration of the first-derivative spectra by use of the available software. The microwave frequency was measured with a microwave frequency counter (EIP Model 575) and the magnetic field values were determined either with an NMR gaussmeter (Bruker ER-035M) or a dual mode cavity along with a standard sample.

Detailed ESR studies were made on cured samples of Thermcon 1000 and phenylacetylene-terminated terthiophene (3T-2AcPh). Separate studies were made both as a function of cure and as a function of iodine content in both thermosets. Additional studies of 3T-2Ac and ETSB were made as a function of cure.

The spin susceptibility and the peak-to-peak linewidths measured in Thermcon 1000 as a function of cure time at 160°C, are shown in Figures 22 and 23. The behavior of the former is qualitatively similar to that reported in a previous cure study of non-conjugated AT resins [24]. In particular, the following three different regions can be distinguished in Figure 22: (1) at the early cure stages (< 90 min cure) an induction period where the spin concentration is low, (2) at intermediate cure times (90 to 900 min) where the spin concentration increases approximately linearly with log(cure time), and (3) at times longer than where the maximum occurs (900 min), the spin concentration decreases with increasing cure time. The linewidth data shown in Figure 23 indicate that there are motional narrowing processes present up till cure times of ~200 min. These motional effects, which are probably associated with the loose polymer network that exists up to the gel-point, account for the lack of radical stability and low radical concentrations at times less than 200 min. The increase in spin susceptibility up to 900 min is therefore a consequence of the increase in the polymer network rigidity. The decrease in spin susceptibility for cure times longer than 900 min is due to an unknown radical reaction. The presence of this reaction indicates that the cured polymer can still undergo slow reactions at times long after gel formation. It is not clear, however, why such slow reactions influence the linewidths and cause them to decrease with increasing cure time, as is depicted in Figure 23.

The spin susceptibility for 3T-2AcPh as a function of cure time at 220°C is shown in Figure 24. The behavior is qualitatively the same as that shown in Figure 22 for Thermcon 1000. The spin concentrations in both these cured resins are primarily due to radicals that are trapped in the rigid polymer network but would otherwise be involved in the free radical crosslinking processes. On the other hand, the behavior of the spin susceptibility versus cure time at 220°C for

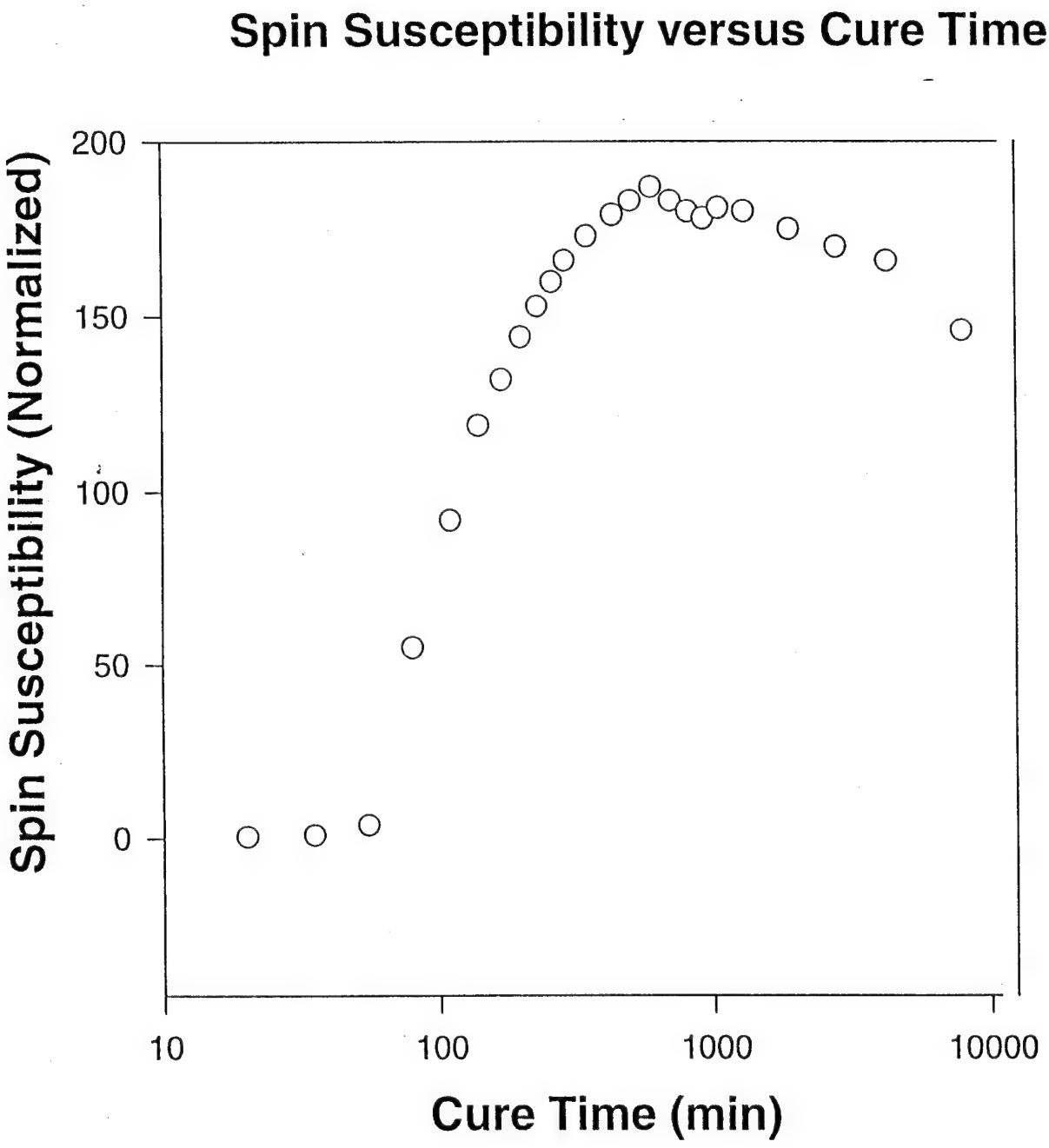

Figure 22. Normalized Spin Susceptibility versus cure time at 160°C for Thermcon 1000.

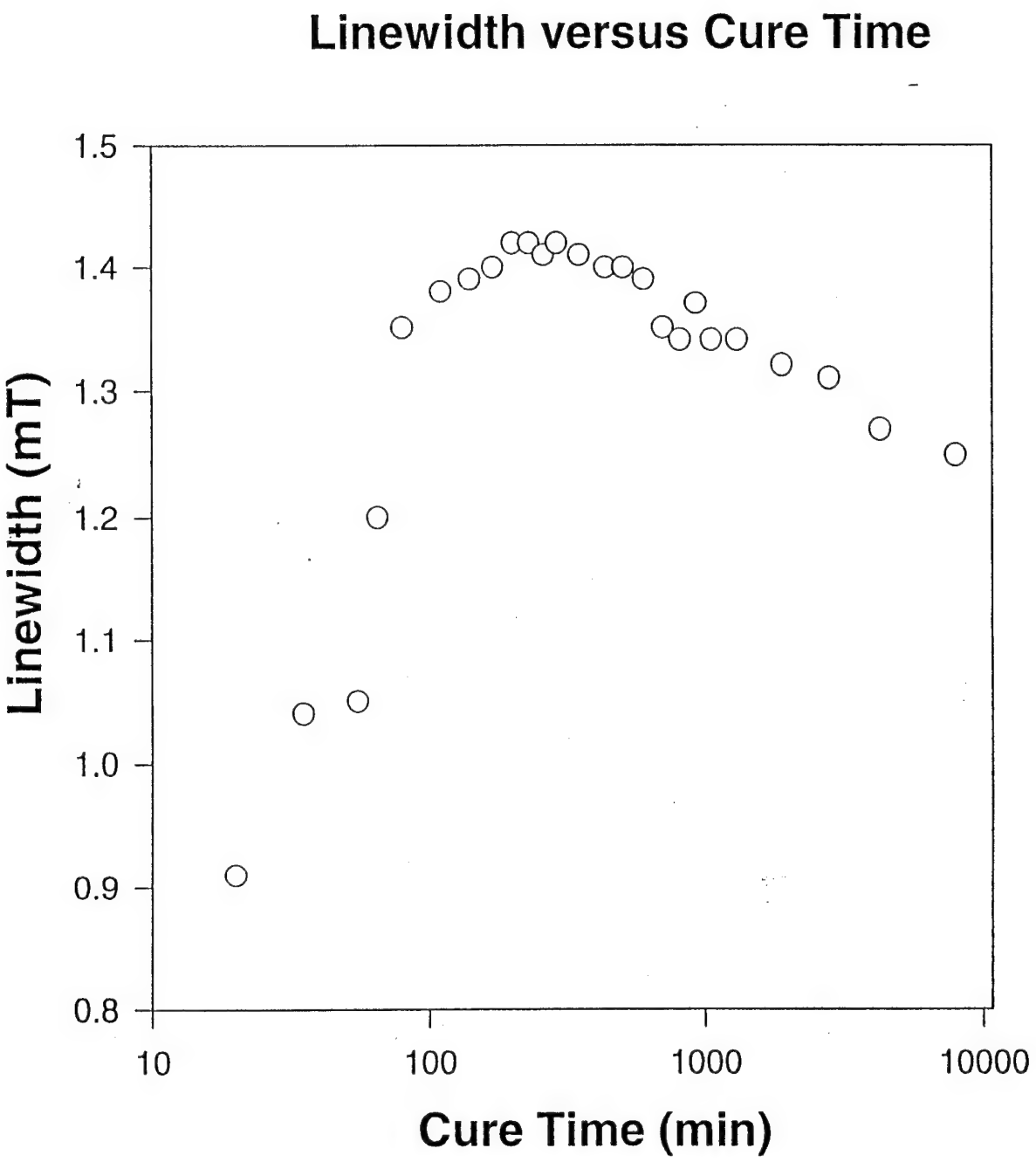

Figure 23. ESR Linewidth versus cure time at 160°C for Thermcon 1000.

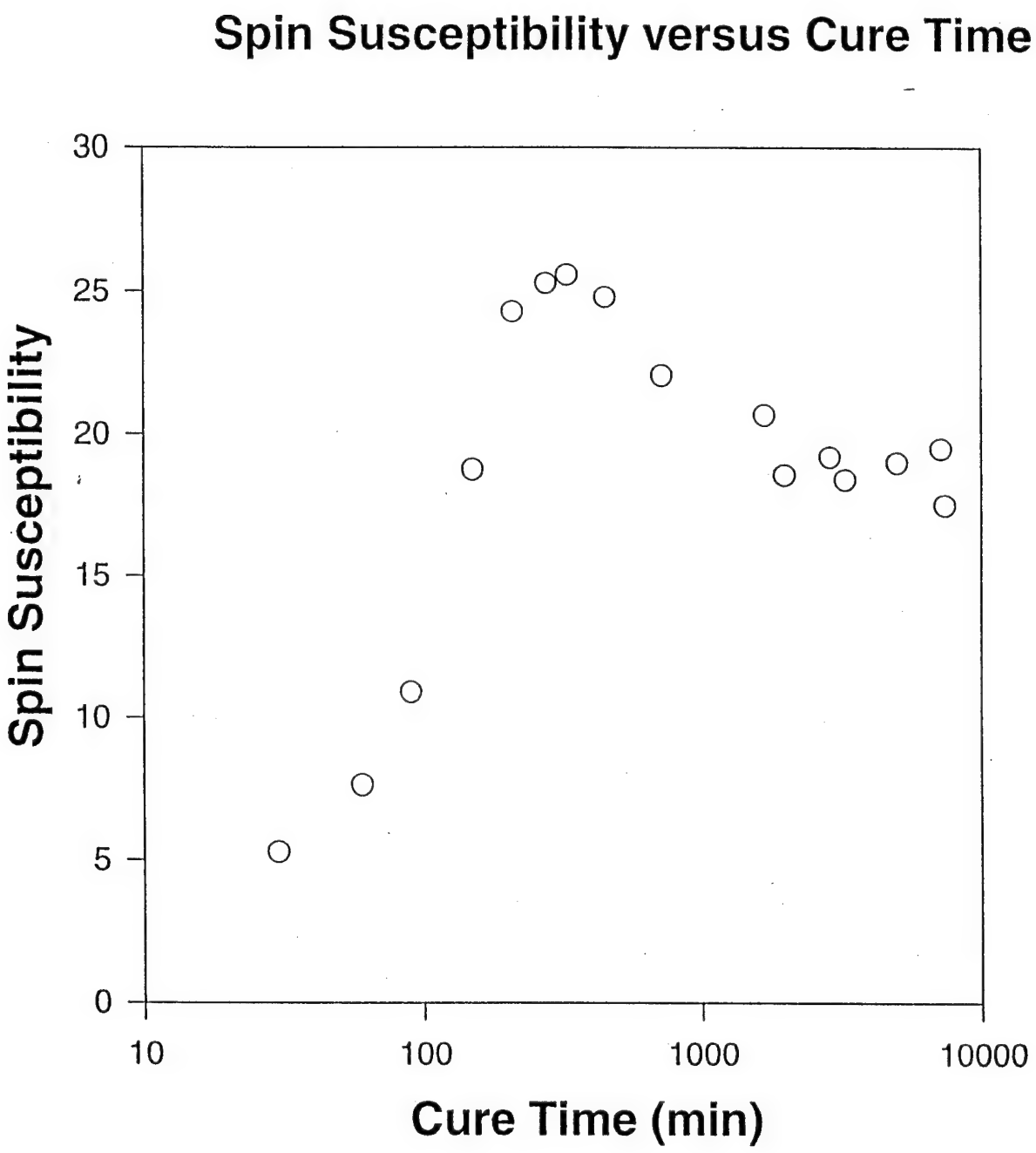

Figure 24. Normalized Spin Susceptibility versus cure time at 220°C for epoxy-terminated Schiff base.

ETSB shown in Figure 25 was similar in that it also showed the same three distinct regions. This result is surprising considering that crosslinking in epoxies is by an anionic ring-opening polymerization, a non-radical reaction [25]. As is shown in Table 1, the spin concentrations are significantly lower in the cured samples of ETSB (a factor of 5 lower than Thermcon 1000) and the maximum in Figure 25 occurs at a significantly later cure time. Both effects indicate that the radical-forming reactions are slower in ETSB and lead us to conclude that the radicals detected in this cured resin are probably formed as a result of thermo-oxidative degradation.

Table 1. The Maximum Spin Concentrations Measured in Thermosets With Different Doping Conditions.

Thermoset Monomer	Number of Repeat Units Containing One Electron Spin	Doping Conditions
Thermcon 1000[(a)]	400	Cure only
Thermcon 1000[(b)]	44	After iodine doping
3T-2AcPh[(c)]	105	Cure only
3T-2AcPh[(d)]	4	After iodine doping
ETSB[(e)]	1800	Cure only
3T-2Ac[(f)]	60	Cure only

(a) After 16 hour cure at 160°C; (b) cured 6 hours at 160°C, postcured 12 hours at 200°C; (c) after 6 hour cure at 220°C; (d) cured 6 hours at 220°C, postcured 12 hours at 245°C; (e) after 165 hour cure at 220°C; and (f) before cure, i.e., as-received monomer.

The spin susceptibility of the resin 3T-2Ac as a function of cure time at 90°C is shown in Figure 26. This behavior is anomolous in that it does not exhibit the three distinct regions described above. The highest spin concentrations were measured in the uncured material with values which were comparable with cured Thermcon 1000 (see Table 1). This result has led us to believe that the 3T-2AC "monomer" was partially polymerized, which could also account for the

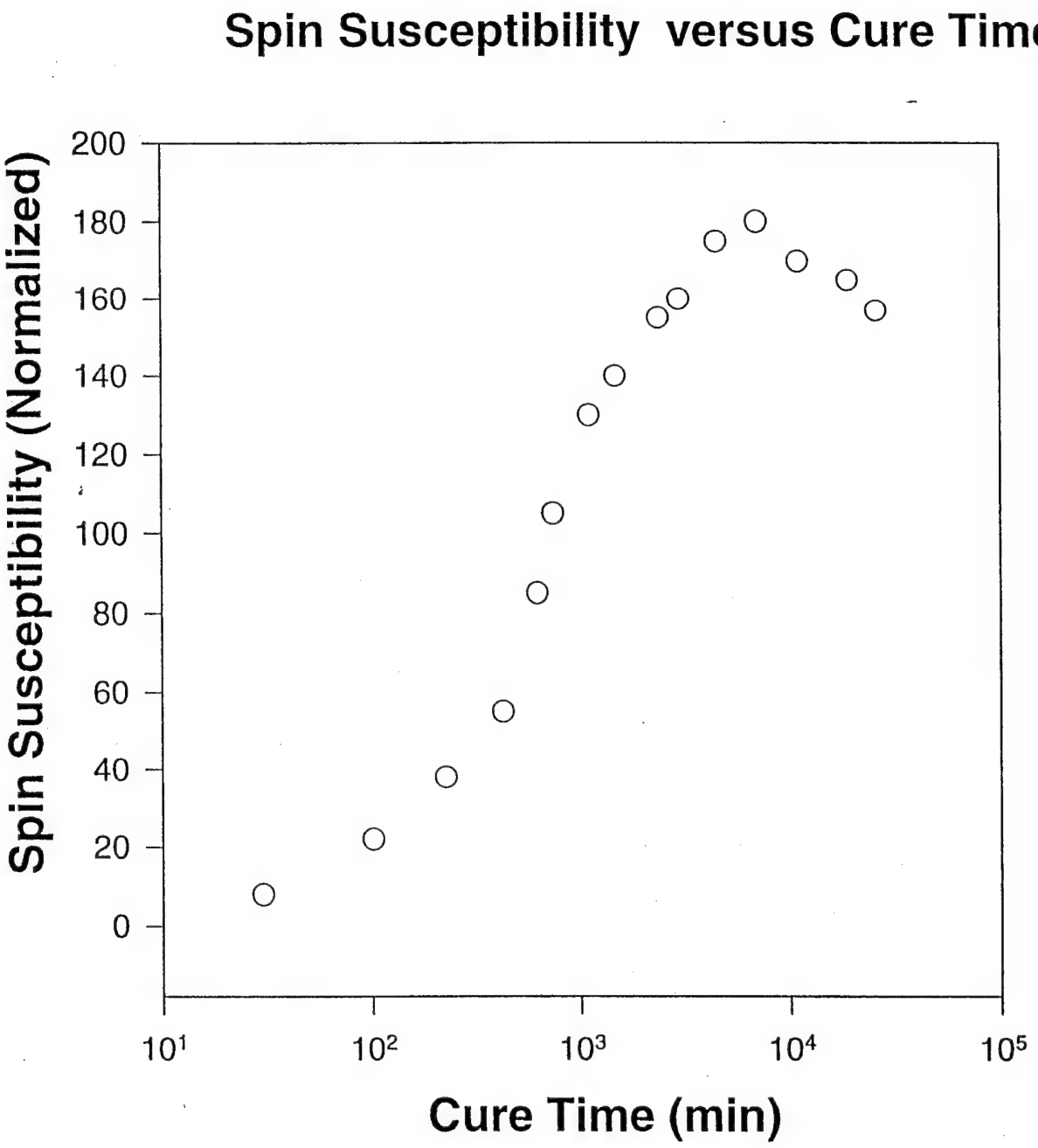

Figure 25. Normalized Spin Susceptibility versus cure time at 220°C for 3T-2AcPh.

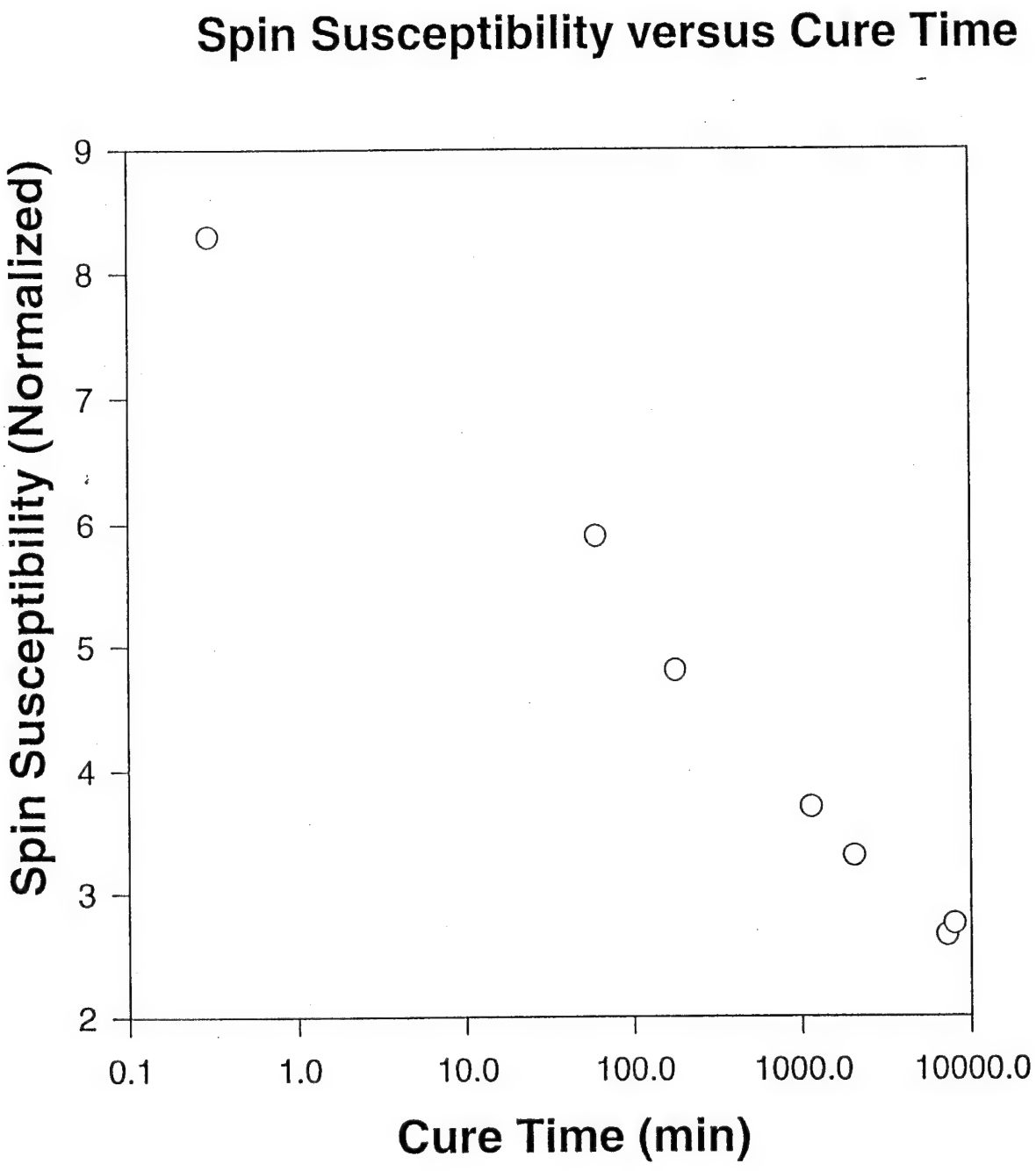

Figure 26. Normalized Spin Susceptibility versus cure time at 90°C for 3T-2Ac.

poor mechanical properties and the low conductivity in iodine-doped samples of this thermoset reported in Section 3.1.1.

In the iodine-doping ESR studies, the Thermcon 1000 monomer was cured at 160°C in air for 24 hours then post-cured at 200°C for 12 hours, whereas the 3T-2AcPh monomer was cured at 230 for 6 hours then post-cured at 245°C for 12 hours. The samples were ground into a fine powder prior to doping. The iodine was added to the powdered polymer in the following manner: the sample was placed in a 4-mm inside a capped vial along with a few crystals of iodine. The vial was then heated in a temperature-controlled oven for times as short as 30 min and as long as 72 h at temperatures varying from 80°C to 115°C. The iodine was removed from the sample by heating the sample in an empty uncapped vial in a vacuum oven at 45°C. The iodine content was determined from the weight increase of the sample.

In the iodine-doping ESR studies no hyperfine splittings were observed in any of the spectra. The spin susceptibility, the effective g-value and the lineshape parameters, (viz., the peak-to-peak linewidth and the asymmetry parameter, A/B), were measured as a function of iodine content in the samples. The definitions of the lineshape parameters and the effective g-value are illustrated in Figure 27(a). The latter is defined as $\langle g \rangle = h\nu/\beta H_o$ where ν is the microwave frequency, β is the Bohr magneton, h is Planck's constant, and H_o is the magnetic field value at which the first derivative crosses the base line. The spin susceptibility, the effective g-value and the lineshape parameters all show both reversible and irreversible changes as iodine is both added and removed from the sample. Since the spin susceptibility as determined from the integrated ESR intensity (i.e., the actual number is obtained from a double integration of the first derivative spectra), it can also be considered a measure of the radical concentrations present.

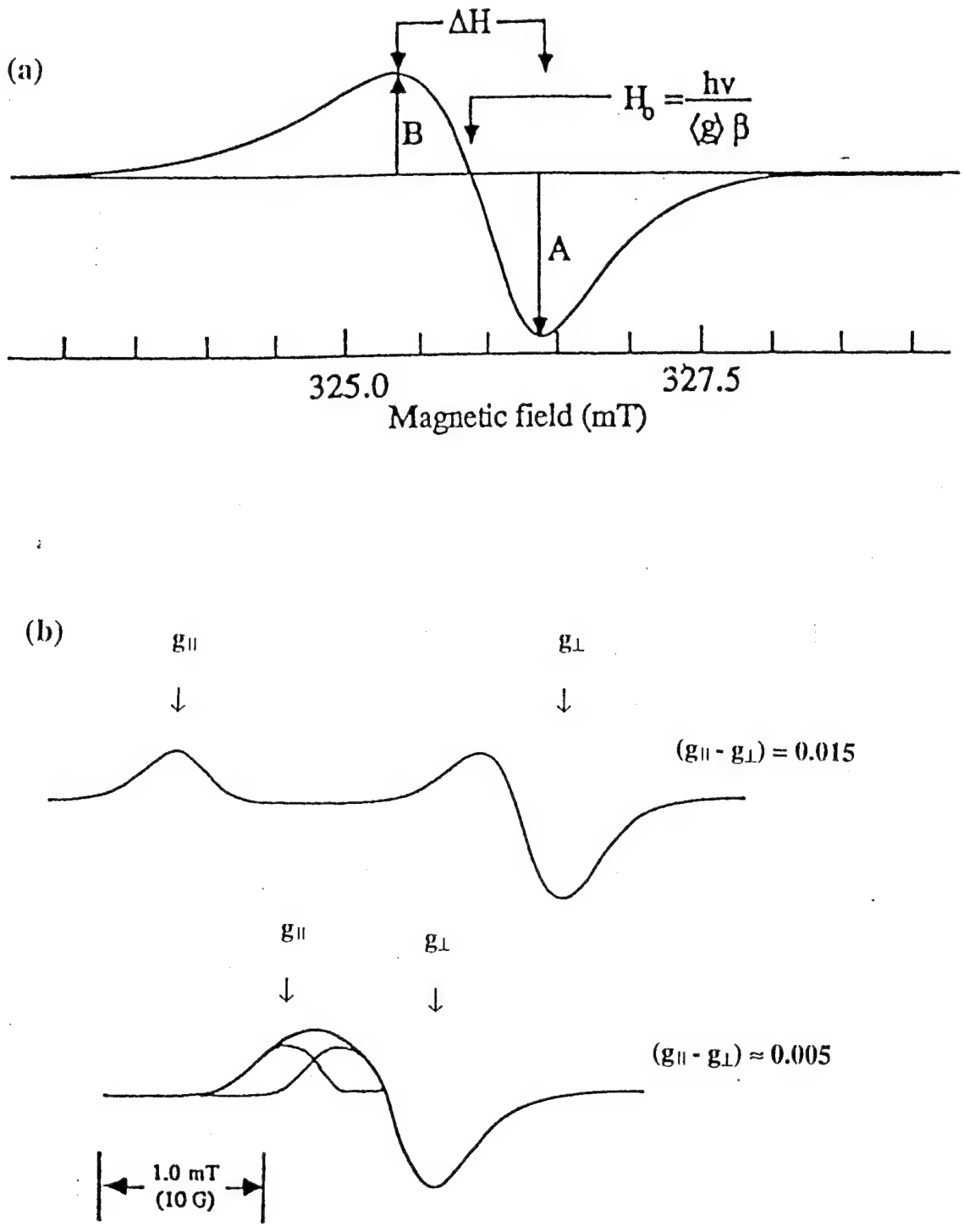

Figure 27. (a) Definitions for ESR lineshape parameters and effective g-value, (b) ESR lineshape expected from a value of $(g_{\parallel} - g_{\perp}) \approx 0.015$, and (c) lineshape expected from a value of $(g_{\parallel} - g_{\perp}) \approx 0.005$.

The results obtained from the Thermcon 1000 samples will be described first. As is shown in Figure 28, on the first addition of iodine the radical concentration increases with increasing

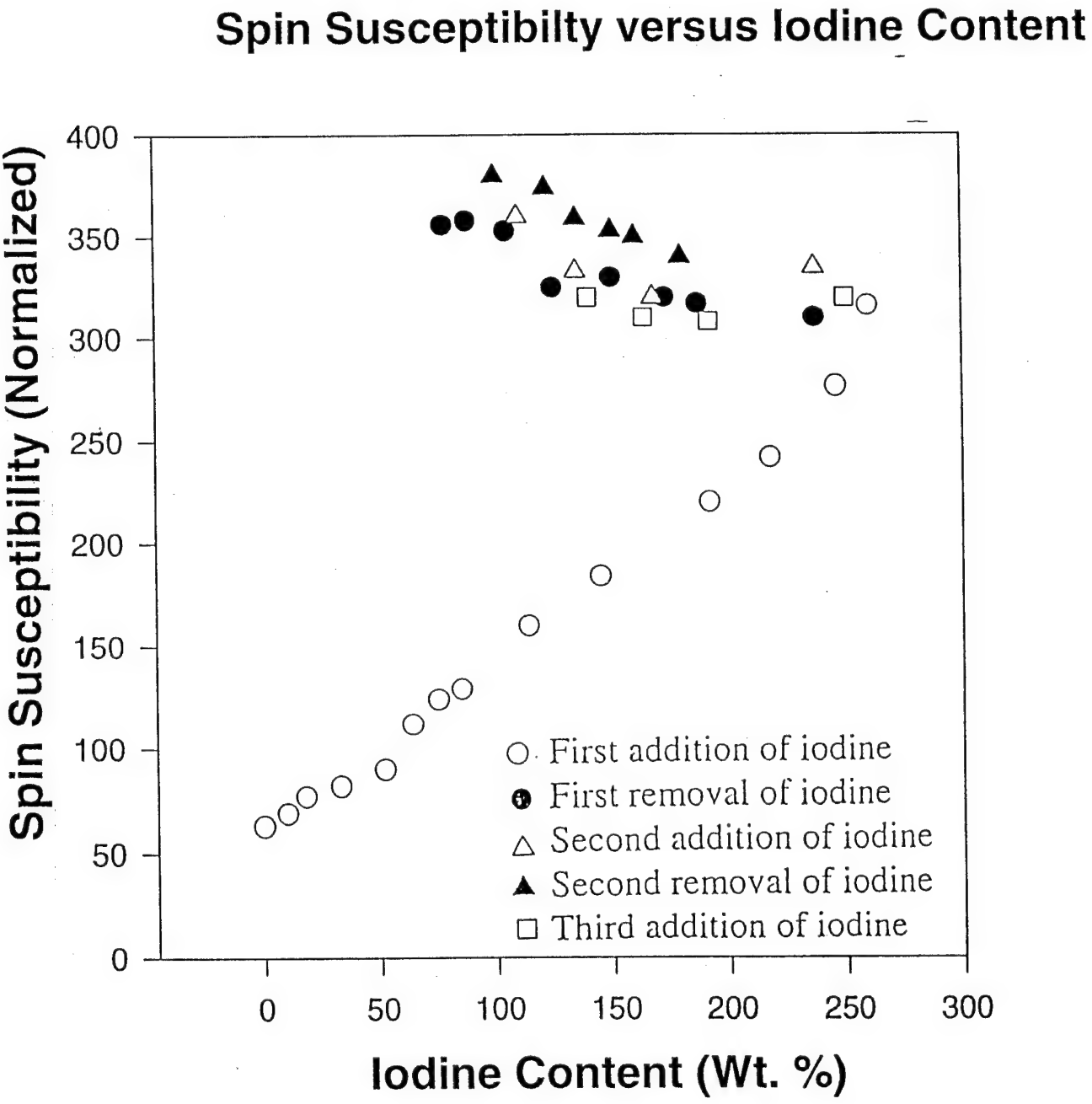

Figure 28. The normalized Spin Susceptibility versus iodine content for cured samples of Thermcon 1000.

iodine content up to at least 150 wt%. On the other hand, when the iodine is removed, the radical concentration remains high and increases slightly with decreasing iodine content. The data also show that after the initial doping, i.e., on the first removal, the second addition and second removal, the measured values of the spin susceptibility are reversible. We explain this behavior in terms of the equilibrium scheme shown in Figure 29, where we have assumed two types of radical

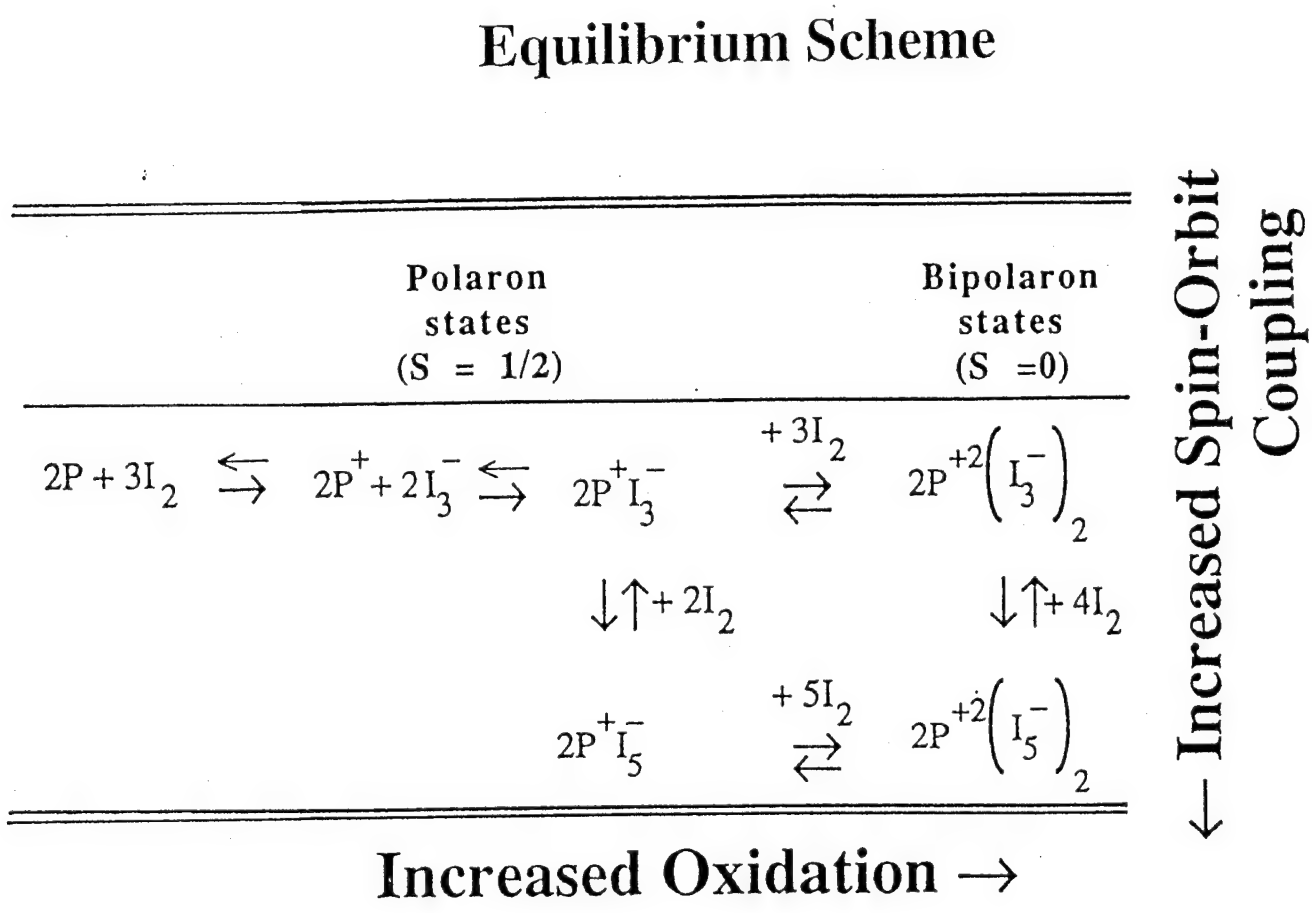

Figure 29. The equilibrium scheme used to explain the reversible changes in the ESR lineshape parameters measured on iodine-doping of the thermosets.

cations are formed in the polymer: the singly charged cation which is paramagnetic (S=1/2) and the doubly charged cation which is diamagnetic (S=0). In solid-state parlance these species correspond to a polaron and bipolaron [26] respectively. In the equilibrium scheme we have also included cationic species with different stoichiometric forms. The examples shown include the charge compensating anions I_3^- and I_5^-. These species were used here for illustrative purposes to account for the changes in <g> and the lineshape parameters. In an actual polymer sample there may be additional stoichiometric forms for the compensating species, e.g., $I_{(2n+1)}^-$ where $n \geq 1$.

According to the equilibrium scheme, at high iodine concentrations (> 150 wt%) both polarons and bipolarons are present in both stoichiometric forms. As the iodine concentration is reduced below 100 wt%, the equilibrium will move to the left, the bipolaron concentration will decrease, the polaron concentration will increase and the spin susceptibility will increase. Thus the equilibrium scheme can explain the observed behavior of the spin susceptibility shown in Figure 28, including its reversibility.

At all iodine concentrations only one ESR line was ever resolved. Therefore, to account for the observed changes in <g> shown in Figure 30 and the lineshape parameters shown in Figures 31 and 32, we consider the spectrum observed at any given iodine concentration to be a superposition of spectra from all stoichiometric forms of the polaron. This superposition may involve a dynamical averaging of some or all of the constituent spectra because of the limited lifetimes of the different stoichiometric species arising from iodine exchange.

Iodine is diamagnetic in the form I_3^- but paramagnetic in the form I_2^-. However, the large anisotropy to be expected will broaden the I_2^- ESR line beyond detection [27]. Hence, although

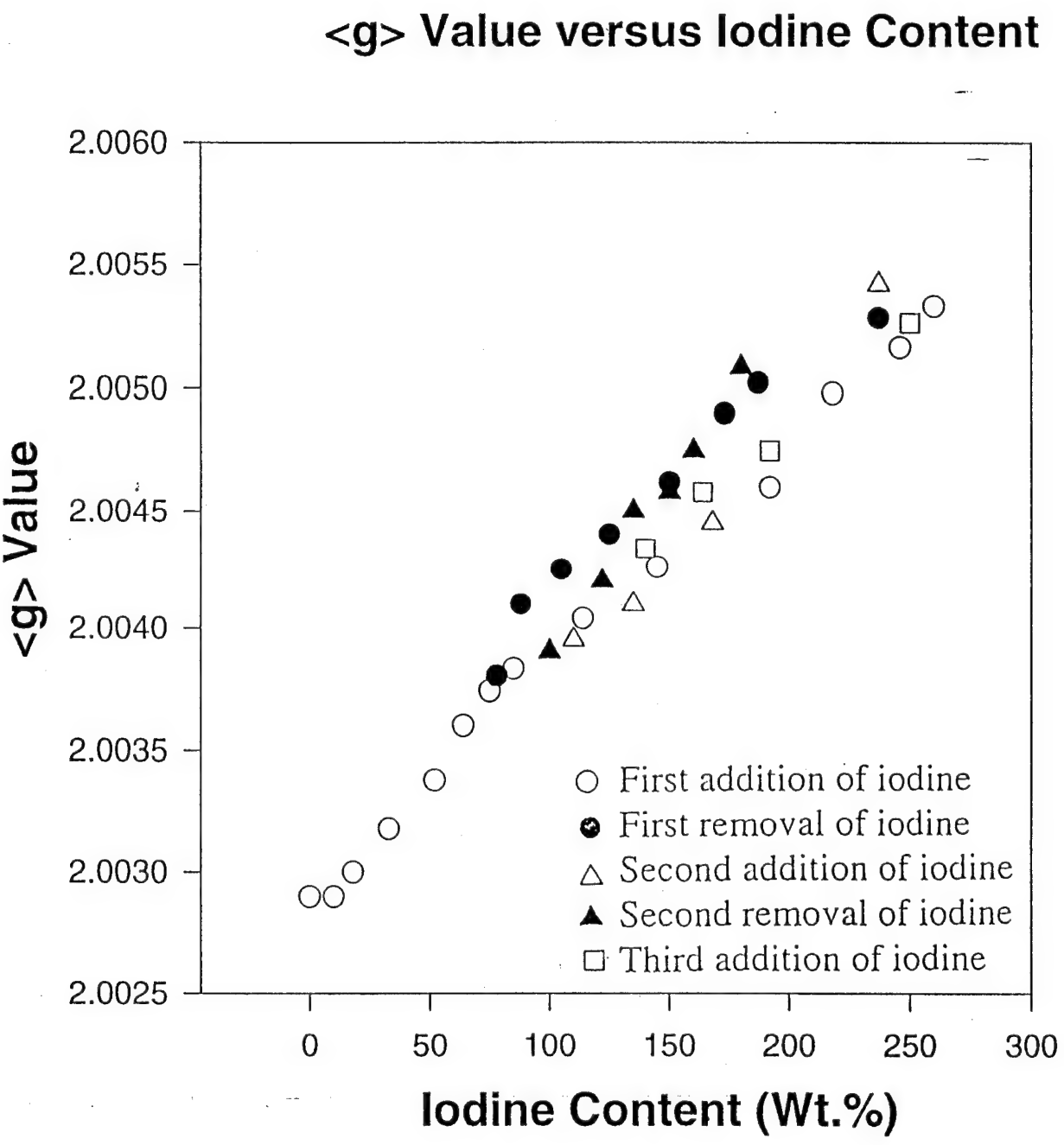

Figure 30. The <g> value versus iodine content for cured samples of Thermcon 1000.

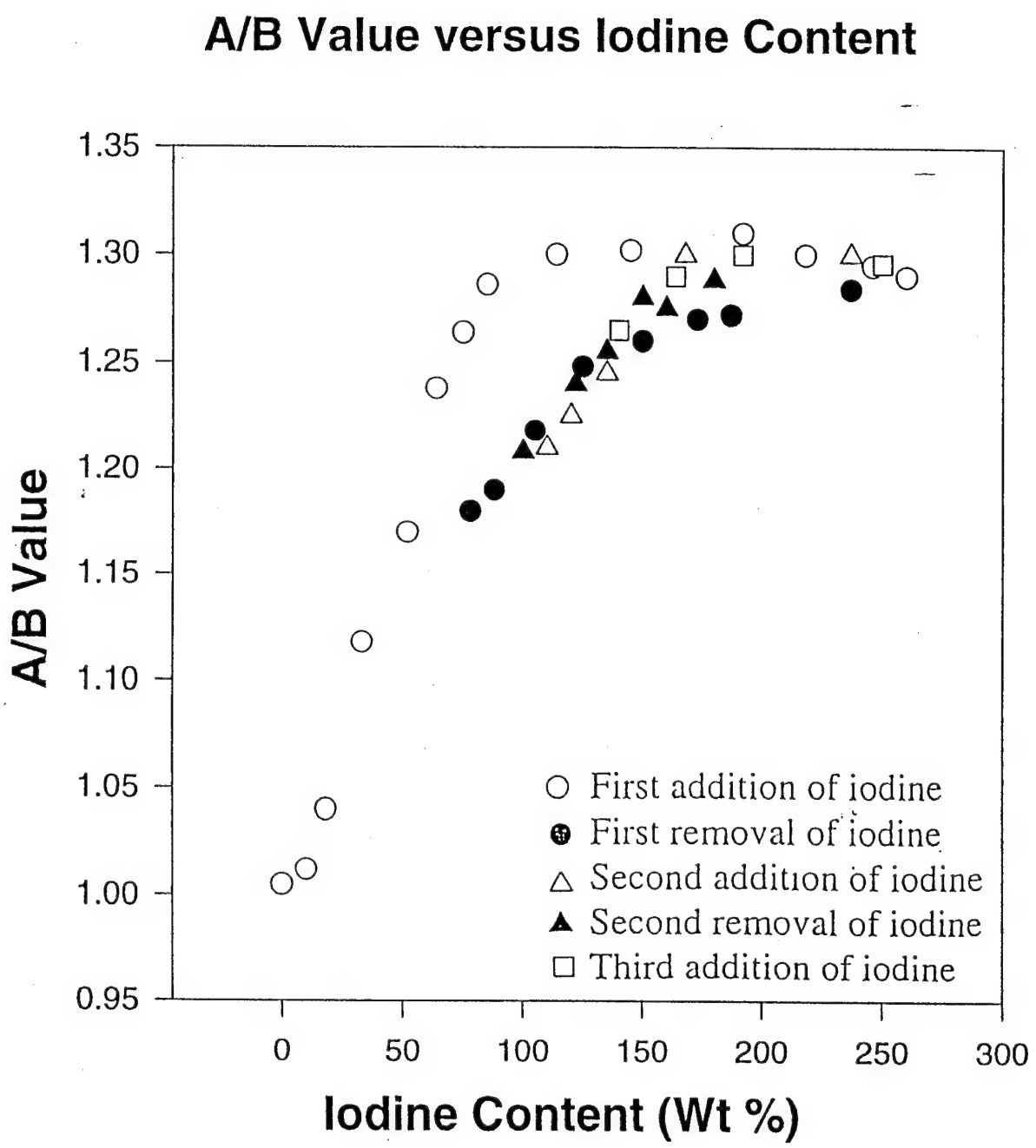

Figure 31. The A/B value versus iodine content for cured samples of Thermcon 1000.

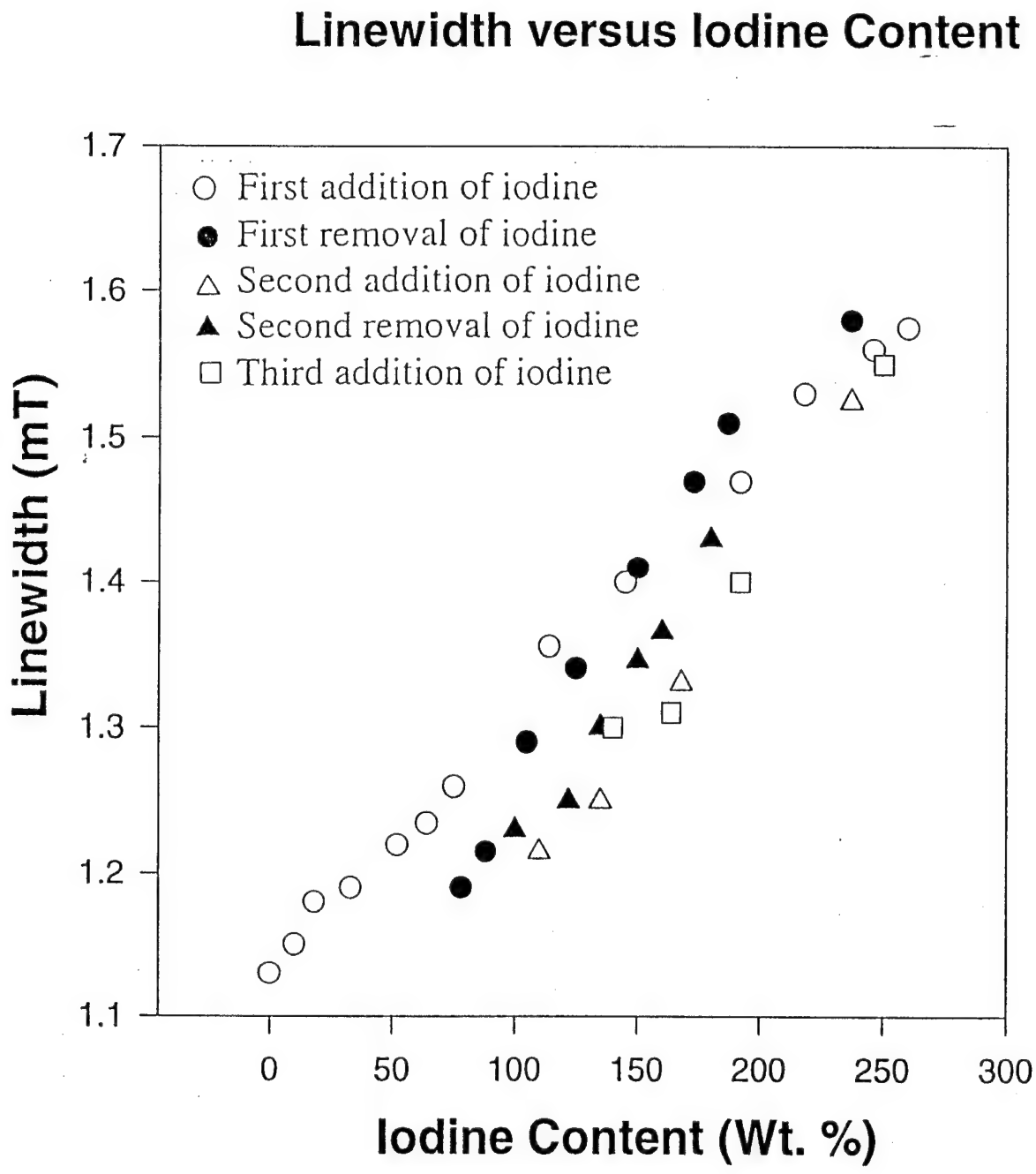

Figure 32. The Linewidth versus iodine content for cured samples of Thermcon 1000.

no ESR spectra other than the single line was observed, it is still possible that some I_2^- is present in the polymer.

The value of <g> depends on the principal values of the g-tensor, and also on the exact nature of the lineshape which, in the case of a rigid polymer host matrix is a superposition of lineshapes from the different types of polaron, each of which is an average over all orientations. The typical lineshapes that can be expected by assuming an axial g-tensor with the g-anisotropy $(g_{II}-g_{\perp}) = 0.015$ and $(g_{II}-g_{\perp}) = 0.005$ are shown in Figure 27(b). We therefore attribute the asymmetry in the lineshape (i.e., $A/B \neq 1$) to g-anisotropy with $(g_{II}-g_{\perp}) \approx 0.005$, where, to a good approximation $\langle g \rangle = (g_{II}+2g_{\perp})/3$.

As the iodine concentration is increased, the equilibrium shown in Figure 29 move vertically downward and the relative concentration of radical species with the higher iodine contents (e.g., $P^+ I_5^-$) increase. These radical species should show higher <g> values because of the increased spin-orbit interaction with a greater number of iodine atoms. The reversible monotonic changes in <g> with changing iodine content, shown in Figure 30, can therefore be explained in terms of the equilibrium scheme.

The actual values of both lineshape parameters, A/B and ΔH, are determined by the g anisotropy, $(g_{II}-g_{\perp})$, the homogeneous packet width and possibly also unresolved proton hyperfine interactions. If we assume that the g-anisotropy increases with increasing g-value, then the reversible monotonic increases (decreases) in A/B and ΔH with increasing (decreasing) iodine content, shown in Figures 31 and 32, respectively, can also be explained in terms of an increase in the relative number of radicals with the higher iodine stoichiometries and consequently higher

spin-orbit coupling values. Thus, the main features of the A/B and ΔH behavior can also be explained in terms of the equilibrium scheme shown in Figure 29.

In Figure 31 there is a broad maximum in the A/B values appearing at an iodine content of 100 wt%. This maximum, which is much more distinct in the 3T-2AcPh A/B data, since the spin concentrations in the latter samples are five times larger, will be described and explained below.

In the case of the data for the iodine-doped thermosets formed from 3T-2AcPh there are also reversible and irreversible changes observed in the ESR lines upon doping and undoping but they differ in some respects from the Thermcon 1000 data. For example, in the spin susceptibility data shown in Figure 33, all the data including that measured during the first doping are reversible. This is different from the Thermcon 1000 data shown in Figure 28. The implication of the differences in these behaviors is that the polaron in the Thermcon 1000 thermoset, i.e., the oxidized form, was more stable than the polaron in the 3T-2AcPh. Our optical studies reported in Section 3.1.4 of doped 3T-2AcPh and Thermcon 1000 also support this observed difference in polaron stability.

The values of <g>, ΔH and A/B for the 3T-2AcPh samples as a function of iodine content are shown in Figures 34, 35, and 36. The values of ΔH and <g> were reversible in that they always increased with increasing iodine content after several doping and undoping procedures. The irreversible effects are evident by a displacement of these ΔH and <g> values with each doping and undoping procedure. Comparing the ΔH and <g> data for 3T-2AcPh with the corresponding data for Thermcon 1000 it was concluded that the irreversible reaction(s) in the former was slower than that in the latter.

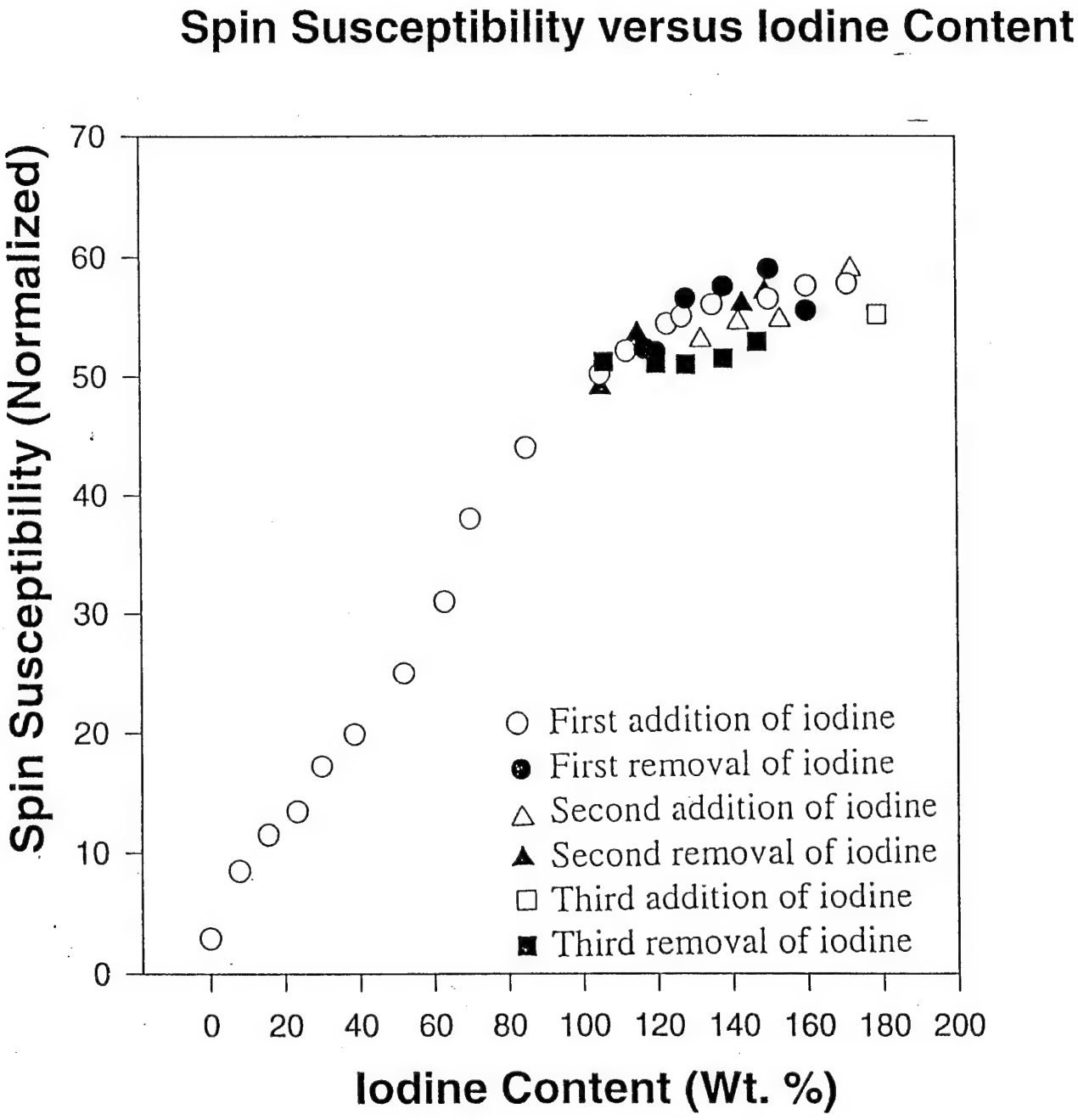

Figure 33. The normalized Spin Susceptibilty versus iodine content for cured samples of 3T-2AcPh.

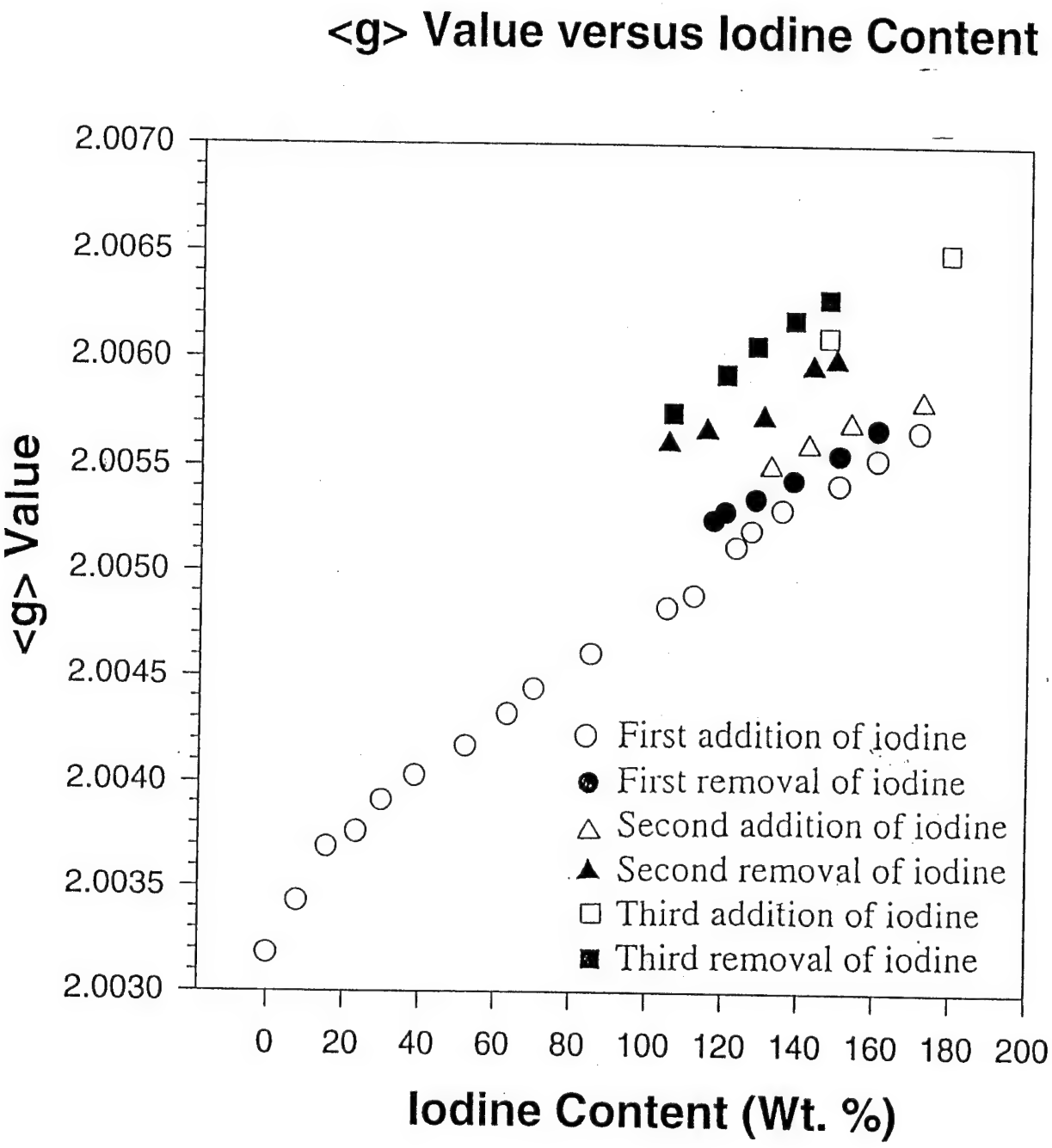

Figure 34. The <g> value versus iodine content for cured samples of 3T-2AcPh.

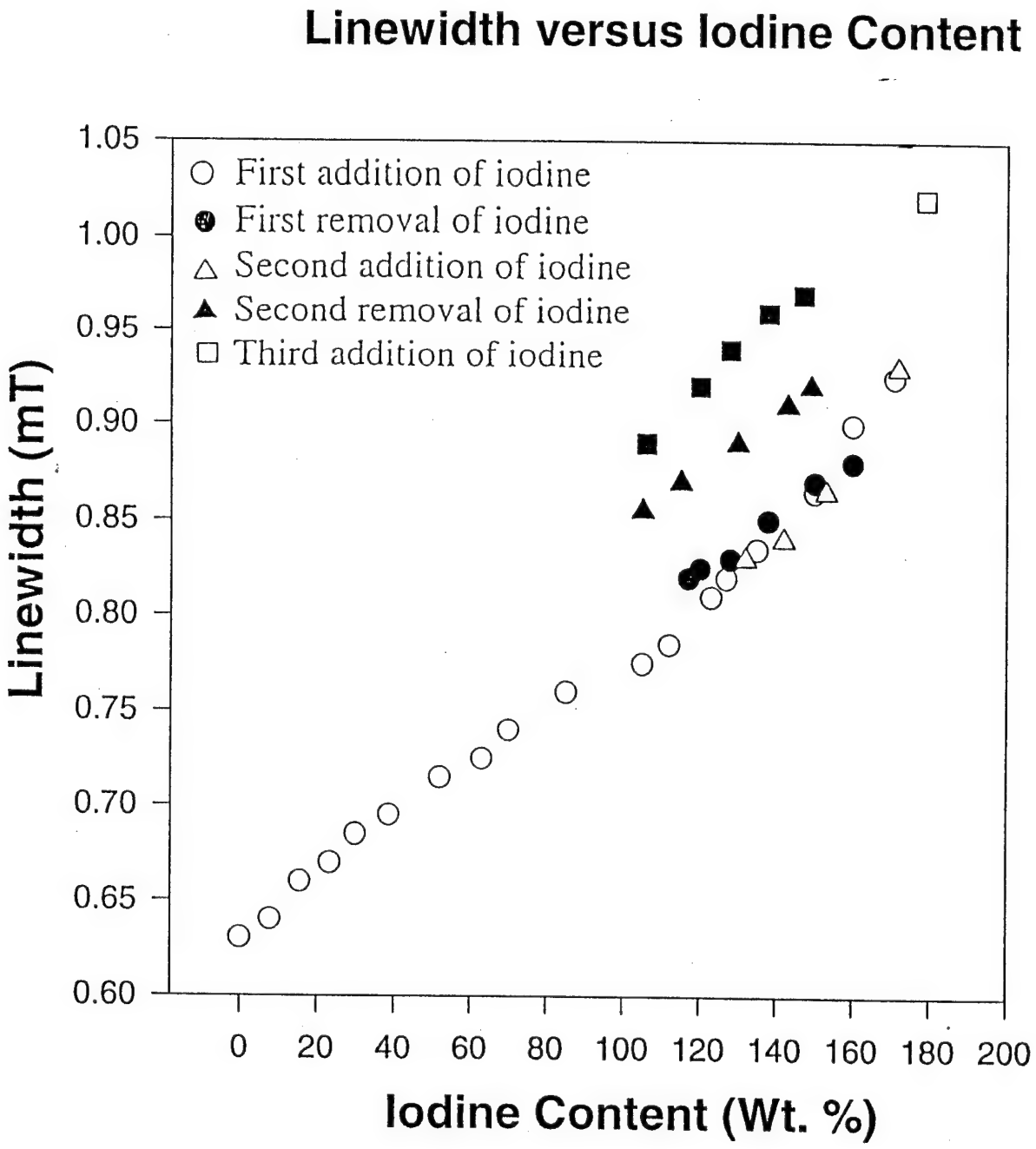

Figure 35. The Linewidth versus iodine content for cured samples of 3T-2AcPh.

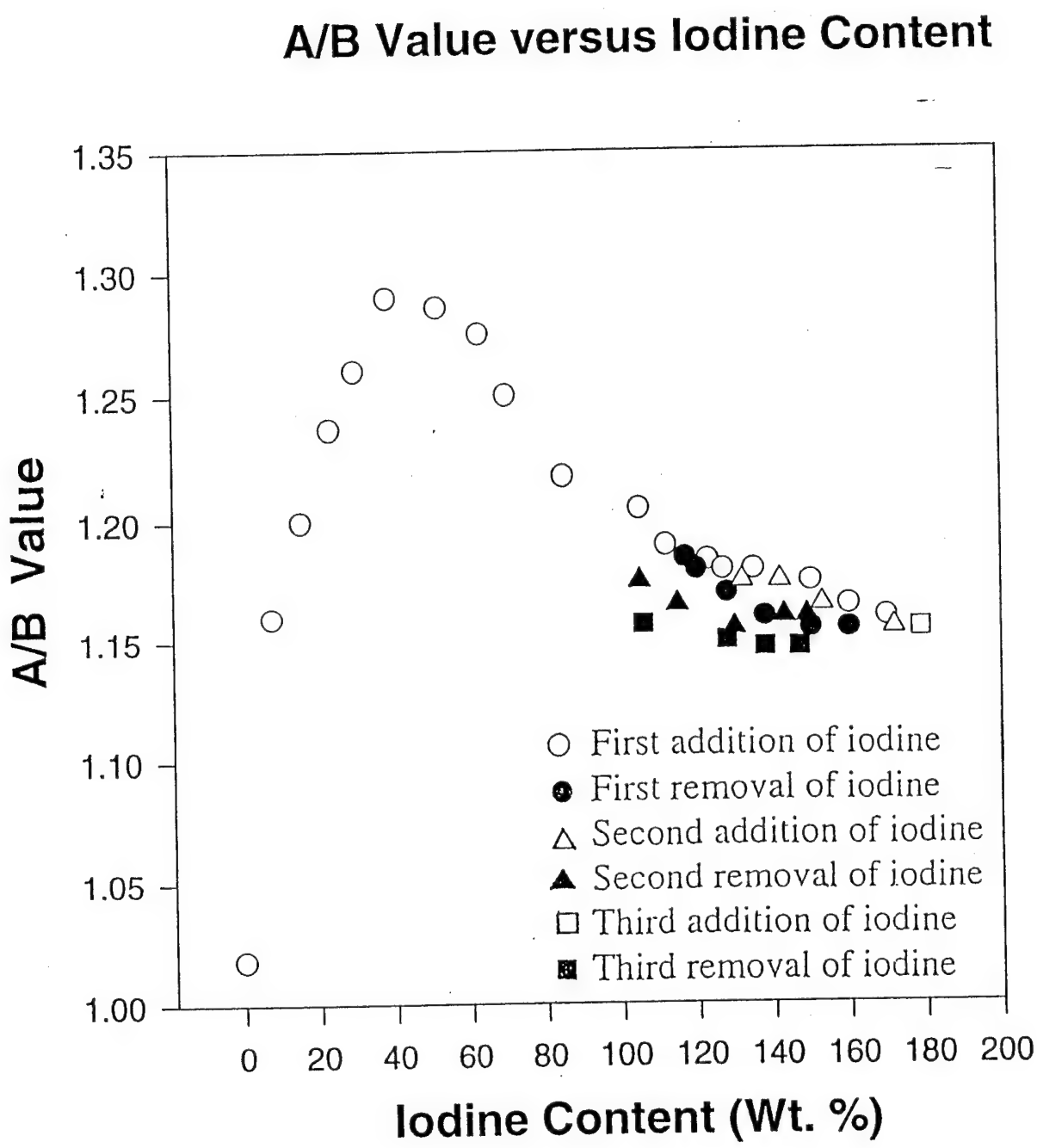

Figure 36. The A/B value versus iodine content for cured samples of 3T-2AcPh.

The distinct maximum in the A/B values that appears in Figure 36 at an iodine concentration of 40 wt% is the result of a dynamical averaging of the ($g_{\parallel}$-$g_{\perp}$) values by spin exchange interactions. It is interesting that A/B is the only lineshape parameter for iodine-doped samples of Thermcon 1000 or 3T-2AcPh that is sensitive to spin exchange brought about at high radical concentrations.

Spin exchange is of the form $H_{ex} = \mathbf{J}\ \mathbf{S}_i.\mathbf{S}_j$ where J is the intermolecular exchange integral that depends on the overlap between the spatial parts of the wavefunction for the ith and jth unpaired electron. These exchange interactions between adjacent spins first lead to a broadening and a shifting of the spin packets towards the isotropic values of the interactions in the spin Hamiltonian [28]. Although the broadening effects are more dramatic in the presence of hyperfine interactions, where they can lead to a removal of the observed hyperfine splittings, they can also affect splittings from other anisotropic interactions such as g-anisotropy. At even higher spin concentrations and consequently larger J values these exchange interactions can eventually lead to exchange narrowing, i.e., a reduction in the linewidths [28]. However, as can be seen from Figure 35, exchange narrowing was never observed, presumably because the spin concentrations were not high enough to narrow up the broadening caused by the spin-orbit effects associated with the iodine. Instead, the spin exchange arising from the intermediate spin concentrations is large enough to average out the unresolved splitting shown in Figure 27, due to the g-anisotropy, i.e., ($g_{\parallel}$-$g_{\perp}$). On increasing the radical concentration, the spin packets associated with this splitting will move together to some average intermediate value, then the A/B value will decrease, whereas the corresponding ΔH value will be little changed.

In summarizing our room temperature ESR results, we have attributed the increase in spin susceptibility observed in a conducting thermoset polymer following the addition of iodine to the formation of polarons. The reversible behavior of the spin susceptibility on addition and removal of the iodine also indicates the formation of a small concentration of bipolarons. We have interpreted the monotonic, reversible behavior of the effective g-value and the lineshape parameters, such as the line asymmetry and the linewidth, in terms of an equilibrium scheme involving different stoichiometric forms of the polaron, e.g., $P^+I_3^-$ and $P^+I_5^-$.

Temperature Dependence of the Lineshape Parameters: Measurements of the values of the lineshape parameters <g>, A/B and ΔH were also made at 77 K. The results summarized in Table 2 indicate a decrease in the <g> value ($\approx (g_\perp + 2g_\parallel)/3$) as well as an increase in the A/B and ΔH values with decreasing temperature for all samples. The latter implies that the g-anisotropy increases with decreasing temperature. As is shown in Table 2, samples with low iodine

Table 2. Temperature Dependence of ESR Lineshape Parameters.

Matrix	Temperature (K)	Linewidth (mT)	A/B	<g>	Iodine Content (Wt%)
Thermcon 1000	300	1.59	1.32	2.0052	235
	77	1.65	1.43	2.0045	235
	300	1.35	1.2	2.0044	141
	77	1.43	1.27	2.0043	141
DGEBA/DETA	300	1.20	1.45	2.0053	264
	77	1.30	1.58	2.0046	264
	300	0.83	1.28	2.0040	159
	77	0.83	1.29	2.0037	159
DGEBA/DDH	300	1.13	1.45	2.0051	395
	77	1.35	1.68	2.0046	395
3T-2AcPh	300	8.05	1.14	2.0053	147
	77	9.0	1.12	2.0048	147
Error		±0.05	±0.01	±0.00005	

contents exhibit smaller changes in the lineshape parameters on lowering the temperature than samples with high iodine content but both show the same temperature dependent trends.

The temperature dependence of <g> can also be explained qualitatively in terms of the equilibrium model depicted in Figure 29. The decrease in <g> with decreasing temperature implies that the complex with lowest spin-orbit interactions, and hence lowest iodine stoichiometry, viz., $P^+I_3^-$, lies lower in energy than the $P^+I_5^-$ complex.

The observed increase in the g-anisotropy with decreasing temperature is more difficult to explain. As was concluded from the room temperature data, the $P^+I_5^-$ has more g-anisotropy than the $P^+I_3^-$ complex. Moreover, since the temperature dependence of <g> suggests an increase of the $P^+I_3^-$ concentration with decreasing temperature, one would expect to observe a decrease of the g-anisotropy with decreasing temperature. One possible explanation involves a motional averaging of the g-anisotropy (but not the <g> value) at room temperature. If this motion is "frozen out" at 77 K , it would account for the increase in g-anisotropy with decreasing temperature. Two types of motion are possible: fast translational motion of the spins down polymer chains in the network or localized motions close to the spins. This fast translational motion down polymer chains seems unlikely in the amine-cured epoxy polymers, DGEBA/DETA and DGEBA/DDH, because of the lack of extended conjugation.

3.1.4 Optical and Infrared Measurements

Optical and infrared techniques were employed to study changes in the properties of the AT-Schiff base and AT-polythiophene monomers during curing and in the thermosets after iodine-doping.

Cure Studies: Some of the acetylene-terminated monomers selected for our electrical studies were monitored during the cure process by infrared absorption spectroscopy. The disappearance of the acetylenic carbon infrared absorption peaks resulting from crosslinking reactions allowed us to determine the degree of cure in the thermoset polymers. Some common absorption peak assignments associated with acetylene groups are the C-H stretching mode at 3295 cm^{-1}, a triple bonded carbon stretch mode at 2108 cm^{-1}, a weak C-H bending mode at 622 cm^{-1}, and a 941 cm^{-1} bending mode of the entire acetylene group [29-32]. All acetylene-terminated monomers examined by infrared spectroscopy measurements exhibited changes in these absorption peaks during the cure. A survey of the results for a number of monomers is presented below.

The samples used for infrared measurements were either fabricated into thin films on transparent substrates using a melt process or were pressed as powders into KBr pellets. For Thermcon 1000 the sample temperature was raised five degrees above the melting point (155°C) for a few minutes and the resulting film was cooled to room temperature. As seen in Figure 37 the observed infrared peaks at 2108 cm^{-1} and 3295 cm^{-1} associated with the acetylene end-groups exhibit strong absorption even after a two hour cure at 160°C, indicating that very little crosslinking has occurred. However, the spectra in Figures 38 and 39 show that as the material cures further at 160°C, for periods of 5.5 and 22.5 hours respectively, these infrared absorption peaks become much weaker, verifying that the acetylene end-groups did undergo crosslinking reactions. Figures 40 and 41 contain more detailed infrared spectra that have been expanded over two regions of interest for a thin film sample of the AT-polythiophene monomer, 3T-2Ac. The absorbance peaks at 3295 cm^{-1} shown in Figure 40 and those at 2108 cm^{-1} shown in Figure 41

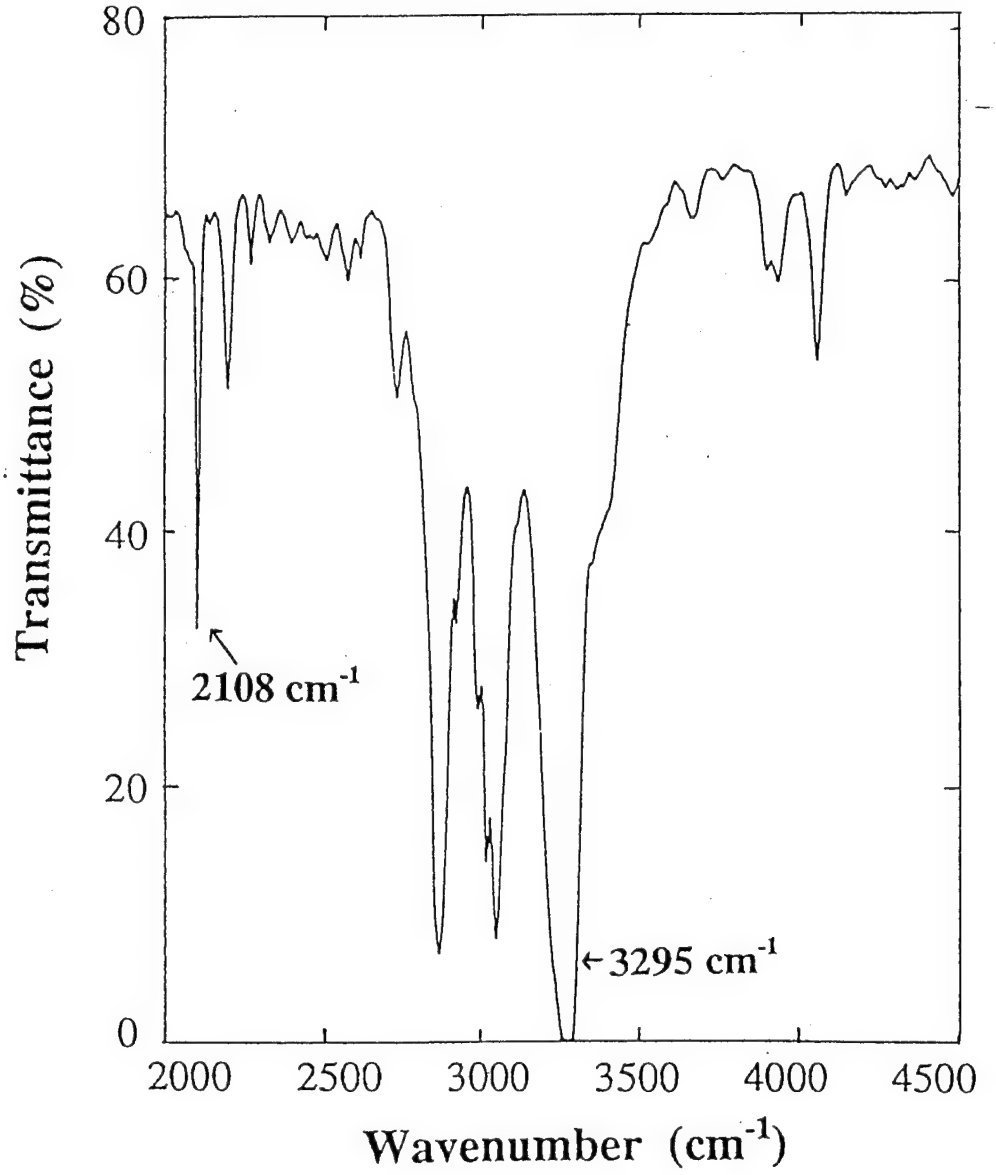

Figure 37. Infrared transmittance spectrum measured in a Thermcon 1000 film after curing at 160°C for 2 hours.

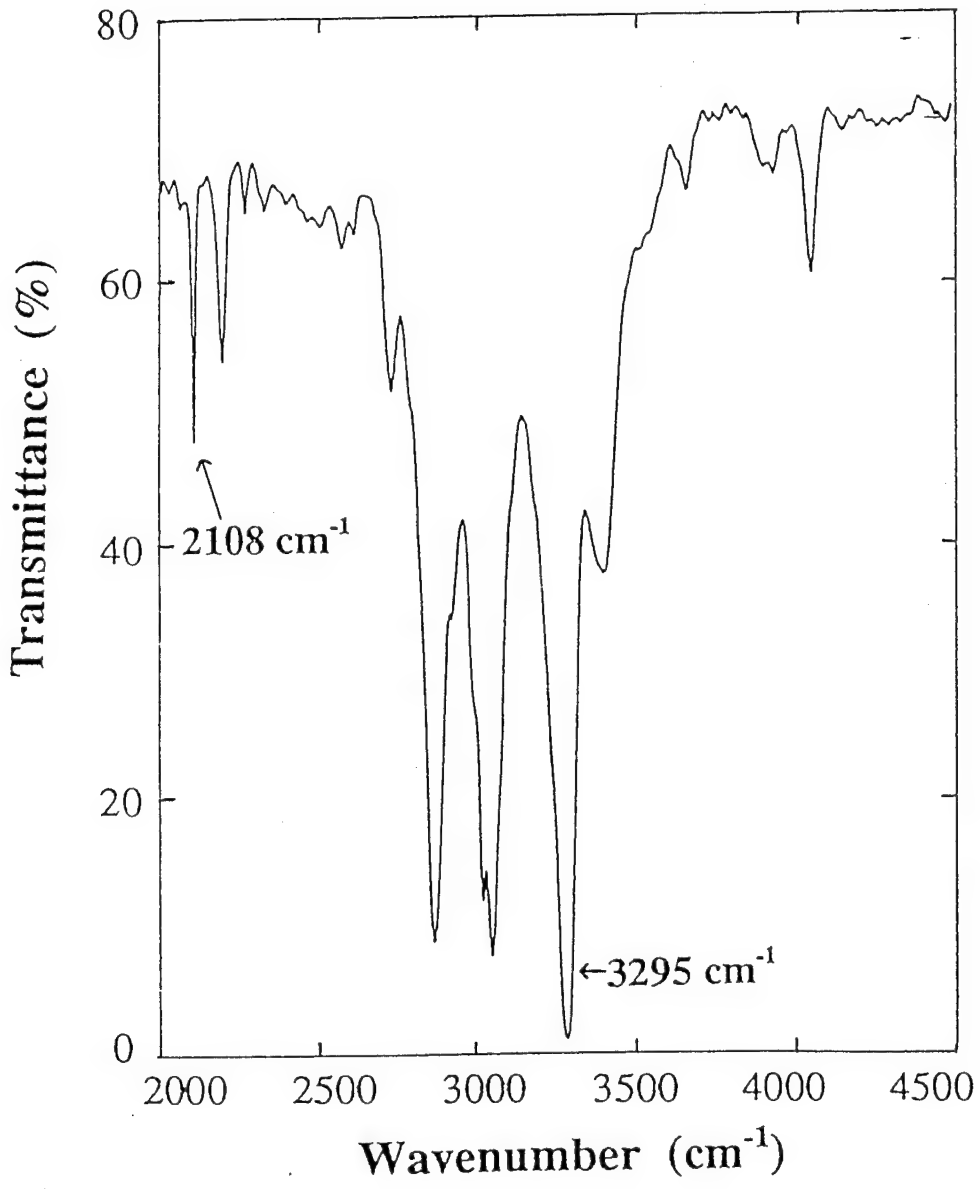

Figure 38. Infrared transmittance spectrum measured in a Thermcon 1000 film after curing at 160°C for 5.5 hours.

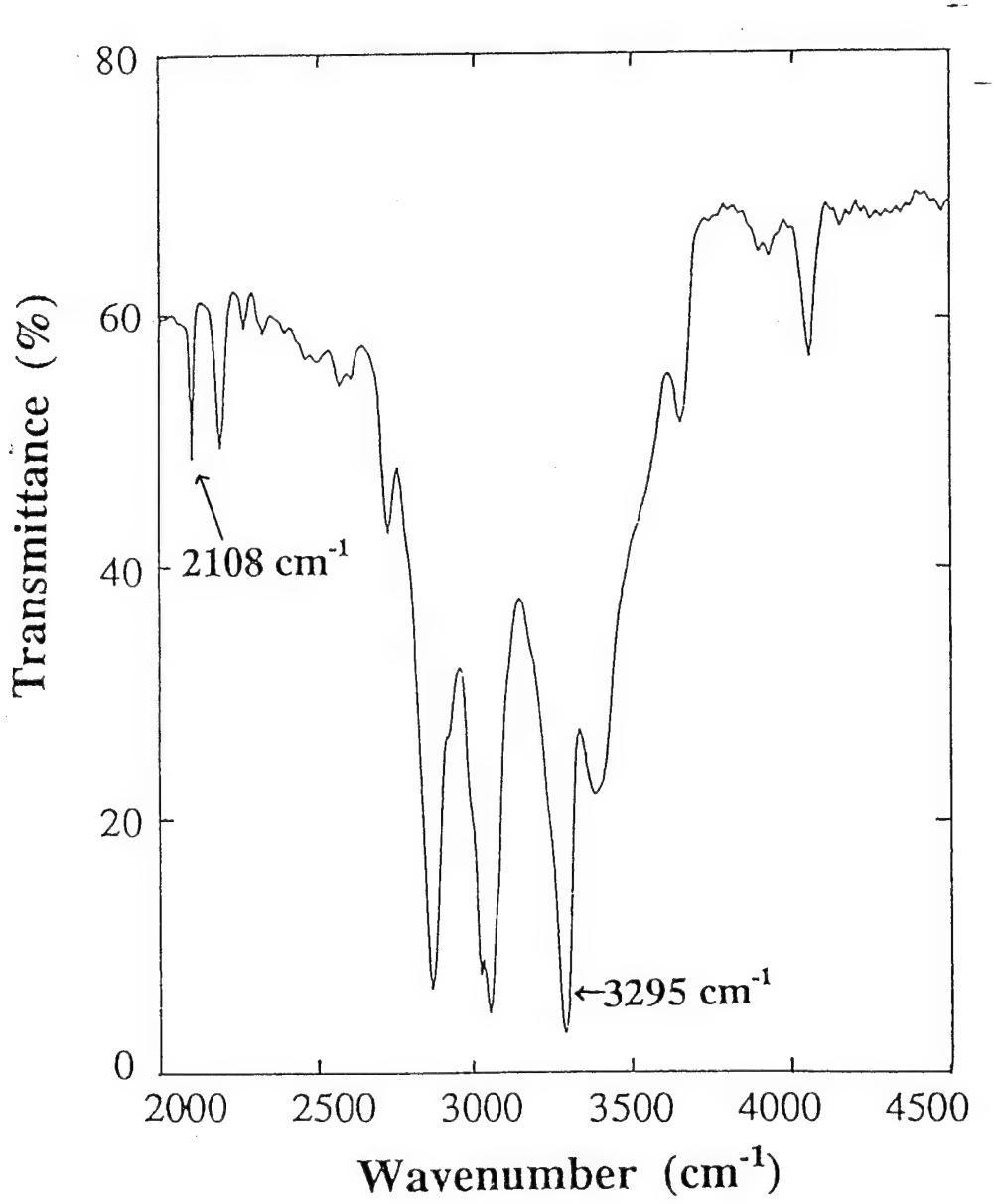

Figure 39. Infrared transmittance spectrum measured in a Thermcon 1000 after curing at 160°C for 22.5 hours.

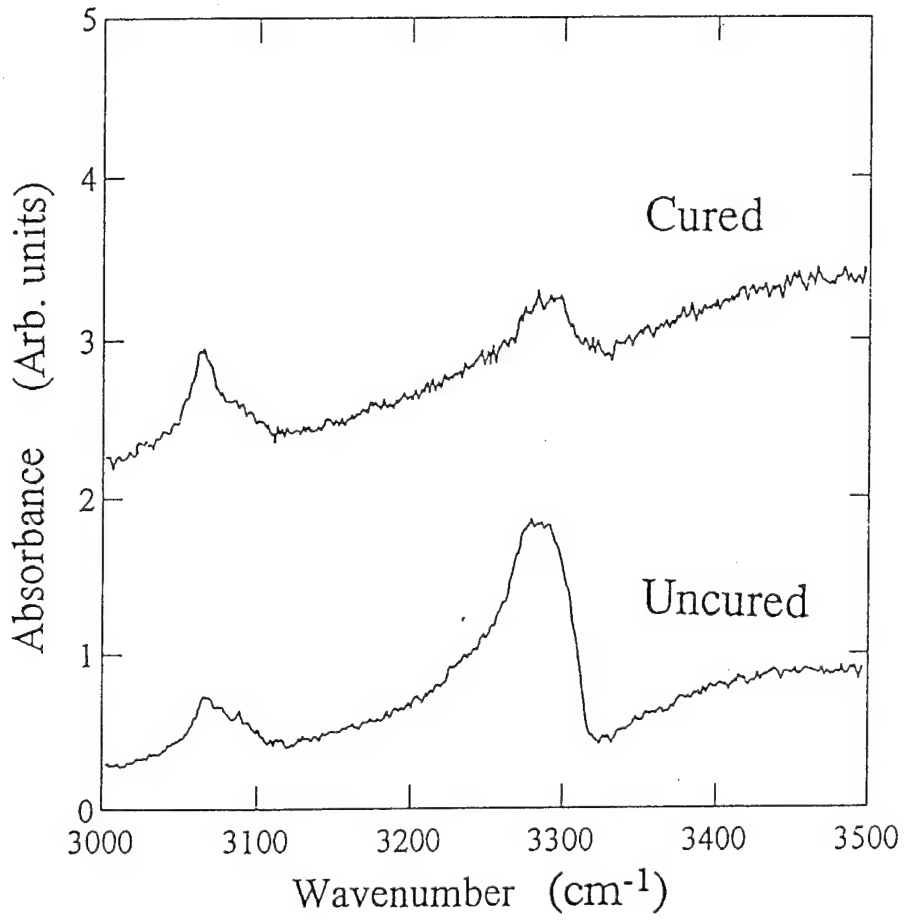

Figure 40. Infrared absorbance spectra measured near the region of the 3295 cm^{-1} acetylenic end-group absorption band in the polythiophene monomer, 3T-2Ac, showing the difference in peak height for the uncured state and after a cure at 95°C for 19 hours.

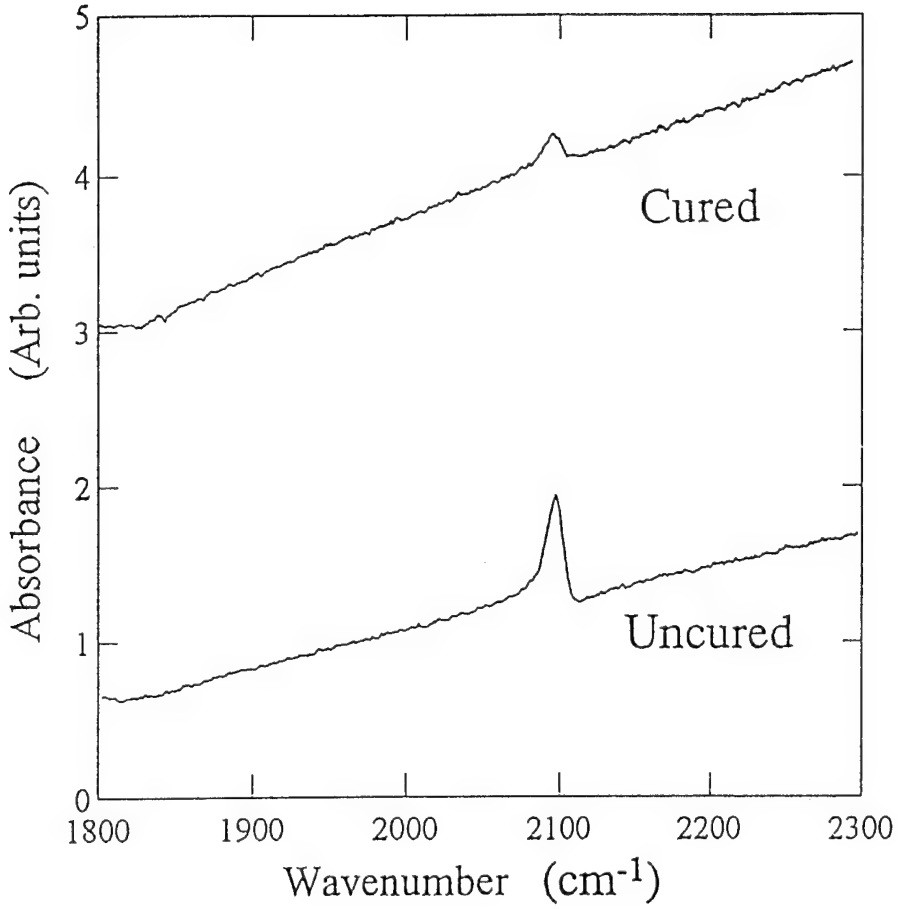

Figure 41. Infrared absorbance spectra measured near the region of the 2108 cm^{-1} acetylene end-group absorption band in a polythiophene monomer, 3T-2Ac, showing the difference in peak height for the uncured state and after a cure at 95°C for 19 hours.

have weakened considerably after curing the material at 95°C for 19 hours. In Figure 42, where the sample is the AT-polythiophene monomer, T-Si-T-2Ac, substantial reductions in the intensity of the 2108 cm^{-1} infrared peak were observed after curing the film at 95°C for 2.5, 6.5, and 22.3 hours respectively. The information obtained from infrared spectra, such as those shown in

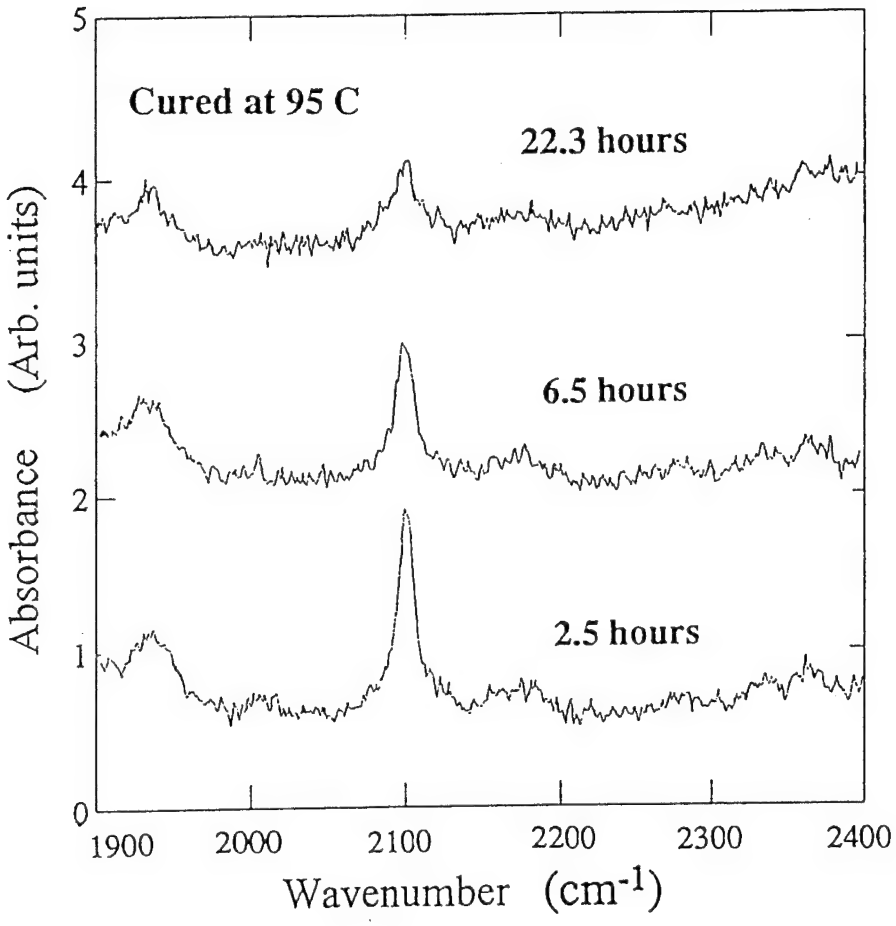

Figure 42. Infrared absorbance spectra measured near the region of the 2108 cm^{-1} acetylene end group absorption band showing the changes in peak height for different lengths of cure time in the polythiophene monomer T-Si-T-2Ac.

Figures 37 to 42, was used to verify that crosslinking had taken place in thin films of the various monomers, and also was used to indicate the relative degree of crosslinking in the resulting thermoset. Such verification was sometimes necessary since it was not always possible to clearly identify an exotherm from the DSC scan, e.g., in the cases of 3T-2Ac, and T-Si-T-2Ac. Moreover, the completeness of these acetylene end-group reactions along with the associated crosslink densities were an important factor to consider in performing doping studies in these thermosets.

We have found that the visible absorption spectra measured in thin thermoset polymer films changed with cure state. In the AT-Schiff base and AT-polythiophene monomers the band-edge was red-shifted after curing. An example of the observed absorption-edge red-shift in Thermcon 1000 is shown in Figure 43. Visually the film was observed to darken as the longer wavelength optical absorbance increased. We attribute this observed red-shift to the extensive crosslinking occurring in these materials, reflecting band-structure changes associated with the transition from a quasi-one-dimensional structure with weak inter-polymer-chain coupling to a three-dimensional heavily crosslinked structure.

We have also found that acetylene-terminated monomers exhibited photoluminescence quantum yields that depended weakly on the degree of cure. An Argon ion laser operating at 514 nm was used to excite the photoluminescence in our thin film samples. We found that the photoluminescence emission measured just below the band edge energy exhibited a small reduction in intensity with increasing cure. For example, in Thermcon 1000 the optical emission from an uncured film was found to be nearly a factor of six greater than that measured after the sample had been cured at 160°C for 19 hours. We attribute the reduced emission to increased

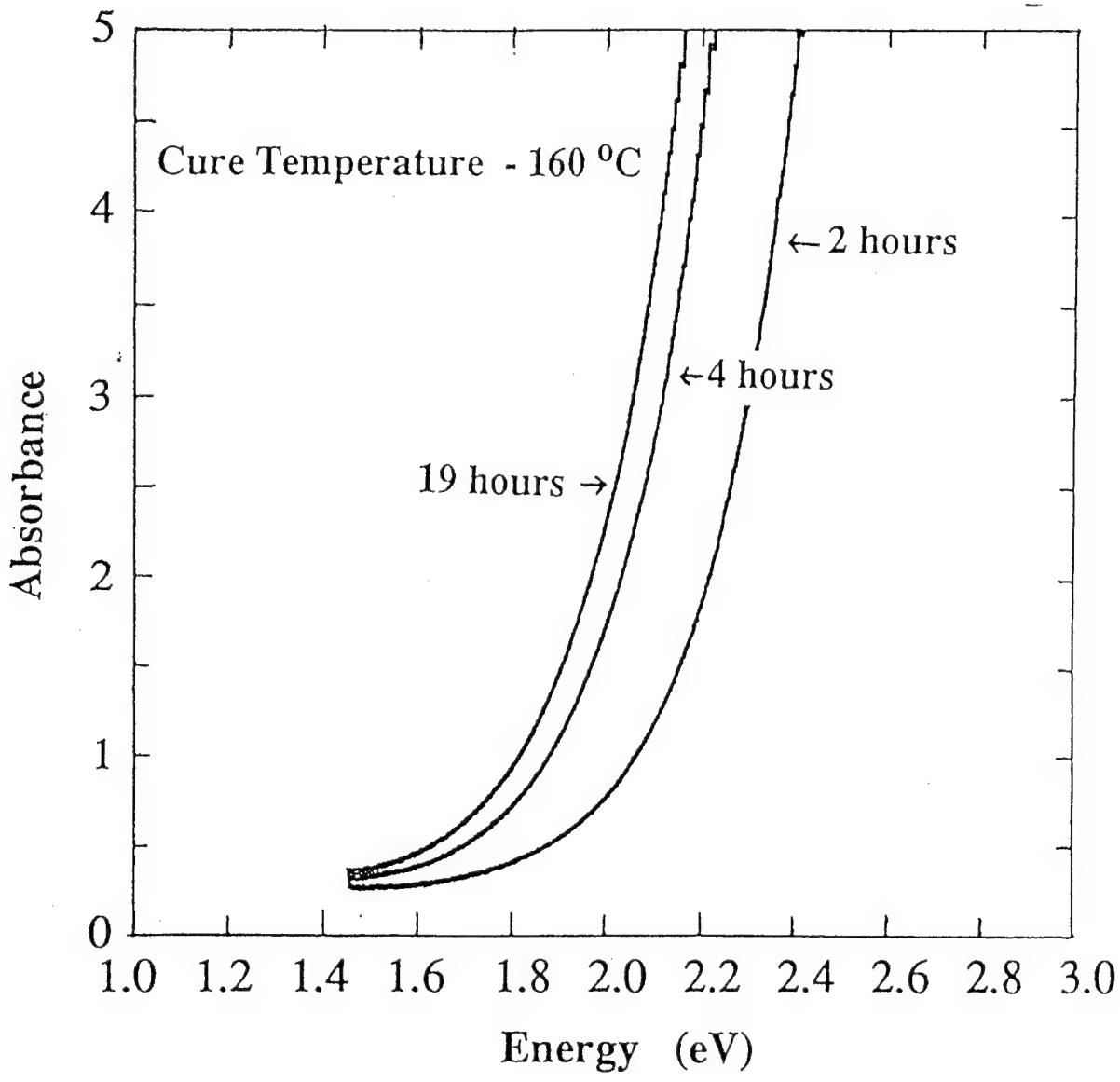

Figure 43. Optical absorption edge measured in a thin film of Thermcon 1000 after curing for different times.

non-radiative recombination, which could be caused by the transition to a more delocalized three-dimensional conjugated structure. In the highly crosslinked structure photo-excited electrons and holes can more easily escape each other and drift apart by diffusion to defects or impurities, where they then have a greater probability of recombining non-radiatively [33]. It is also possible that the reduced emission is caused by an increased defect density in cured films. It is worth noting that no significant difference was found in the photoluminescence emission measured in Thermcon 1000 material that had been purified by recrystallization. This implies that chain defects are probably the major source of non-radiative recombination in these materials. The optical and infrared techniques described above were used to monitor changes in the physical and chemical properties of acetylene-terminated thermosets during the curing process prior to performing the doping studies.

Doping Studies: Optical spectroscopy techniques were also employed to study the electronic properties of iodine-doped, conducting, thermoset films. These absorption studies contribute toward our understanding of conducting polymers through band structural changes that are inferred from changes in the measured spectral features. For example, questions arise as to the nature of charge transport through the extensively conjugated crosslinked network in the thermoset polymers. An examination of absorption features at energies below the band gap energy can indicate whether polaron and/or bipolaron charge carriers form [33-35]. We have measured absorption through thin conducting doped films in the visible and infrared regions of the spectrum to determine where oscillator strength changes occur, and also, to provide supporting evidence, along with the ESR data, for the formation of polarons and/or bipolarons. In addition

we have examined photoluminescence in undoped and iodine-doped thermosets, to verify if recombination occurs primarily through polaron states.

In these polymers polaron recombination should show up as an emission peak below the band edge energy. In addition, any photoconductive response observed in thermoset materials should provide a qualitative measure of charge carrier mobility through the three-dimensional amorphous network. If trapping states exist below the band edges or a large degree of disorder is present, the photoresponse will be small, indicating that charge carriers are highly localized and relatively immobile.

Thin films of Thermcon 1000 and 2000 were prepared for optical studies by melting and curing prior to doping with iodine vapor. We found it difficult to diffuse iodine into the fully cured thin films formed on substrates. After repeated exposures to iodine vapor at 70°C the optical properties were unchanged, suggesting that little iodine was being incorporated into the films. Considering our success in doping bulk samples of fully cured Thermcon 1000 for electrical measurements and powders for ESR measurements we conclude that iodine diffuses more slowly into fully cured thin films on substrates. As was described in Section 3.1.1 we found evidence for microcracking in iodine-doped bulk thermosets which may play a role in enhancing iodine diffusion into the sample. Stress-induced microcracking found in bulk materials may be less likely to occur in thin films since adhesion to the substrate (glass) may prevent crack propagation and also may limit possible physical expansion which would occur if iodine diffuses into the thermoset. Thus the influx of iodine that would normally follow stress-relieving microcracking is not readily observed in the thin films that were fabricated on substrates for our optical studies. To circumvent these limitations of incorporating iodine into our thin films we

performed our optical studies of the effects of iodine-doping only on partially cured thermosets with correspondingly lower crosslink densities.

Figure 44 shows optical absorption spectra measured in a Thermcon 1000 thermoset

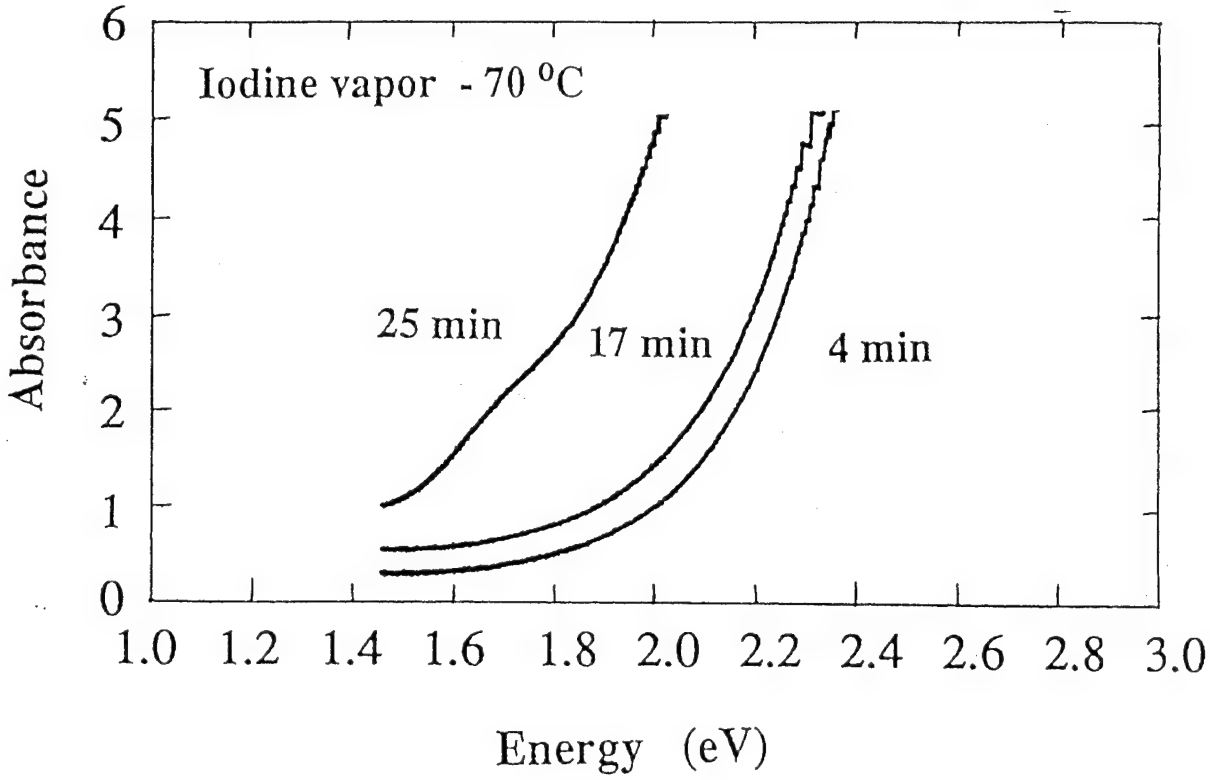

Figure 44. Optical absorption edge measured in a Thermcon 1000 film after doping with iodine vapor. The edge shifted toward lower energy and a peak at 1.7 eV appeared with increased exposure to iodine vapor (i.e., increased iodine uptake).

sample after repeated exposures to iodine vapor at 70°C for different periods of time, and Figure 45 shows similar spectra measured in a Thermcon 2000 film exposed to iodine vapor at 60°C for longer periods of time. The films used for these doping measurements were first partially cured at 160°C. In both cases the optical absorption edge near 2 eV is observed to shift toward lower energy as iodine is incorporated into the film, and, after further exposures, a peak begins to

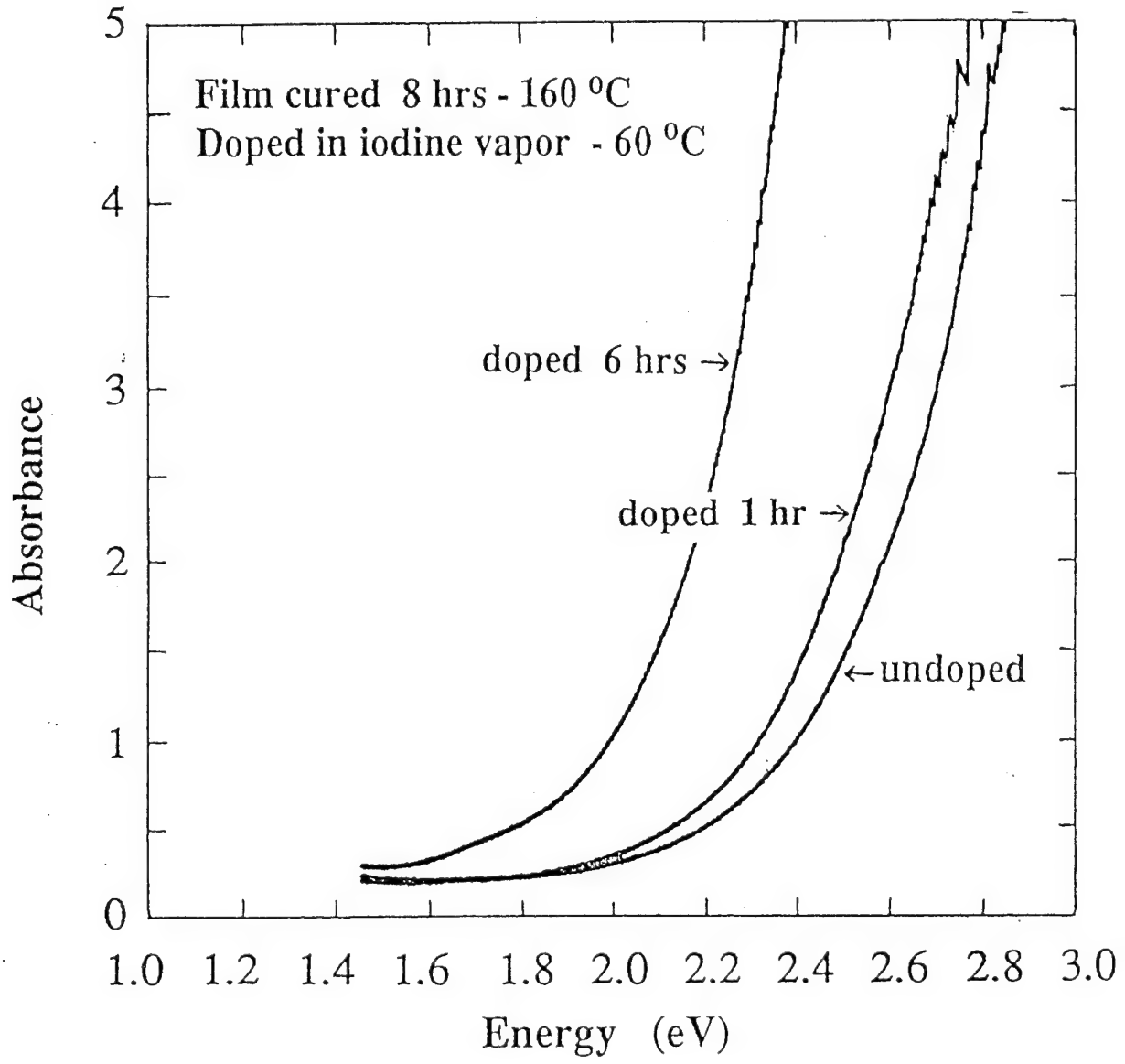

Figure 45. Optical absorption edge measured in a Thermcon 2000 film after doping with iodine vapor. The edge shifted to lower energy and a peak near 1.7 eV appeared with increased iodine uptake.

emerge at 1.7 eV. We associate this observed absorption peak at 1.7 eV, which occurs below the band edge optical transitions, with the formation of polarons in these thermosets [33-35]. This conclusion is also supported by our ESR measurements, which show a marked increase in the spin susceptibilty following iodine doping indicating the formation of S = 1/2 particles residing on the polymer chains. Similar doping-induced optical changes observed in thin films of 3T-2AcPh thermosets are shown in Figure 46. Once again, the absorption edge is found to shift toward

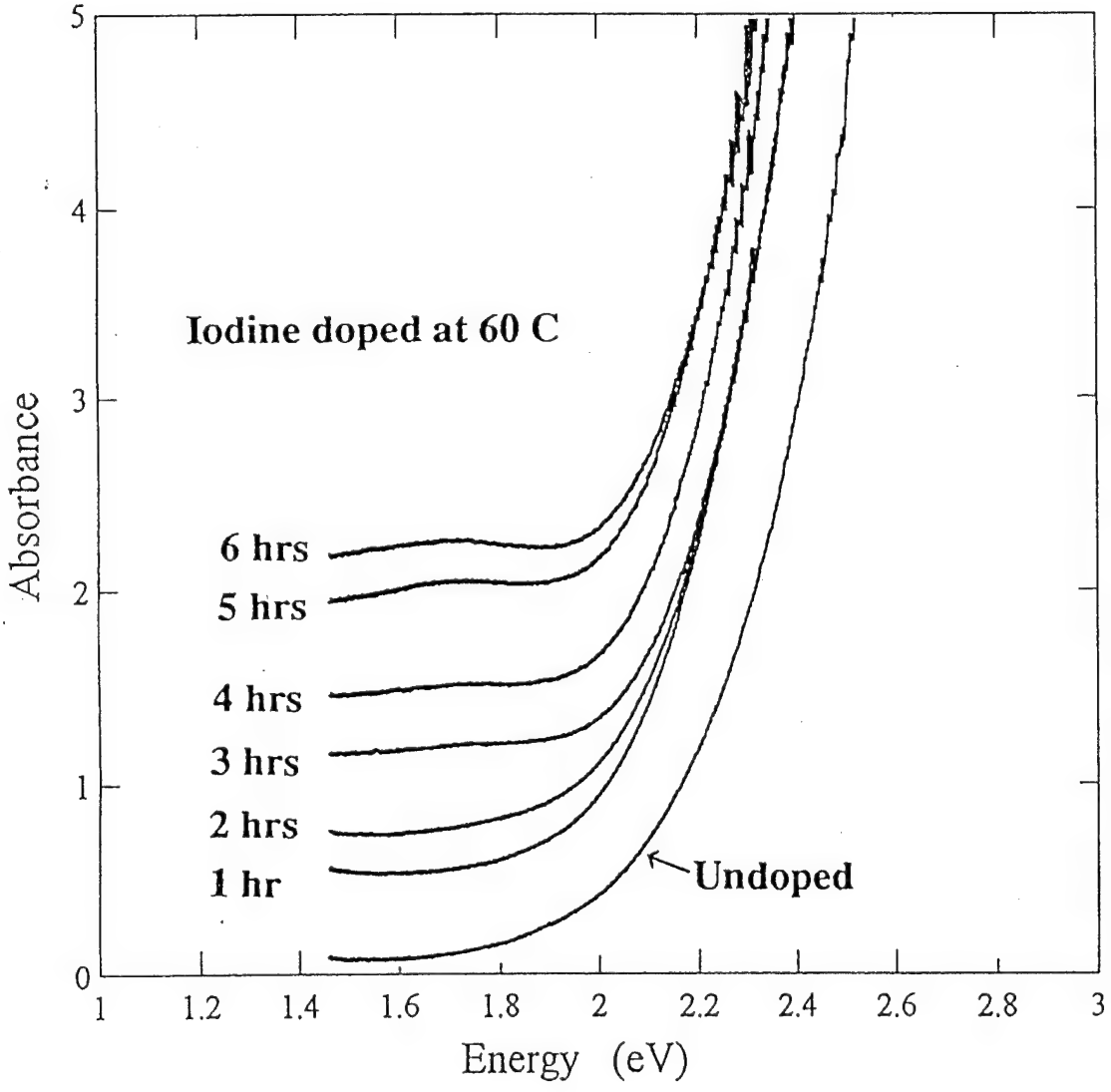

Figure 46. Optical absorption edge measured in a 3T-2AcPh film after doping with iodine vapor. The edge shifted to lower energy and a peak at 1.7 eV appeared with increased iodine content.

lower energy and an absorption peak at 1.7 eV eventually appears below the band edge after progressive sequential hourly exposures to iodine vapor at 60°C.

Further evidence for polaron formation in Thermcon 1000 thermosets is provided by a low energy shoulder near 1.7 eV in the photoluminescence spectra, as shown in Figure 47. The main

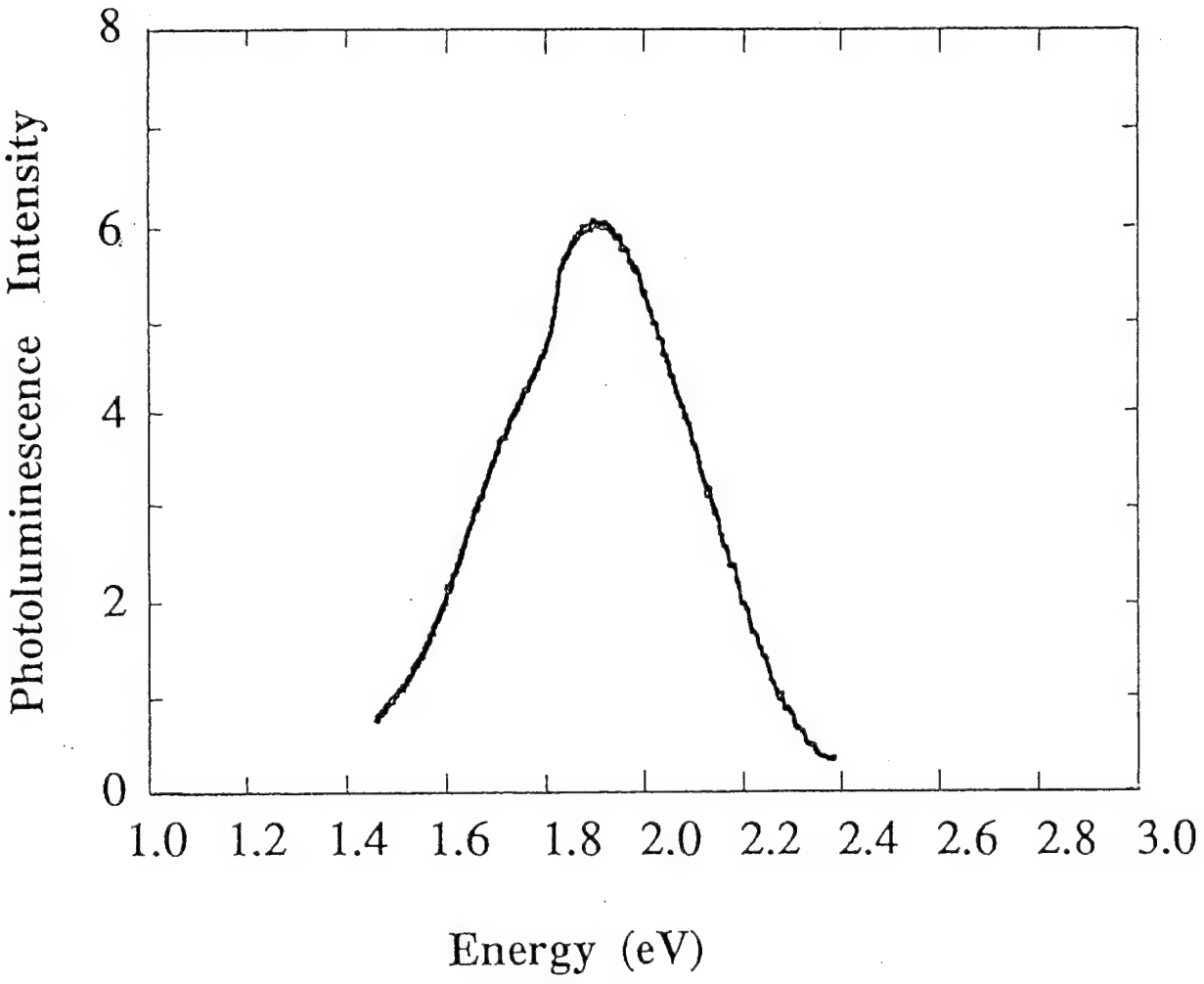

Figure 47. Photoluminescence spectrum measured in a partially cured Thermcon 1000 film.

peak near 2 eV is attributed to emission through band-edge tail states as photoexcited electrons and holes recombine radiatively. The 1.7 eV luminescence shoulder corresponds to the absorptive transition observed in iodine-doped material which, along with the ESR results, suggests the formation of polarons. Thus, instead of recombining radiatively immediately following creation, a fraction of the photoexcited charges first form polaron states. These photo-induced polaron charges then relax to the ground state through a lower energy radiative transition at 1.7 eV, which is where the additional absorption peak was observed in iodine-doped Thermcon 1000 thermoset.

We have also found that the photoluminescence intensity decays with time during exposure to laser light, as illustrated in Figure 48. A likely explanation for this involves photo-

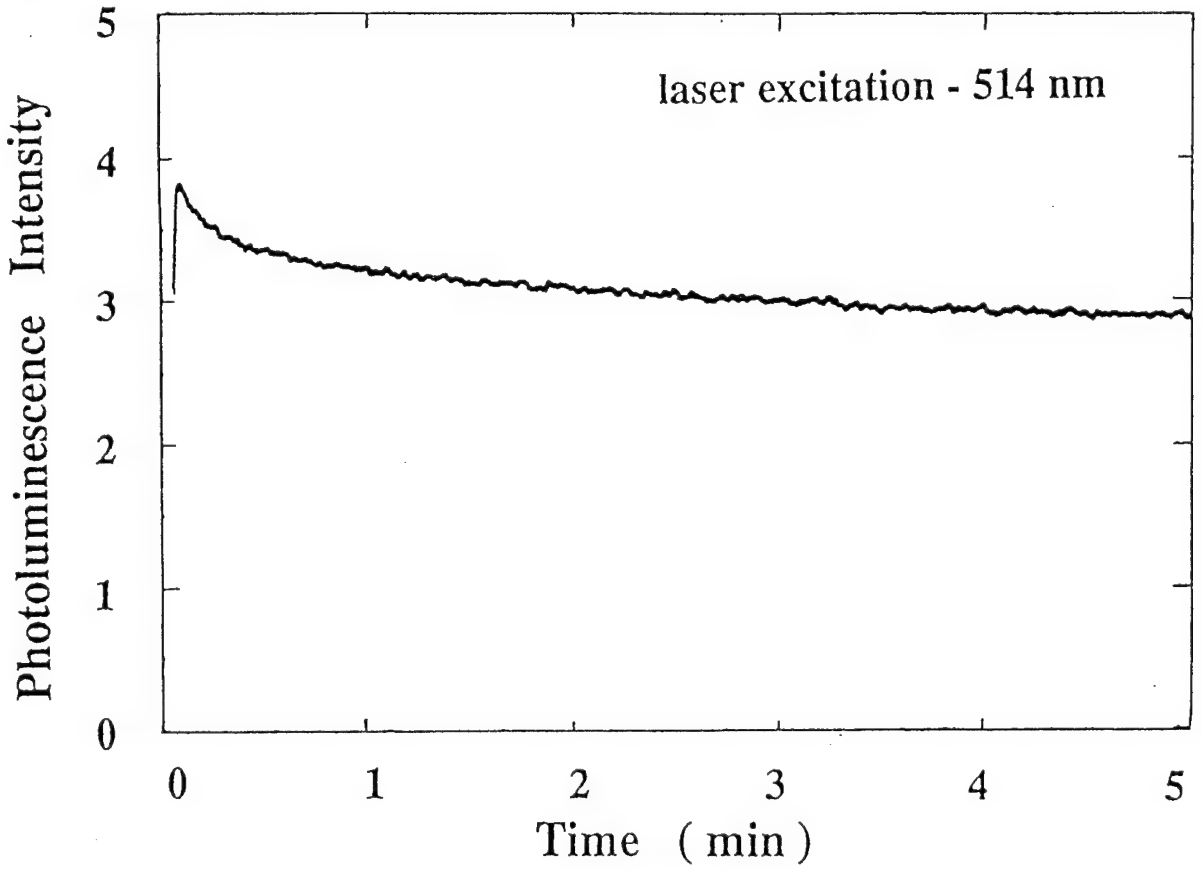

Figure 48. Time dependent decay of the photoluminescence intensity measured in a Thermcon 1000 film.

excited charges trapped at defects or impurities on the polymer chains. As some fraction of the photo-excited charges generated near defects become trapped, additional non-radiative recombination pathways open up for any newly-created photo-induced charges, resulting in an observed decay of the photoluminescence intensity with time [33]. Thus the non-radiative decay path changes with time due to the increasing density of trapped charge. The observed photoluminescence emission decay is found to occur only during the time the sample is exposed to laser light. For example, Figure 49 shows the time dependent photoluminescence signal in

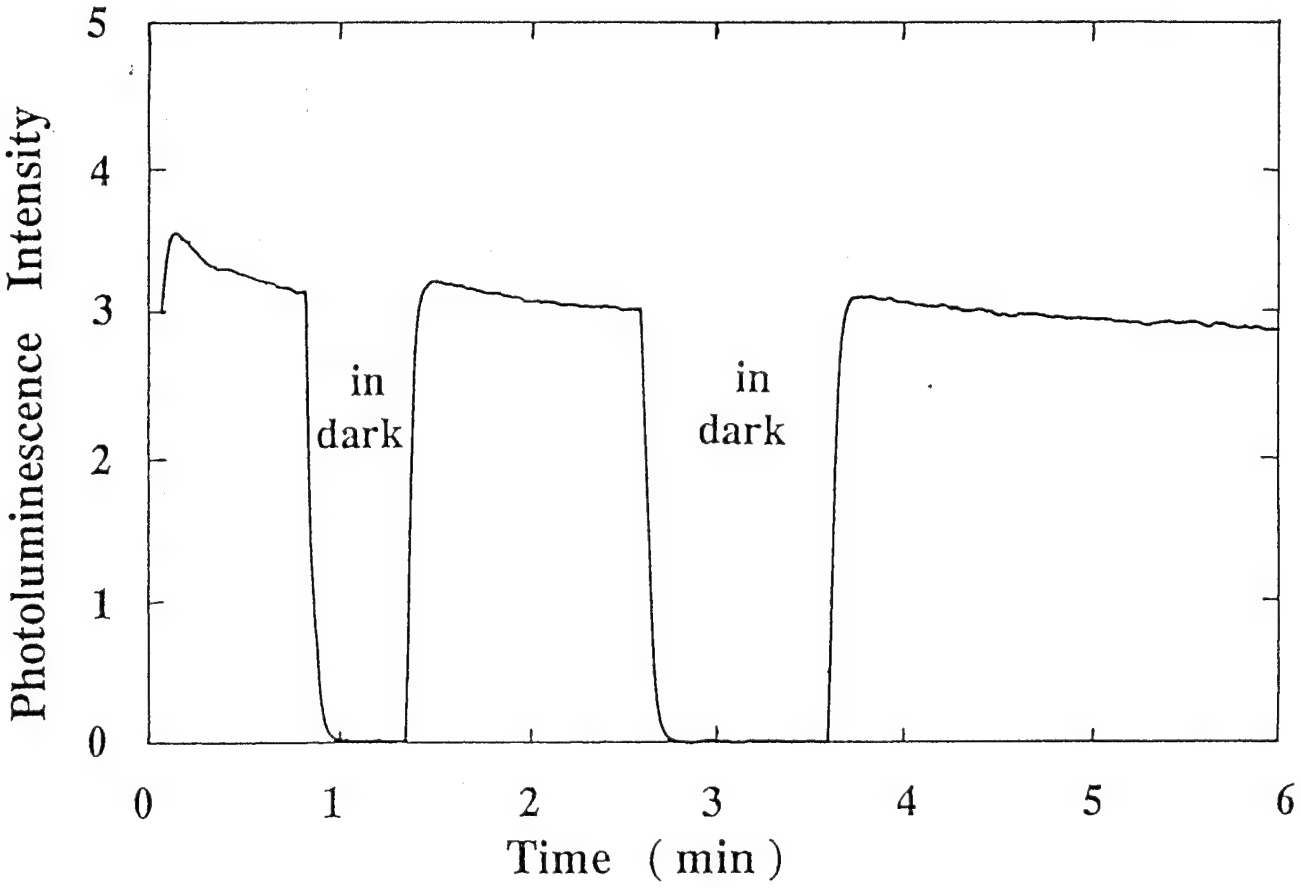

Figure 49. Time dependent decay and partial dark recovery of the photoluminescence intensity measured in a Thermcon 1000 film.

Thermcon 1000 with the laser light on, and after brief periods in the dark. A reduction of the photoluminescence intensity occurs only during the time the sample is exposed to light. In fact, a partial recovery of the luminescence intensity is observed just after the dark periods. The decay is found to be reversible if the sample remains in the dark for long periods of time. This result implies that any excess charges trapped at defects eventually decay back to the ground state, and render the additional competing non-radiative recombination pathways less effective.

Support for the trapped-charge-induced quenching of luminescence is provided by the measured photoluminescence emission which became much weaker after doping with iodine. However, we have also found that after a long waiting time the photoluminescence response in doped samples partially recovers. Figure 50 shows photoluminescence spectra measured in a Thermcon 1000 thermoset sample before doping with iodine, and long times after doping. After 3 days the luminescence intensity is roughly 4% of the initial signal height and after 13 days it has recovered to nearly 8%. These data suggest that iodine slowly diffuses out of the thermoset after long periods of time at room temperature.

We have also found that some of the other observed optical changes induced by doping are reversible, which provides additional evidence that a fraction of the iodine is able to diffuse out of the sample. After shifting to lower energy upon doping, the absorption edge was found to return to higher energy when measured in samples that had remained at room temperature for several days. This absorption-edge reversibility effect demonstrated by Thermcon 1000 samples is shown in Figure 51. However, the optical absorption edge in doped films never completely recovers to that measured in the undoped material, indicating the effect is not completely reversible. Apart from these reversible changes in the optical absorption edge, the doping induced

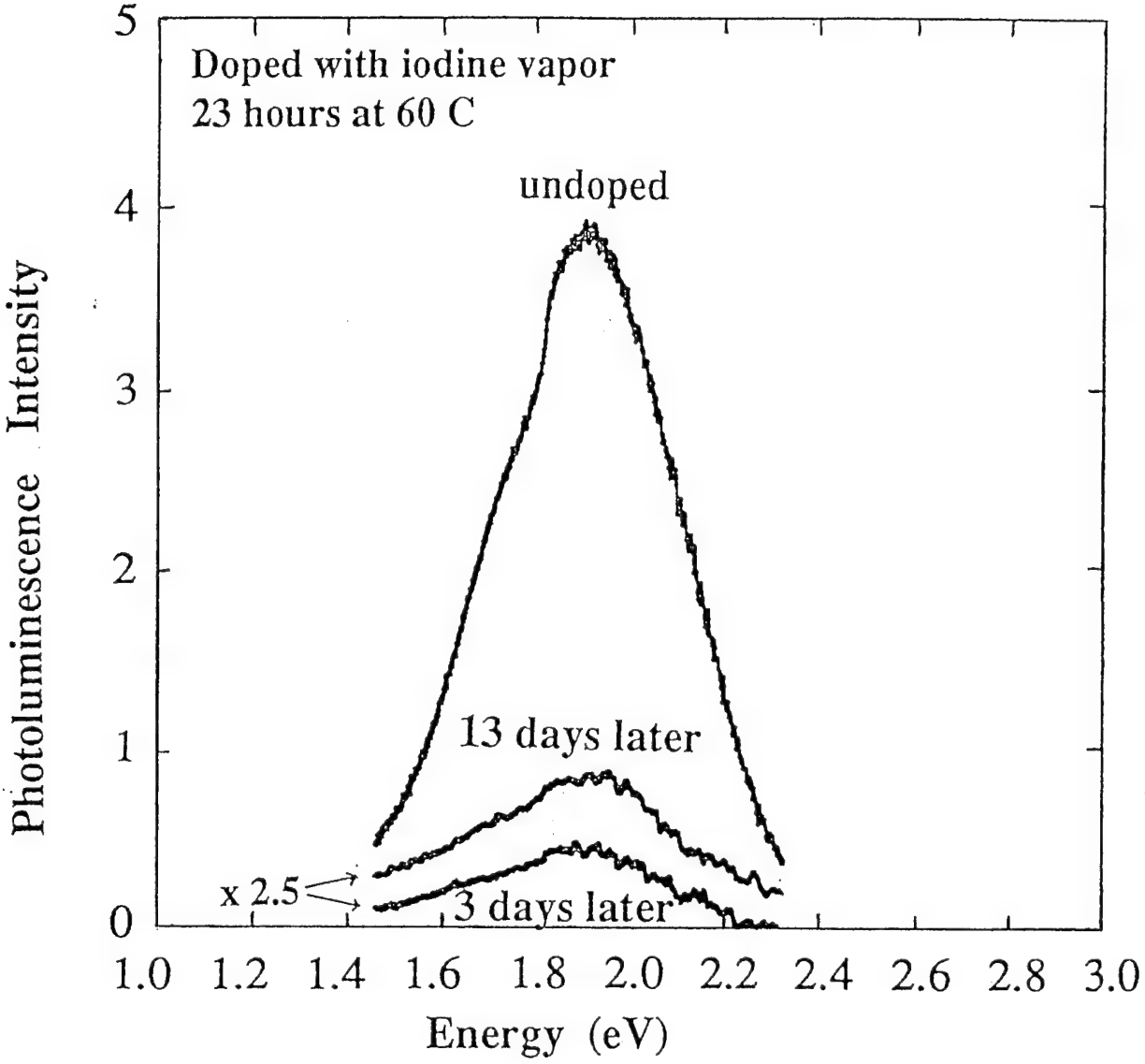

Figure 50. Photoluminescence spectra measured in a Thermcon 1000 film before and after doping with iodine vapor and waiting for the periods of time indicated.

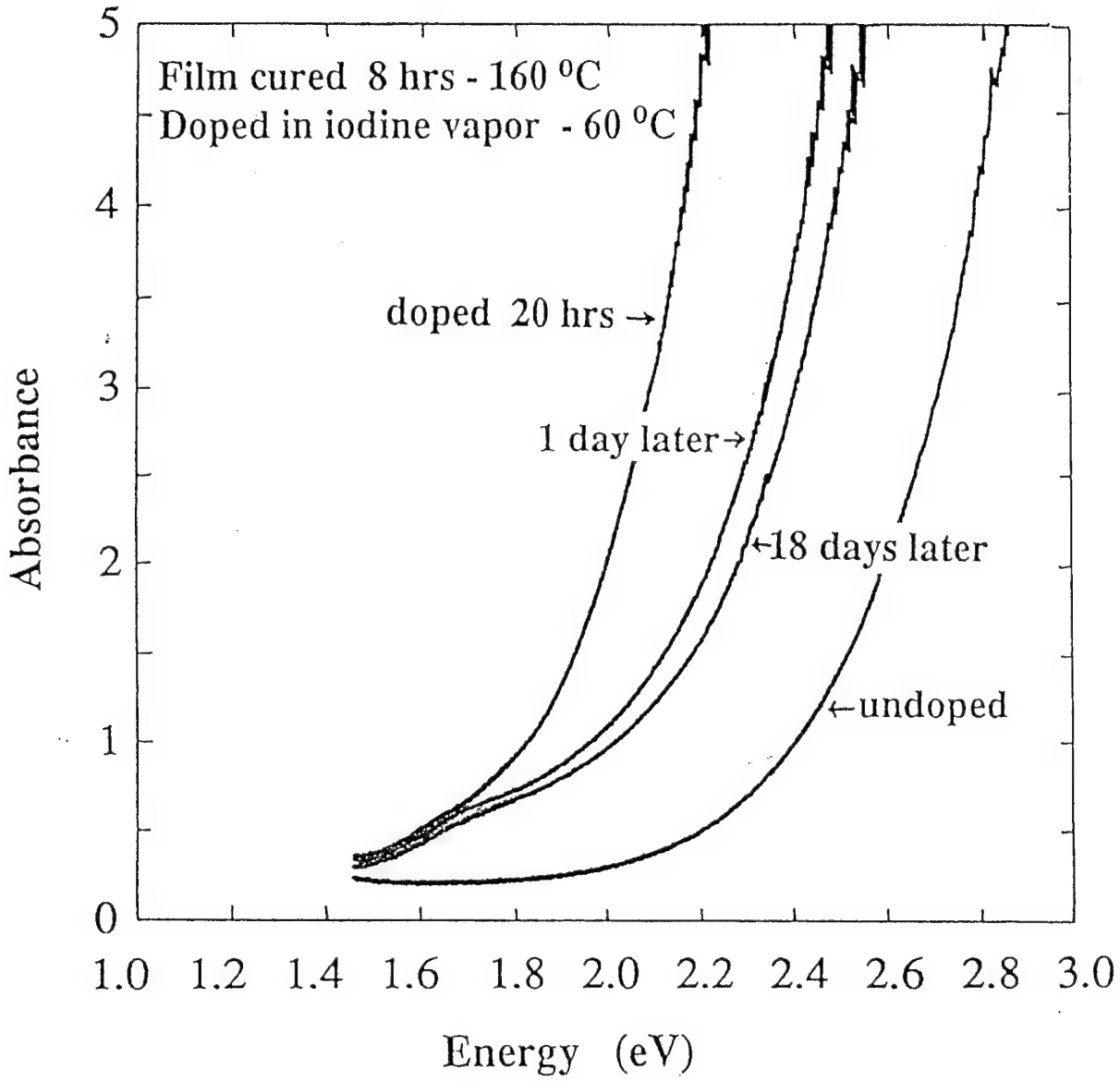

Figure 51. Optical absorption edge measured in a Thermcon 1000 film before and after doping with iodine vapor and waiting for the periods of time indicated.

absorption peak associated with polarons observed near 1.7 eV in Thermcon 1000 thermosets exhibited no further measurable change when the material remained at room temperature for many days. This implies that the iodine counter-ion species involved in transferring charge on to the polymer chain in the form of polarons remained in the material for very long periods of time at room temperature. However, this was not the case in 3T-2AcPh, where the 1.7 eV peak diminished with time after doping. Our ESR spin susceptibility results, shown in Figures 28 and 33, also support this difference in the behavior of polarons in the iodine-doped Thermcon 1000 and 3T-2AcPh thermosets.

To provide a better understanding of the possible limitations on the electrical conductivity we have attempted to measure photoconductivity in acetylene terminated thermoset polymers. Closely-spaced, coplanar electrical contacts were evaporated on top of cured thermoset films and the electrical resistivity was measured during illumination with above-band-gap 514 nm blue laser light. A photoconductive response was measured, but it was found to be small. For example, the measured film resistivity in Thermcon 1000 (~3 x 10^8 ohm cm) decreased by only 30% when the sample was exposed to 100 mW of 514 nm laser light. This qualitative result suggests that charge carrier mobilities are low in the acetylene terminated thermosets and implies that photogenerated charges are trapped in localized states below the band edges. A likely cause for this low charge mobility is some form of disorder arising from the amorphous structure associated with the thermoset polymer. The conjugated band structure is expected to be significantly perturbed by misalignment of the neighboring p_z orbitals constituting the π-electrons, due to disorder along the polymer chains. Thus, the electrical transport is most likely limited by polaron charges hopping between disorder-induced localized states within the band gap. This has important implications

regarding the possible reasons for the limited maximum conductivity's measured in these systems. We conclude that iodine doping efficiently transfers charges to the polymer chains to create polarons, but that the mobility of these polarons is low basically due to the intrinsic amorphous structure of these thermoset polymers. Several consequences of this amorphous structure, including explicit examples of the molecular structures that result in a misalignment of the p_z orbitals will be discussed in more detail in Section 4.4.3.

3.2 AT-Polyaniline Studies

The objective of this task was the investigation of the polyaniline-based and polyaniline derivative-based oligomers terminated with reactive acetylene groups that would undergo crosslinking to form a conducting thermoset resin. The structures of these oligomers are shown in Figure 52. This task involved the following five major efforts: (i) synthesis, (ii) characterization, (iii) modification of the oxidation state, (iv) doping and measurement of electrical conductivity, as well as (v) processing and curing.

3.2.1 Oligomer Synthesis

Oligomers of polyaniline and polyaniline derivatives were synthesized using two different approaches. The first was the modified-Honzl-Wudl (MHW) approach [36,37], and the second was the Manassen-Khalif (MK) approach [38]. Both are described below.

Synthesis of ATPAs Using the Modified-Honzl-Wudl (MHW) Approach: The initial approach involved the preparation of acetylene-terminated oligomers of polyaniline (ATPA) by an adaptation of the two-step procedure described by Wudl et al., for the synthesis of polyaniline (PA) [37] and phenyl-terminated aniline oligomers [39]. This synthesis involved the condensation of 1,4-phenylenediamine (PDA) and 3-ethynylaniline (EA) with

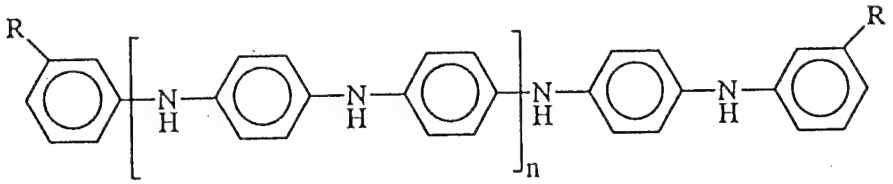

PPAI (R = H; n=large)
ATPA-7 (R = C≡CH; n=3)

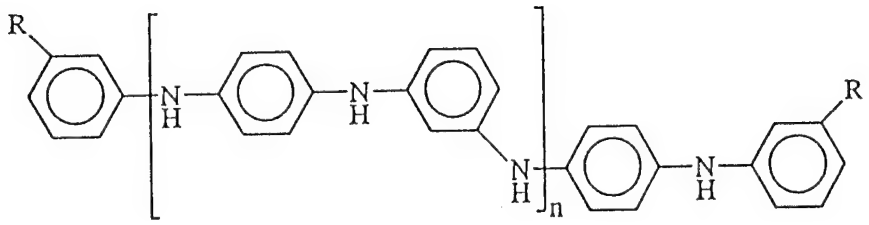

m,p-PPAI (R = H; n=large)
m,p-ATPA-7 (R = C≡CH; n=3)

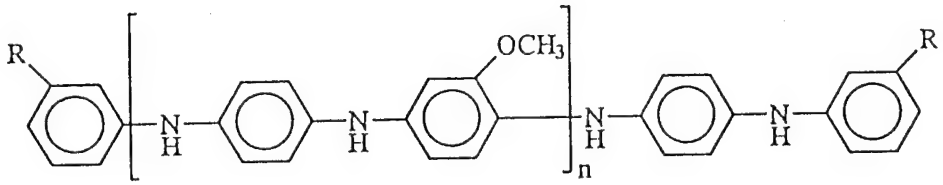

MeO-PPAI (R = H; n=large)
MeO-ATPA-7 (R = C≡CH; n=3)

(aniline-co-anisidine)

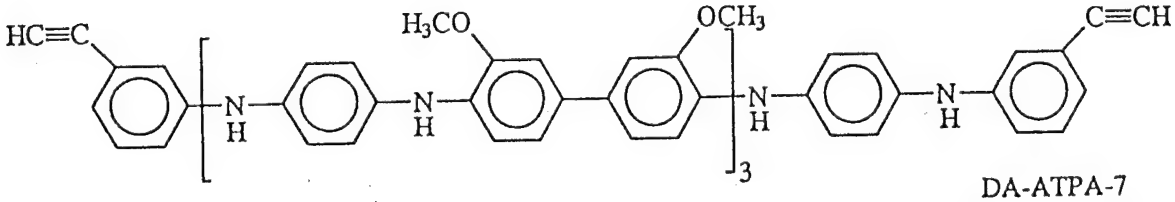

DA-ATPA-7

Figure 52. Structures (leuco forms) of polyaniline-type oligomers and polymers investigated in this work.

2,5-dioxo-1,4-cyclohexanedicarboxylic acid (DCCA) in m-cresol at 65°C under an inert atmosphere. The preparation of DCCA and ATPA are shown in Figure 53 as Scheme VIII, and in Figure 54 as Scheme IX, respectively. The initial partially unsaturated condensation product was subsequently converted to a conjugated, more emeraldine base-like oligomer by air oxidation at 65°C.

Scheme VIII

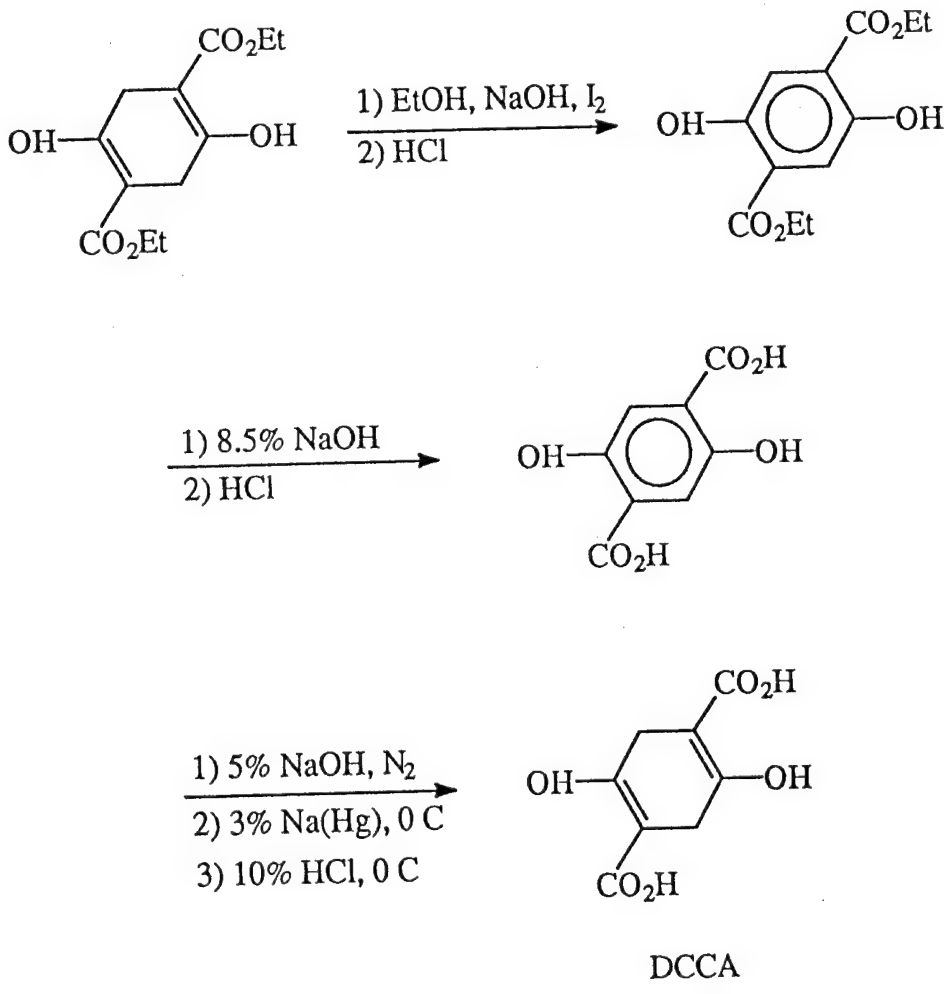

DCCA

Figure 53. Scheme VIII: Procedure used to synthesize 2,5-dioxo-1,4- cyclohexanedicarboxylic acid (DCCA).

Scheme IX

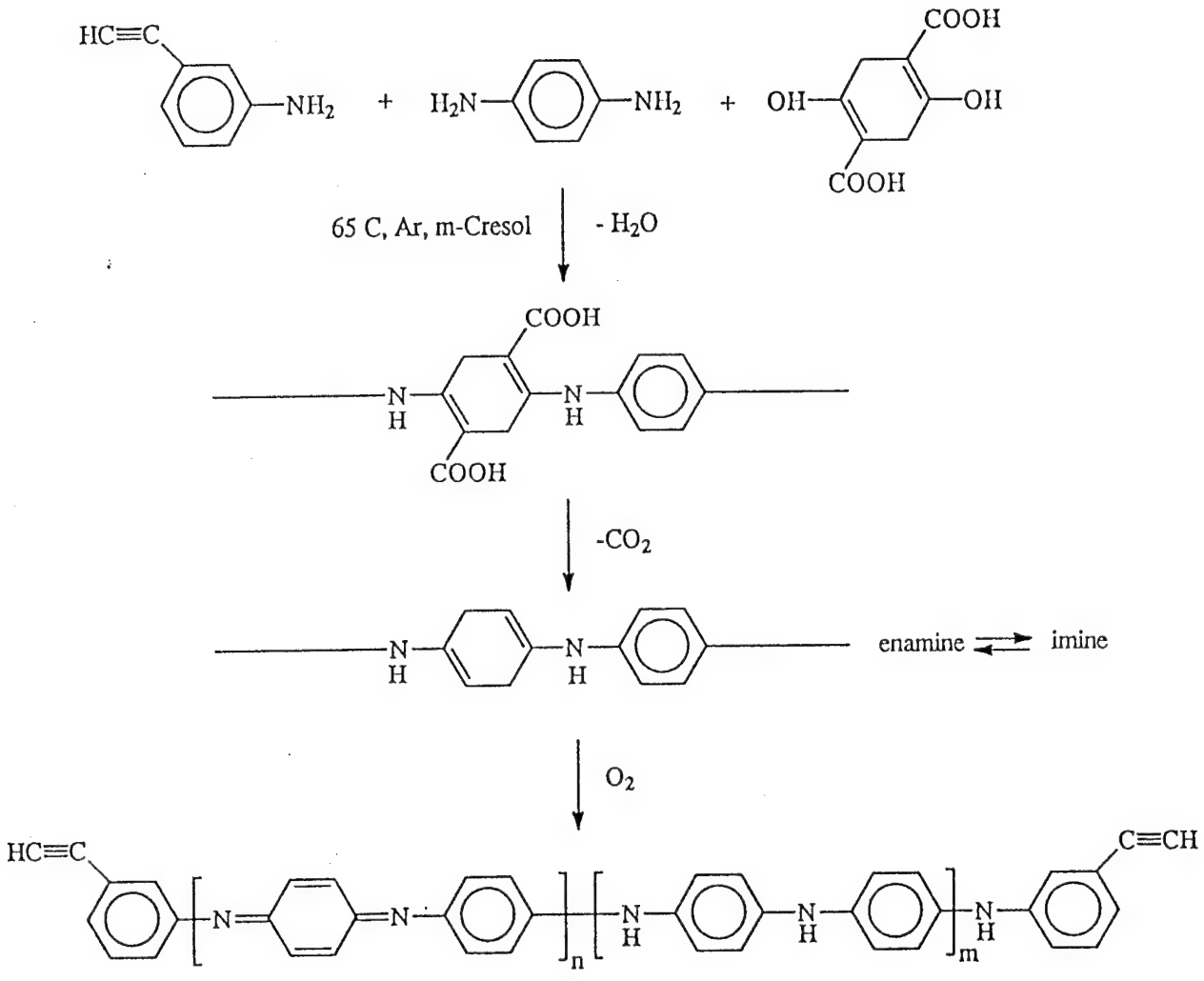

Figure 54. Scheme IX: Procedure of Wudl et al., used to synthesize polyaniline oligomers.

The MHW scheme was used to prepare several acetylene-terminated polyanilines. The synthesis of ATPA-9 was extensively investigated to determine the optimum reaction conditions. This oligomer had 9 internal benzene rings (including benzenoid and quinoid forms), 10 nitrogens and 2 terminal ethynylbenzenes. The best results were obtained when the end-capping agent, EA, was added after 48 h in about 70% excess to the reaction mixture consisting of 1,4-phenylenediamine and DCCA (molar ratio = 4/5) in *m*-cresol (5% solution). Two shorter acetylene-terminated oligomers, ATPA-3 (containing 4 nitrogens, i.e., the 'tetramer') and ATPA-7 (containing 8 nitrogens, i.e., the 'octamer') were prepared in a similar fashion to ATPA-9.

Synthesis Using Manassen-Khalif (MK) Schiff-Base Approach: Because the MHW synthesis involved the synthesis and use of highly unstable DCCA, a more convenient synthetic approach was sought. The MK approach [38], which employed 1,4-cyclohexanedione (CHD) in place of DCCA was found to be both convenient and reliable. Synthesis with CHD proceeded by the classical Schiff-base chemistry, shown in Figure 55 as Scheme X, to afford essentially the same quality ATPA-3 and ATPA-7 as prepared by the MHW procedure. The ability to substitute CHD for DCCA in this procedure is of great importance for the following two reasons: (1) it precludes the laborious and expensive preparation of DCCA outlined in Figure 53, and (2) it makes it very easy to combine reactants in the correct stoichiometry. In the MHW approach, the tendency of DCCA to decompose and liberate CO_2 makes it very difficult to guarantee correct stoichiometry and thus optimize the oligomer length.

A typical synthesis used to prepare ATPA involved the reaction of 1,4-phenylenediamine with 1,4-cyclohexanedione (CHD) in m-cresol at 65-70°C for 72 hours in an argon atmosphere followed by the addition of an excess amount of m-ethynylaniline (EA). The reaction was then

Scheme X

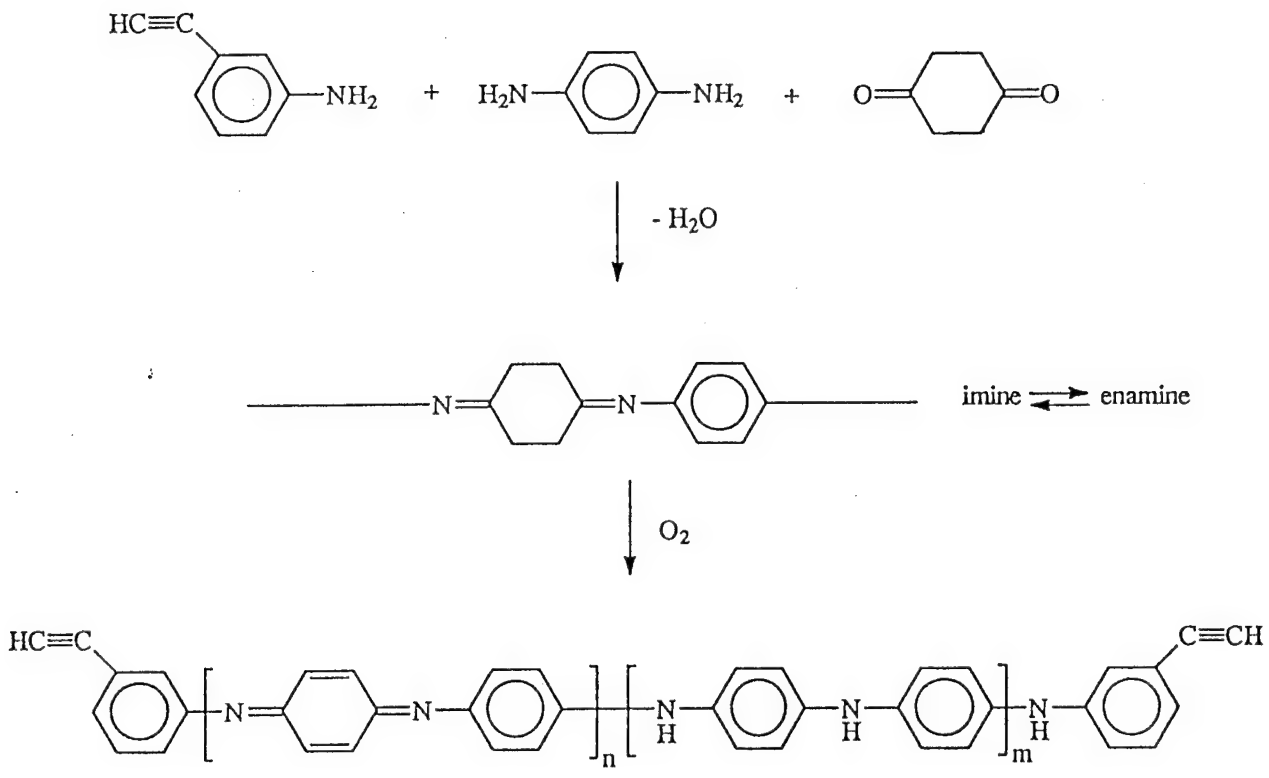

Figure 55. Scheme X: Our adaptation of the procedure of Manassen and Khalif used to synthesize polyaniline oligomers.

continued for an additional 72 to 96 hours before exposure to the atmosphere for periods of 20 to 22 hours. The product was obtained as a gray powder. Yields ranged from 43 to 53%.

A comparison of Figures 54 and 55 shows that both the MHW and the MK approach produce polyaniline oligomers through the same partially saturated intermediate. In Figure 54, this intermediate is drawn as an enamine, whereas in Figure 55 it is drawn as its imine tautomer.

In both cases this intermediate becomes both aromatized and oxidized upon heating in the presence of atmospheric oxygen. However, samples prepared using either the MHW or MK method were typically not completely oxidized to the emeraldine base form shown in Figure 56. In certain cases, further air oxidation led to improved conductivity.

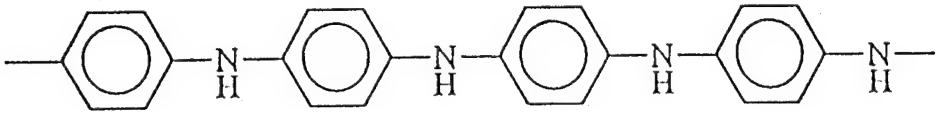

Leucoemeraldine

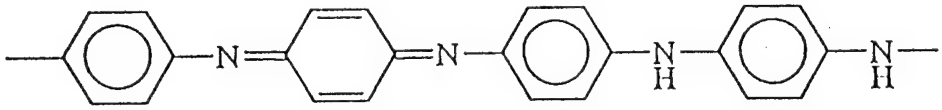

Emeraldine Base

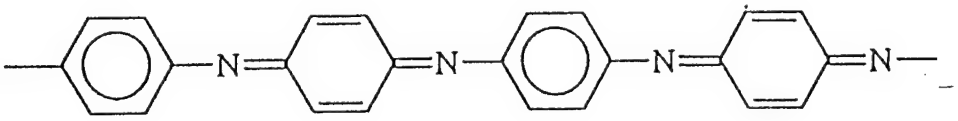

Pernigraniline

Figure 56. Schematic of a typical polyaniline-type material in various oxidation states: (a) leucoemeraldine, (b) emeraldine, and (c) pernigraniline.

The following related compounds were synthesized using the MK approach:

Phenyl-Capped Octaaniline (COA): The octamer COA having non-crosslinkable phenyl endcaps was synthesized for comparison with the crosslinkable acetylene-terminated polyaniline oligomers. The initial reaction of CHD and PDA to form the oligomer, was followed by end-capping with aniline, instead of EA, to make a phenyl-terminated product. The crude product consisted of only a slightly oxidized oligomer as determined from its electronic spectrum shown in Figure 57 which indicates a weak absorption at 592 nm.

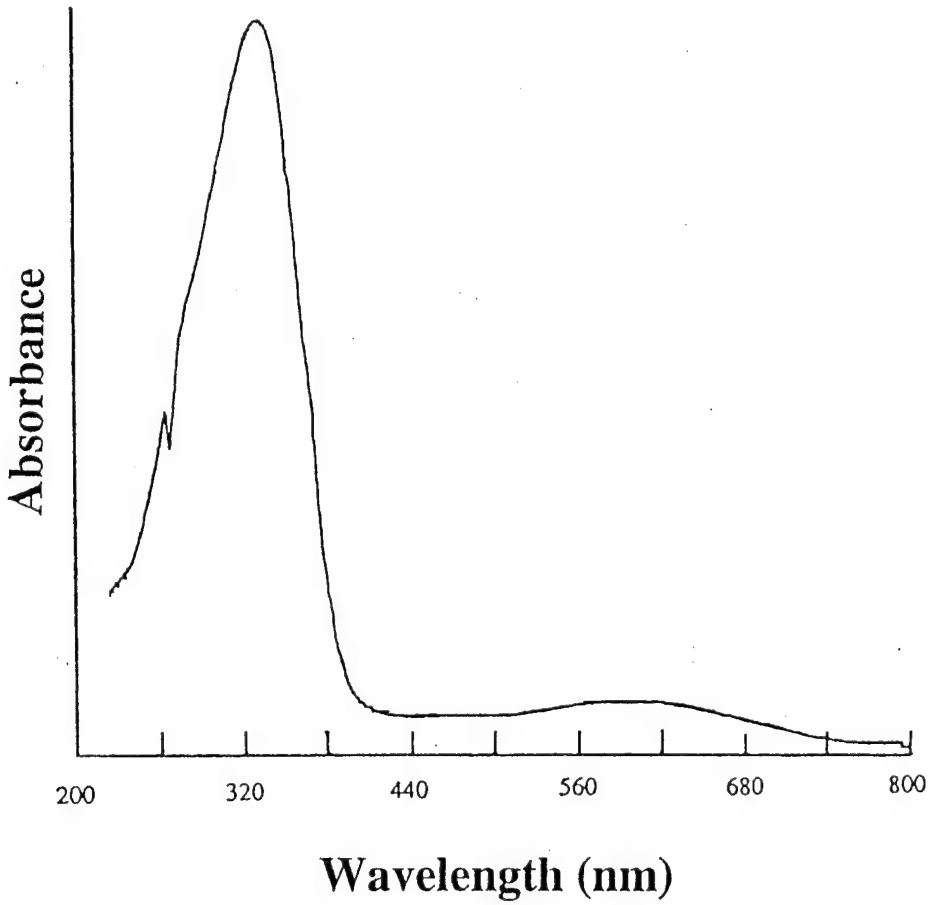

Figure 57. UV-VIS spectrum from phenyl-capped aniline oligomers (COA) prepared using MK approach. Very weak peak at ~600 nm indicates this sample was only slightly oxidized.

Polyphenyleneamineimine (PPAI; polyaniline): PPAI, which is essentially polyaniline, was prepared in order to evaluate the effectiveness of the MK synthesis for producing conductive materials having a polyaniline structure. Unlike the MHW synthesis, a tan precipitate did not form during the MK synthesis until the reaction mixture had been exposed to the atmosphere for about two hours. The PPAI(MK) product was obtained in highest yield (88%) when molecular oxygen was bubbled into the m-cresol reaction mixture at 68°C for 22 h after the tan precipitate had formed.

Modified Polymers and Oligomers for Improved Processability: In order to increase the processability (i.e., low melting point and low temperature cure) of ATPA-type oligomers, alkoxy-substituted and meta-substituted aromatic diamines were incorporated into the oligomers as shown in Figure 52. The syntheses of these compounds are described briefly below:

m,p-Polyaniline (m,p-PPAI): This polymer was prepared in addition to its structurally similar octamer (see below) because it was suspected that the polymeric form would be more conducting than the octamer. The outcome of this comparison would therefore allow a quantitative evaluation of the effect of meta substitution on polyaniline. The product was obtained as a dark solid which consisted of two fractions, one that was very soluble in N-methylpyrrolidone (NMP) and another that was only slightly soluble. Both were oxidatively treated with a solution of ammonium persulfate, $(NH_4)_2S_2O_8$, in 1 M HCl. The UV-vis spectra of the fraction slightly soluble in NMP lacked absorption in the 600 nm region, indicating the absence of the quinoid rings required for conductivity.

m,p-ATPA-7: The product was obtained as a dark brown solid in 51% yield. The IR spectrum was similar to that of normal p-ATPA-7. The 600 nm absorption was absent from the

UV-VIS spectrum, indicating the absence of the quinoid rings required for conductivity. The UV-VIS spectrum of a sample treated with oxygen for 20 hours was unchanged. Unlike ATPA-7, m,p-ATPA-7 apparently resists further oxidation.

Methoxy-Substituted ATPA-7 (MeO-ATPA-7): This oligomer was obtained in 62% yield as a black powder. It was more soluble in acetone and methanol than other ATPA-7s, which may provide better solvent processability. The IR spectrum supported the proposed structure and indicated the presence of N-H, C=C-H, CH_3O (2923 cm^{-1}), quinoid (1606 and 1599 cm^{-1}), and benzenoid (1502 cm)$^{-1}$ groups. A dilute, light purple solution in DMF produced a UV-VIS spectrum having absorption peaks at 284 nm and 513 nm. Doping with concentrated HCl caused a small shift to 581 nm. This is in contrast to the larger shift and color change from blue to green that occurred when a DMF solution of ATPA-7 was acidified with HCl.

Dianisidine ATPA-7 (DA-ATPA-7): This material was obtained in rather low yield (34%) as a light gray solid. The reaction was carried out at 110°C for one week before addition of EA, further reaction for 4 days at 65, and exposure to air. The IR and ^1H NMR spectra support the proposed structure shown in Figure 52, but also indicate the presence of some unreacted carbonyl groups. The product was partly soluble in chloroform and acetone and very soluble in DMF and DMSO. A dilute solution in DMF was almost colorless and gave a maximum UV-VIS absorption at 353 nm.

3.2.2 Characterization of Oligomers

Several techniques were used to characterize the oligomers synthesized. The most commonly used techniques were IR and UV-VIS spectroscopies. NMR was used to a lesser

extent, and mass spectrometry (MS), TGA, ESR were only used in selected samples. The results are described below:

IR and UV-VIS Characterization of ATPAs Prepared Using MHW Approach: The FTIR spectrum from ATPA-7 in KBr is shown in Figure 58 and is very similar to that of polyaniline [37]. A more detailed examination of the FTIR of ATPA-7 and UV-VIS spectra of ATPA-9 in

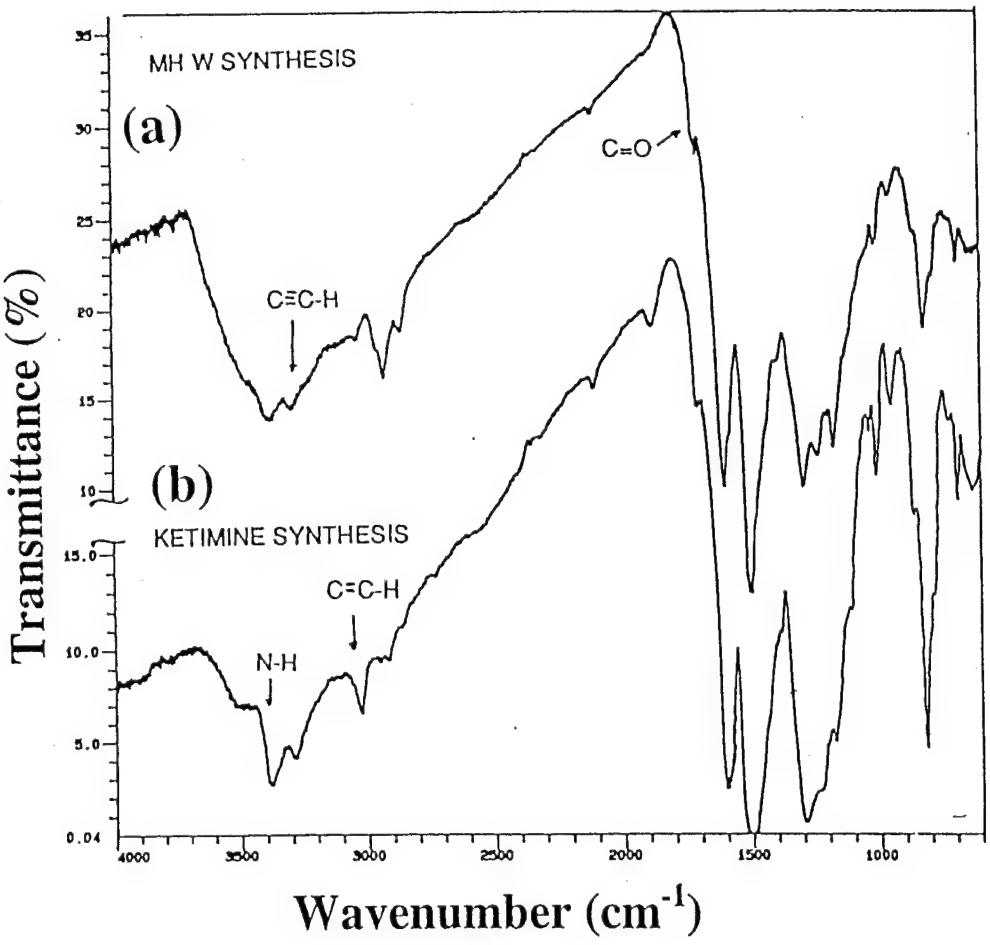

Figure 58. IR spectra recorded from acetylene-terminated polyaniline oligomers: (a) ATPA-7 synthesized using the MHW approach. Peak at 2900 cm^{-1} indicates some residual CH_2 present (i.e., this particular sample was not fully aromatized) and (b) ATPA-7 synthesized using the MK approach.

DMF shown in Figure 59 indicated that ATPA synthesized by the MHW method contained mostly benzenoid units (1502 cm^{-1}, λ_{max} = 300 nm) and some quinoid units (1600 cm^{-1}, λ_{max} = 610 nm). The presence of N-H (~3380 cm^{-1}) and the absence of C=O (1717 cm^{-1}) in the-IR spectrum was additional evidence that the reaction product had a polyaniline-type structure. Absorption at 3290 cm^{-1} confirmed the presence of the terminal ethynylbenzene groups. The IR and UV-VIS spectra of the ATPA-3, ATPA-7, and ATPA-9 were all essentially the same.

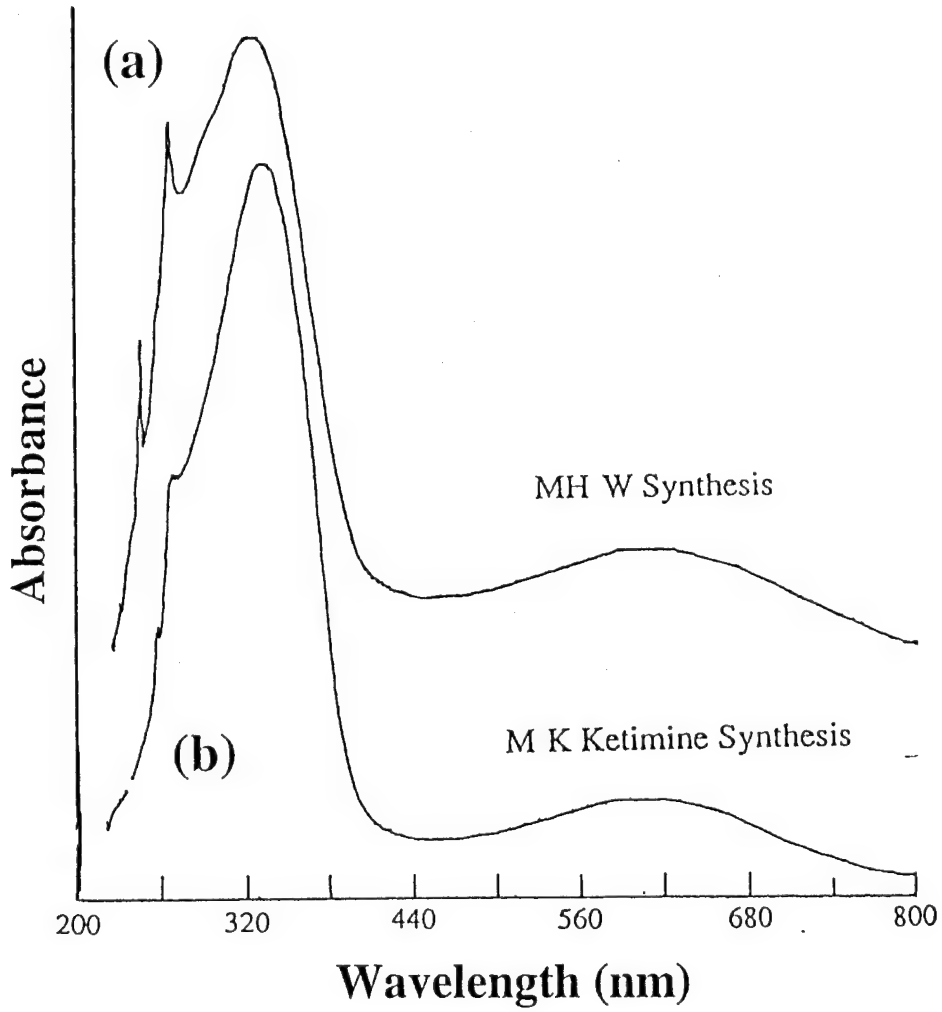

Figure 59. UV-VIS spectra recorded from acetylene-terminated polyaniline oligomers: (a) ATPA-9 synthesized using the MHW approach and (b) ATPA-7 synthesized using the MK approach. In both cases the relatively weak absorption at ~600 nm indicates the samples were only slightly oxidized.

The relative intensities of the quinoid and benzenoid peaks in the IR and UV-VIS spectra indicated that, in general, the fraction of quinoid units was lower than that required for the sample to be totally in the emeraldine oxidation state necessary for conductivity. This fraction could be significantly increased by subjecting samples to further air oxidation.

The relatively low fraction of quinoid rings in the ATPAs was consistent with the results of Wudl et al. [37], who obtained similar UV-VIS spectra from polyaniline synthesized using the MHW approach. As is shown in Figure 60, polyaniline synthesized using the conventional ammonium persulfate oxidation of aniline had a higher fraction of quinoid units.

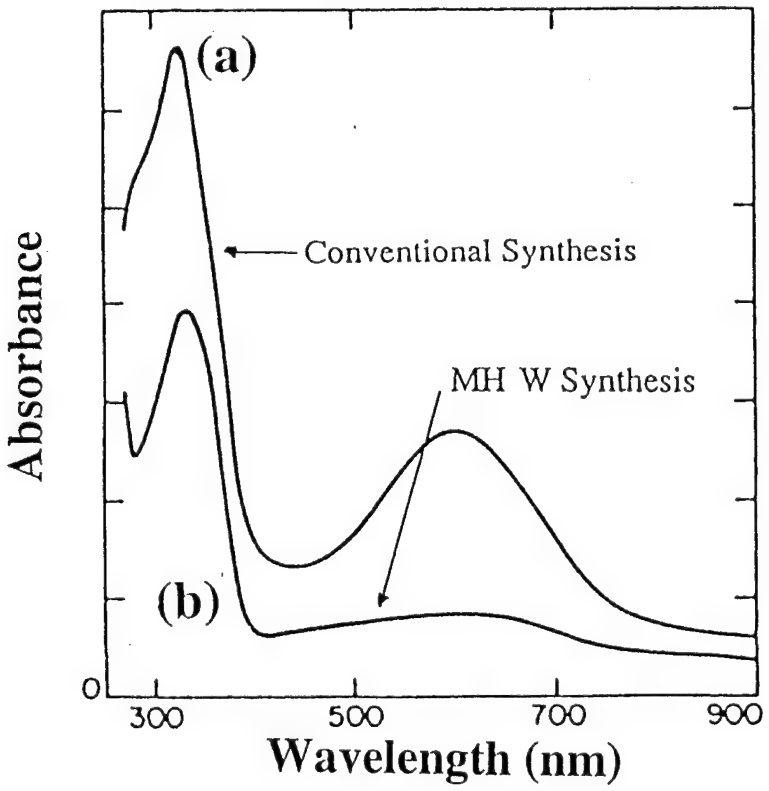

Figure 60. UV-VIS spectra of polyaniline: (a) prepared by chemical oxidation of aniline using ammonium persulfate and (b) prepared using MHW approach.

IR and UV-VIS Characterization of ATPAs Prepared Using MK Approach: The FTIR spectra in KBr and UV-VIS spectra in DMF of ATPA prepared by the MK synthesis are shown in Figures 58 and 59 respectively. These spectra indicate that these oligomers have the same structures as those synthesized using the MHW approach. The ATPA existed mostly in the leuco form. For example, the FTIR spectrum of ATPA-7 showed a ratio of 1:4 for the quinoid:benzenoid absorptions, and the UV-VIS spectrum shown in Figure 61(a) has absorptions at 328 and 600 nm with an intensity ratio of 15:1. Again this indicates a low quinoid content.

Characterization of ATPAs Using MS and TGA: The MS total-ion-current data from MHW ATPA, shown in Figures 62 and 63, indicated that MHW ATPA produced polyaniline-type fragments upon pyrolysis.

The TGA derivative plots of ATPA synthesized by both the MHW and the MK techniques, shown in Figures 62 and 64, looked similar to the above MS data. These results indicated that not only MHW ATPAs, but also MK ATPAs had polyaniline-type structures.

IR and UV-VIS Characterization of COA: The COA had FTIR and UV-VIS spectra similar to the ATPAs, except that no C-H peak appeared at 3290 cm^{-1} in the IR spectrum of the COA shown in Figure 65. The UV-VIS spectrum of Figure 57, which has only weak quinoid absorption at 592 nm, indicates that the as-synthesized material consisted of only slightly oxidized oligomer. The FTIR spectrum shown in Figure 65 confirmed this low oxidation state. There is only a weak quinoid peak at 1599 cm^{-1} compared with the stronger benzenoid peak at 1501 cm^{-1} (1:4 ratio). Figure 66 shows a literature IR spectrum [40] of fully oxidized pernigraniline for comparison. In this case the quinoid to benzenoid peak ratio was approximately 1:1.

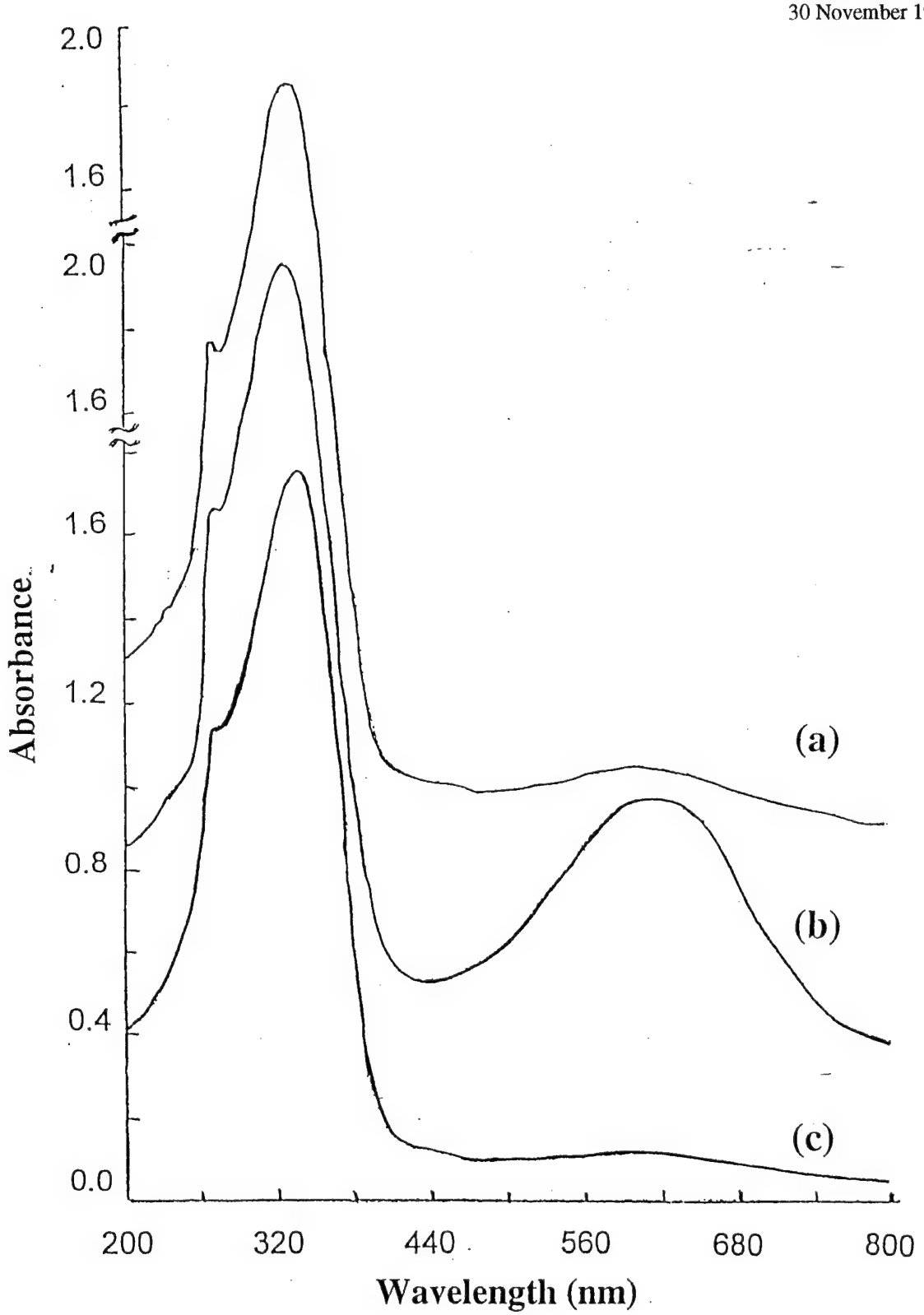

Figure 61. UV-VIS spectra of ATPA-7(MK): (a) as-synthesized, (b) following oxidation with O_2, and (c) following reduction with phenylhydrazine.

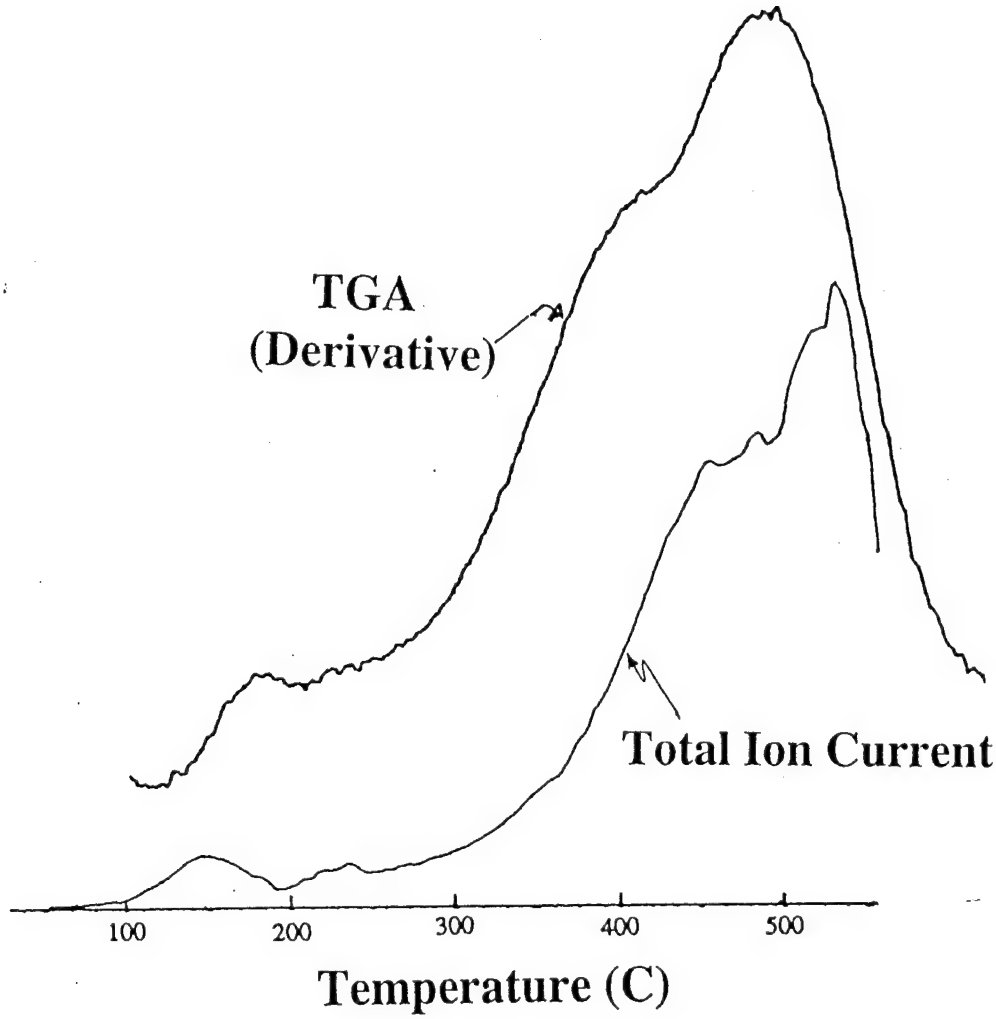

Figure 62. TGA (derivative) and mass-spectrum total ion current from ATPA prepared using MHW approach.

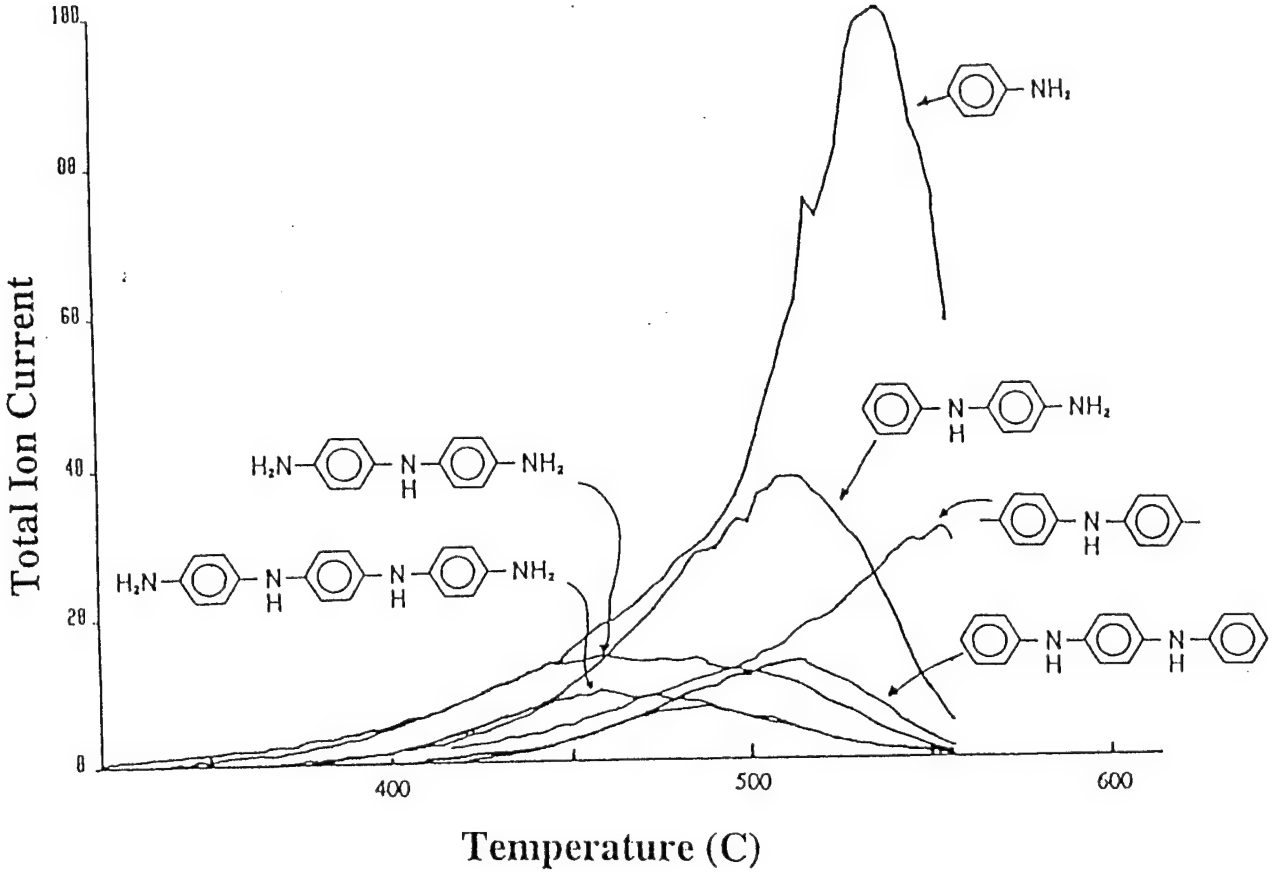

Figure 63. Fragments contributing to mass-spectrum total ion current from ATPA prepared using MHW approach.

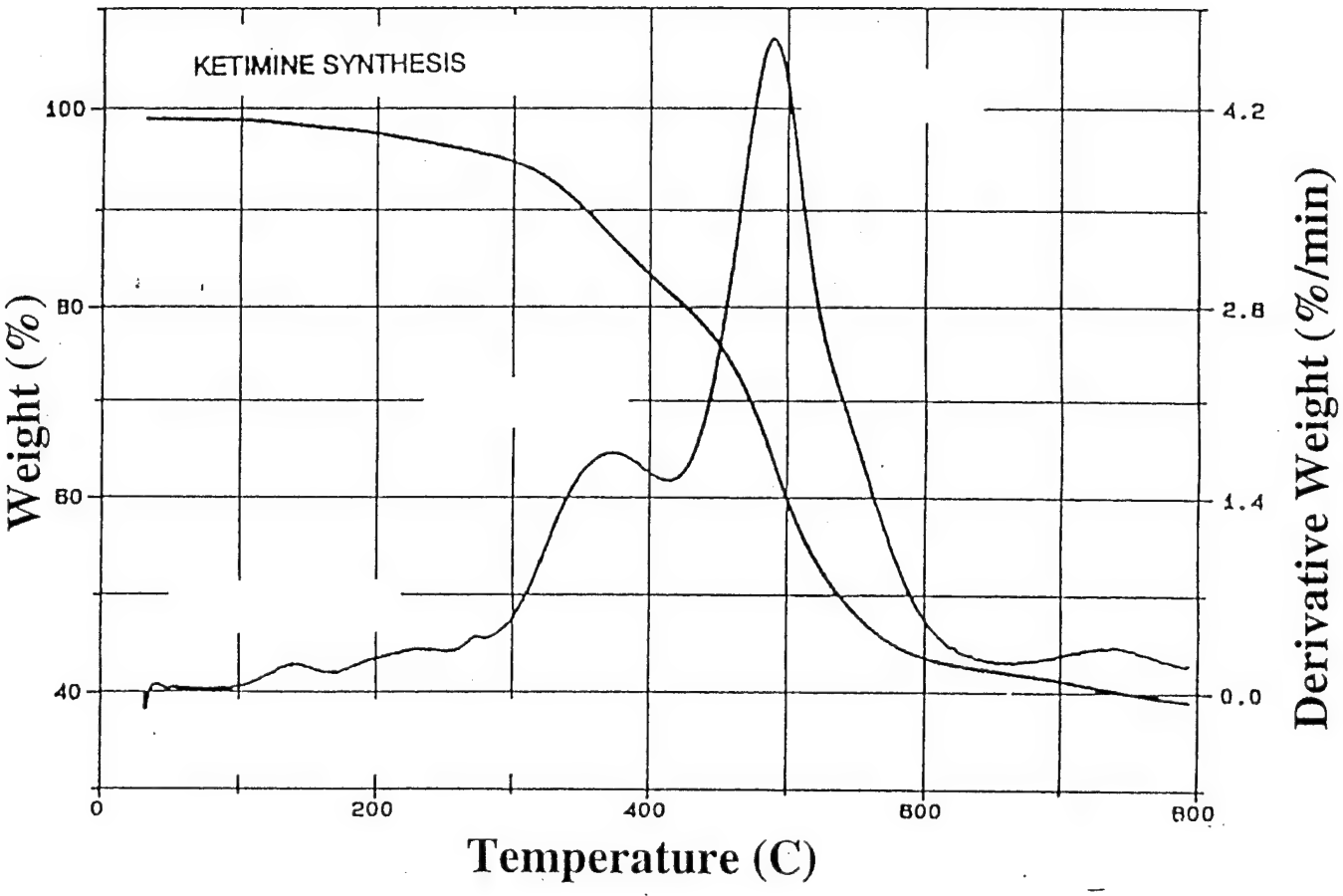

Figure 64. TGA from ATPA-7 prepared using MK approach.

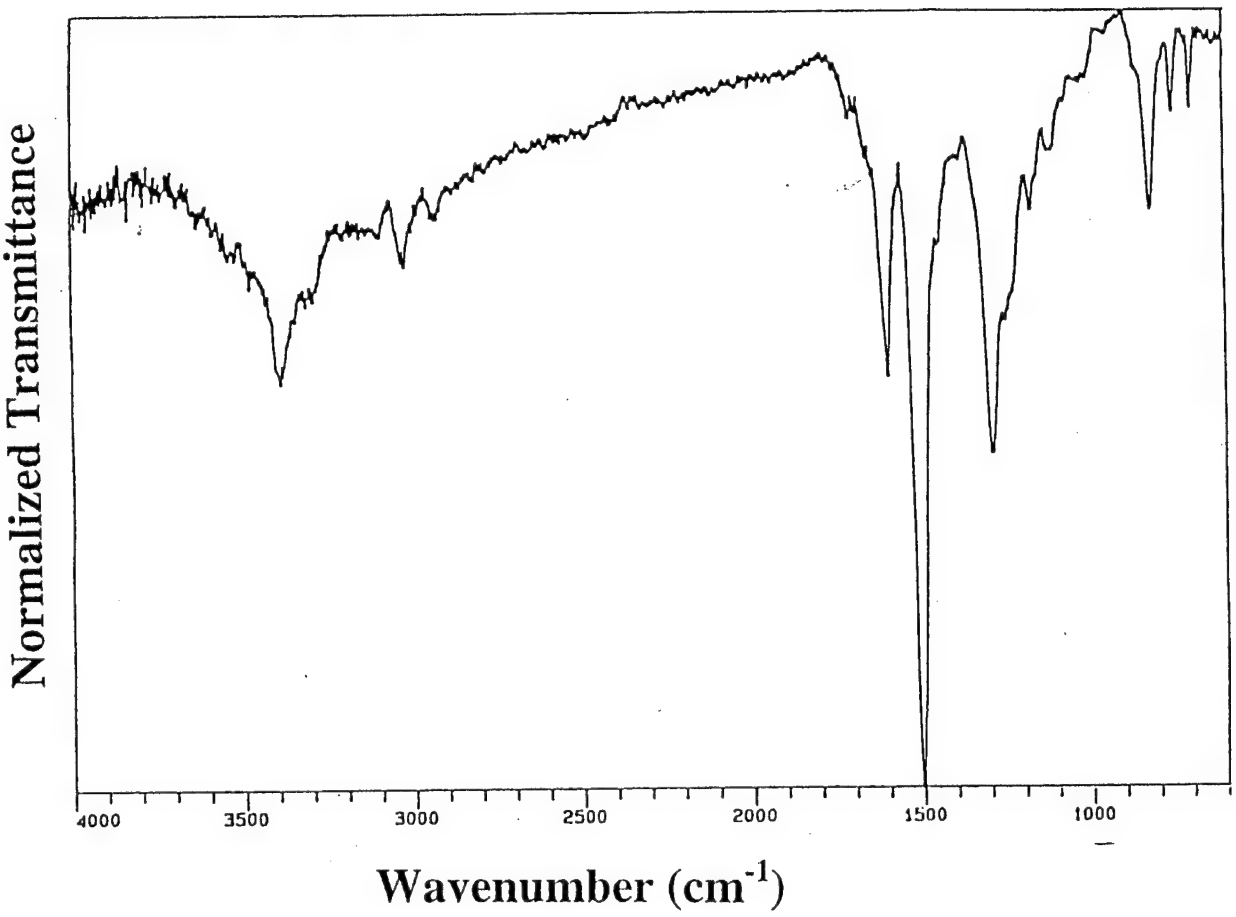

Figure 65. IR spectrum from phenyl-capped aniline oligomers (COA) prepared using MK approach. Weak peak at ~1600 cm^{-1} indicates a low concentration of quinoid rings (i.e., low oxidation) in the sample.

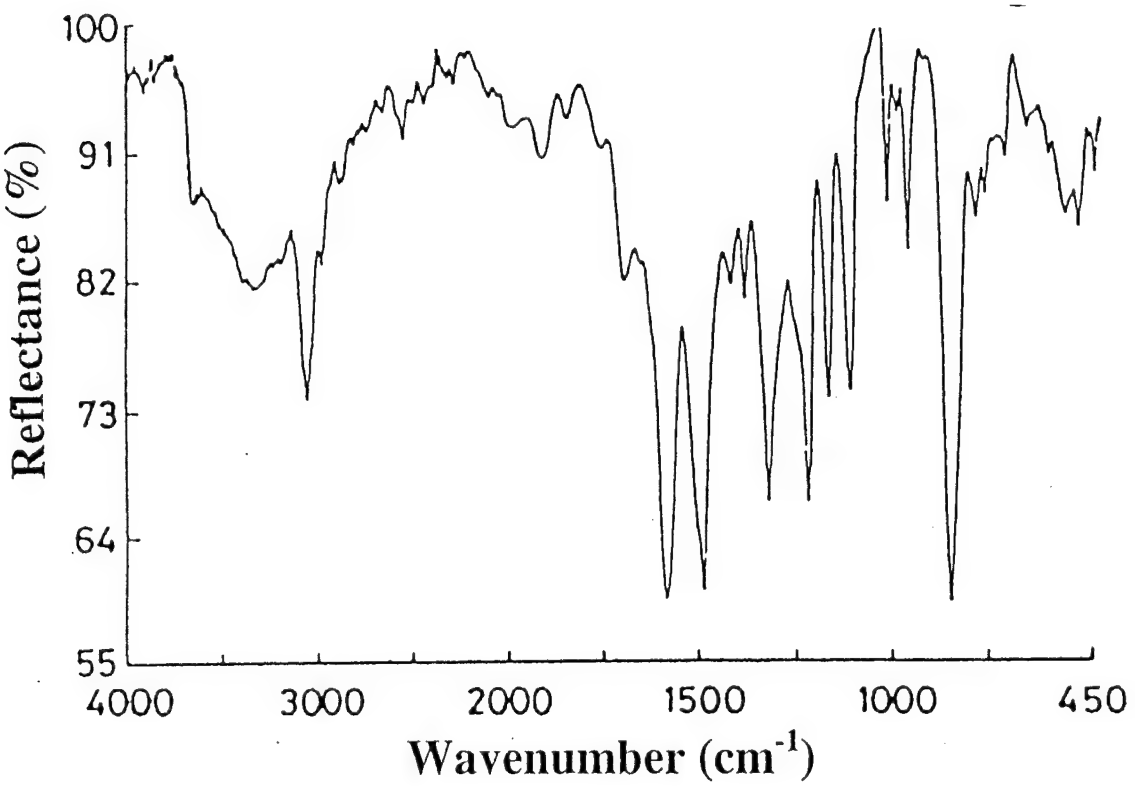

Figure 66. IR spectrum from fully oxidized polyaniline (i.e., pernigraniline state), with equal numbers of quinoid (Q) and benzenoid (B) rings in the sample.

ESR Measurements of uncured ATPA and COA: Samples examined by ESR were in the form of doped and undoped powders. Typical spectra are shown in Figures 67 and 68, with linewidth and intensity data reported in Table 3. The integrated intensities did not depend significantly on whether the MHW or MH approach was used for sample synthesis. In each case the intensities increased by a factor of ~25 upon doping with HCl. Conductivity of the doped

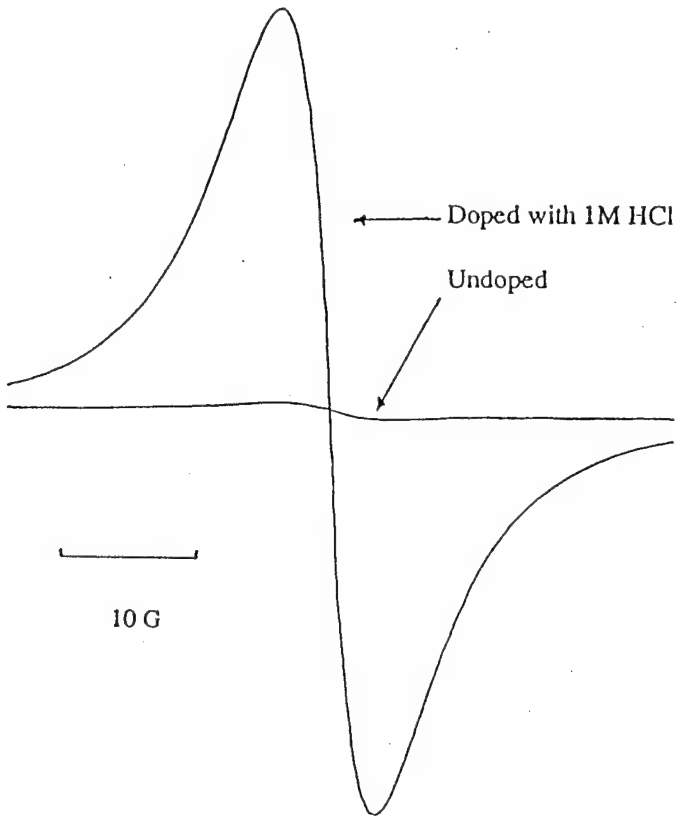

Figure 67. ESR spectra from undoped and HCl-doped ATPA prepared using MHW approach.

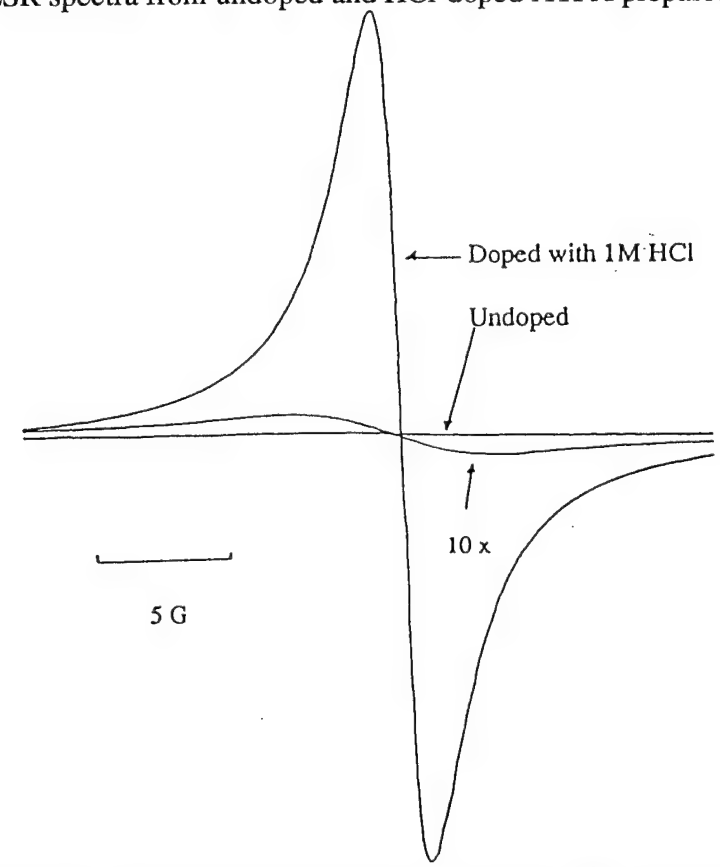

Figure 68. ESR spectra from undoped and HCl-doped ATPA prepared using MK approach.

Table 3. ESR Parameters for Uncured Aniline Oligomers.

Sample*	Doped Relative Intensity	Doped Intensity / Undoped Intensity	Doped Linewidth (mT)	Conductivity (S/cm)
ATPA-7(MK)	14.6	28	-	10^{-2}
ATPA-7(MK)	-	-	0.15	$4x10^{-3}$
ATPA-3(MK)	23.4	20	0.26	$2x10^{-3}$
COA(MK)	-	-	0.70	$4x10^{-4}$
ATPA-7(MHW)	17.6	48	0.80	$<10^{-5}$

*MK and MHW refer to Manassen Khalifand Modified Honzl-Wudls yntheses procedures.

samples correlated with ESR linewidth, but not with signal intensity. The most conductive samples had the narrowest ESR lines. This is consistent with highly delocalised electrons having narrow ESR lines.

Electrochemical Determination of Oxidation State of ATPA-7: Following the procedure of MacDiarmid et al. [41], a sample of ATPA-7 was mixed with powdered carbon (3:2 ratio), pressed between platinum and zinc electrodes, and immersed in 1 M zinc chloride electrolyte. The sample was then reduced over a period of 8 h using a constant current of 100 microamps. As is shown in Figure 69, during reduction the potential at first decreased only gradually, but when reduction was nearly complete, the potential changed more rapidly. The total charge required to reduce the sample was determined from the point where the potential began to change rapidly. From the total coulombs passed and the initial mass of the sample, it was determined that the sample was in an oxidation state intermediate between leucoemeraldine and emeraldine. Thus, if pernigraniline, emeraldine, and leucoemeraldine correspond to 0%, 50%, and 100% reduction, respectively, the ATPA-7 sample was 60% reduced. These data are consistent with UV-VIS data which indicated that as-synthesized ATPA-7 is typically in a low oxidation state.

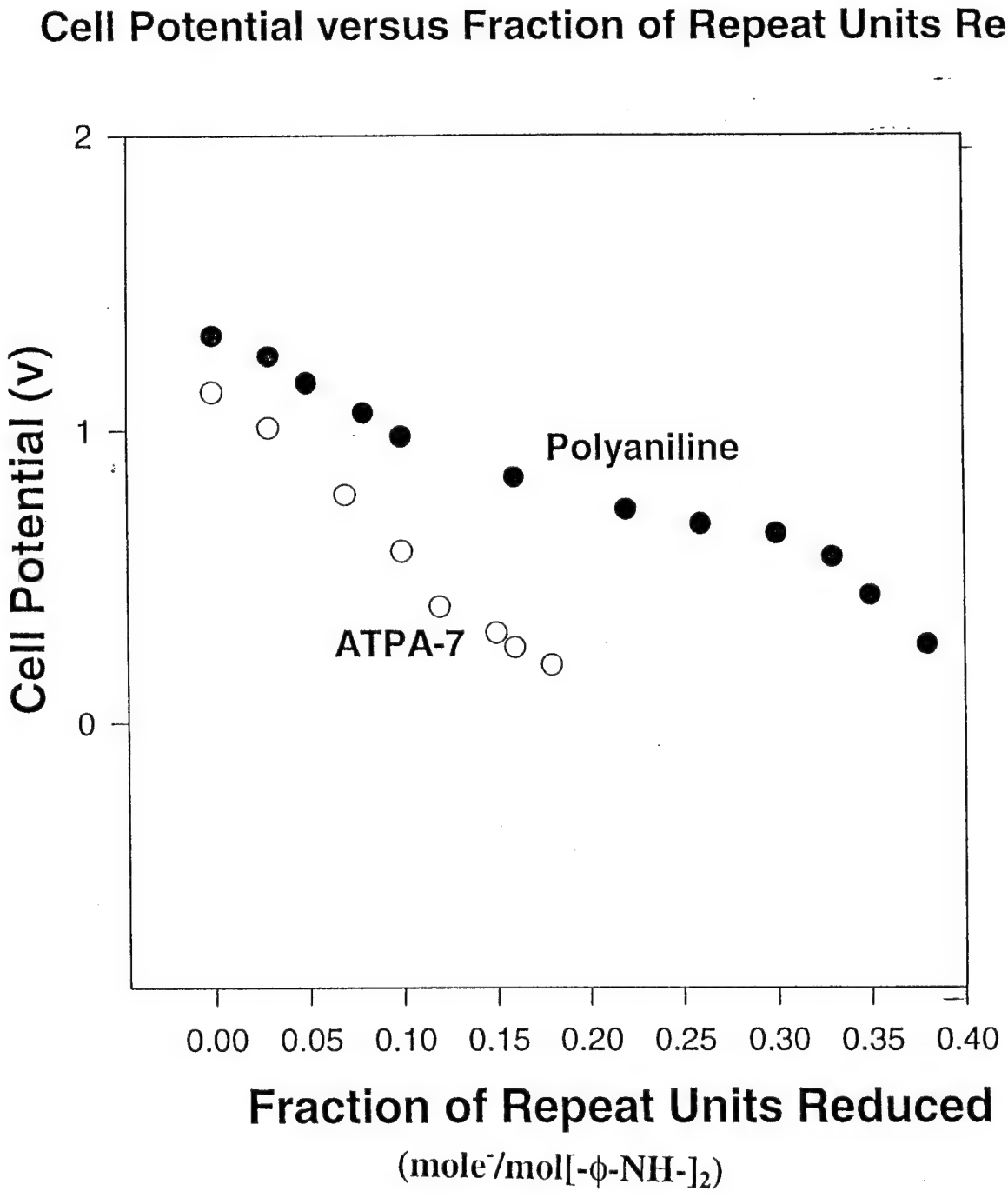

Figure 69. Electrochemical cell potential as a function of fraction of repeat units reduced for (a) Conventional polyaniline, and (b) typical as-synthesized ATPA-7(MK). Note a value of 1.0 refers to one electron deposited for every aniline repeat unit in the chain. Emeraldine would be completely reduced upon reaching a value of 0.5.

NMR Characterization of ATPA and COA: NMR experiments focused on answering two questions: (1) What was the degree of polymerization of a typical ATPA-7 sample, and (2) was the sample completely aromatized? Prior to NMR analysis, samples were reduced with phenylhydrazine both to assure good solubility in DMF and to simplify the spectra. A typical result is shown in Figure 70, which includes spectra of reduced COA and reduced ATPA-7. Comparison of the two spectra suggests that the acetylenic hydrogen peak occurs at 4.0 ppm. The ratio of the area of this peak (8 units) to the area of the aromatic region (125 units) indicates a degree of polymerization (DP) of 28. The reason for this apparent high DP may be that partial reduction of the acetylene groups had occurred.

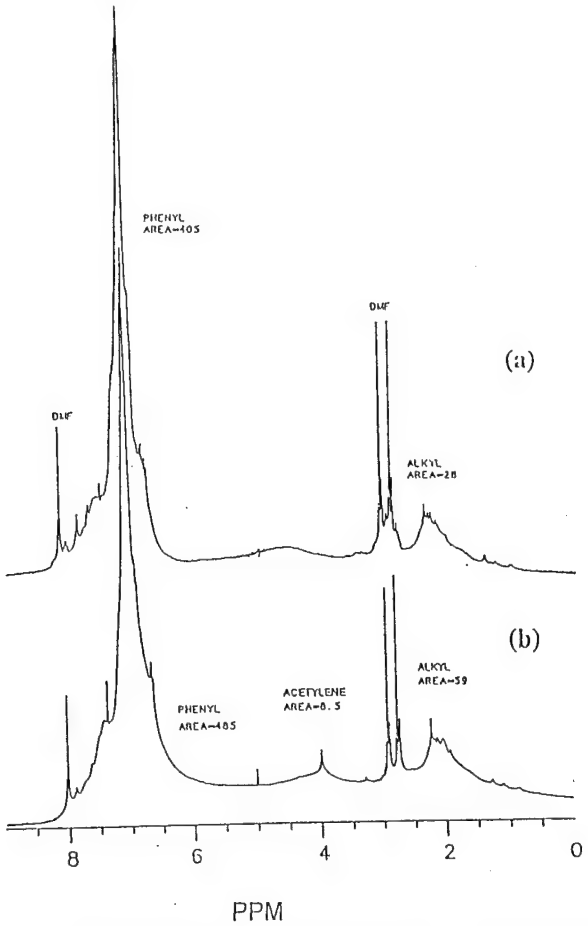

Figure 70. ^{1}H NMR spectra of ATPA-7(MK) and COA(MK), both following the reduction with phenylhydrazine. (a) COA(MK) and (b)ATPA-7(MK).

Both the COA and ATPA-7 NMR spectra have peaks in the aliphatic region, indicating that these materials are not fully aromatized. Low aromatization should result in reduced conductivity for these samples, which is consistent with their actual conductivity data (see below). The literature suggests using o-chloranil to accomplish more complete aromatization [42].

GPC Analysis of ATPA-7 and COA: Two groups of GPC data were taken. The first group was from ATPA or COA dissolved in pure THF. The second group was from ATPA or COA dissolved in a 5% solution of di-n-butylamine (DNBA) in THF. The DNBA was used to break up any clusters of oligomer that might form. The results of both groups of experiments were the same. Figure 71(a) and Figure 72 show data from ATPA-7 in pure THF and in DNBA/THF, respectively. In both cases the molecular weights are uncorrected values, referenced to polystyrene standards. (More nearly correct molecular weights can be calculated using a GPC 'Q factor' appropriate for aniline-type oligomers. According to Wei et al. [43], a typical Q factor for these materials would be 2.5.) Figure 72 indicates that ATPA-7 oligomers have (uncorrected) molecular weights that range from 500 to 7500. This distribution yields a number-average molecular weight (M_n) of ~1270, and weight-average molecular weight (M_W) of ~5000. Average molecular weight values calculated from three separate ATPA-7 samples are: M_n = ~1250 and M_W = ~4550. The values of M_n appear to be consistent with the stoichiometry of the synthesis, which should yield ATPA having a nominal M_n of ~900.

Three factors affect the quality of this data: (1) The highest molecular weight fractions of the ATPA samples were at, or beyond the upper limits of resolution for the GPC column (the column was calibrated for M_n = 7600). This tends to underestimate the molecular weights of the ATPA-7 samples. (2) Application of the literature Q value (= 2.5) suggests a M_n of only 500,

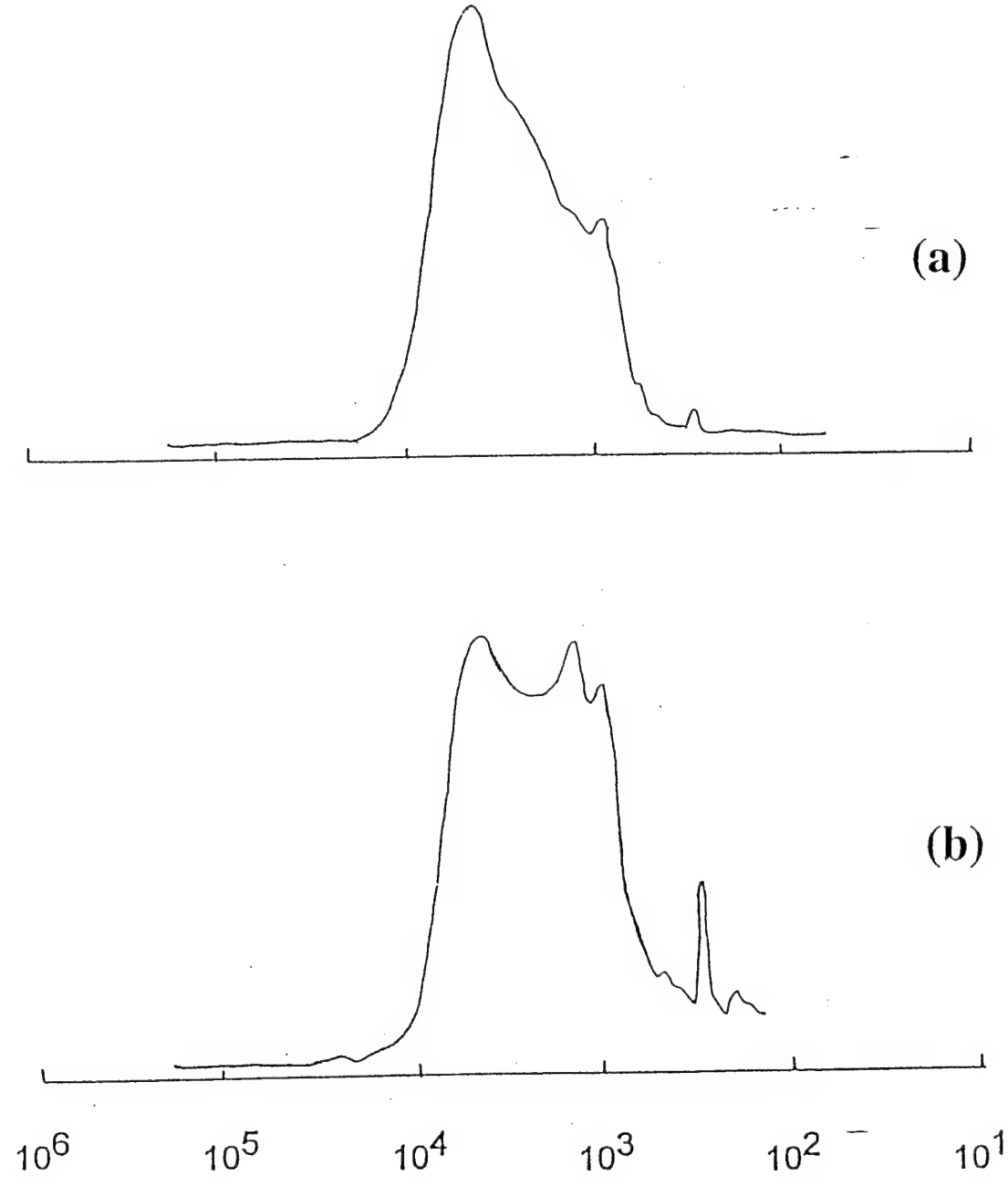

Figure 71. GPC chromatograms for ATPA-(MK) prior to and following reduction using phenylhydrazine. (a) Before reduction and (b) after reduction.

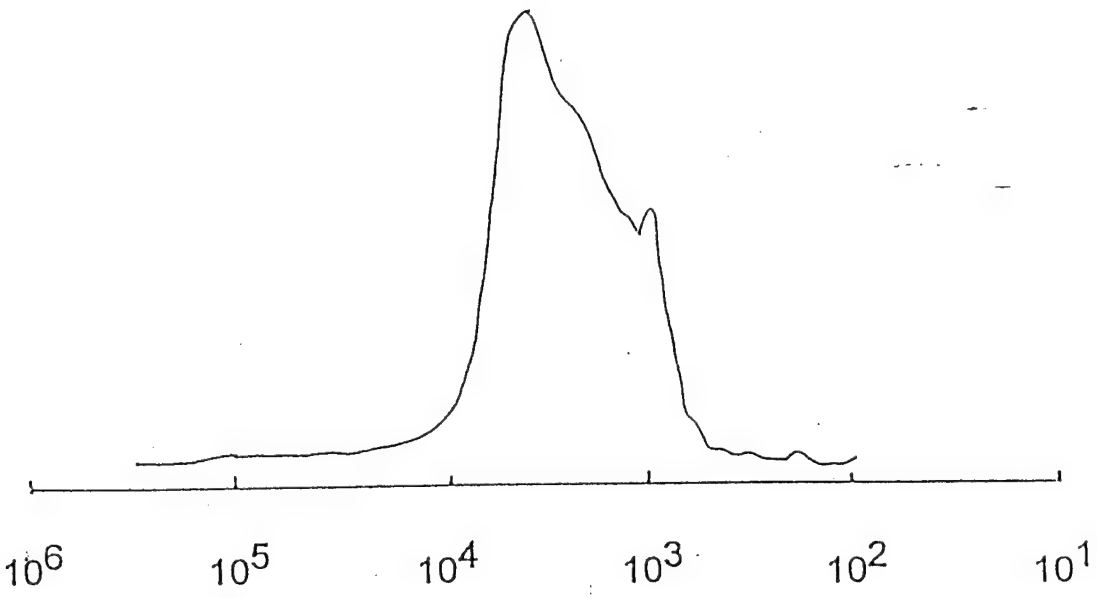

Figure 72. GPC chromatogram for ATPA-(MK) in 5% DNBA/THF.

indicating that our uncorrected M_n value of 1250 is an overestimate of the true M_n and (3) Any fraction of ATPA-7 that is not soluble in THF is not part of the GPC chromatogram. This would make our observed M_n value an underestimate of the true M_n value. GPC analysis employing a better solvent, such as DMF, was not available.

Overall, it appears that as-synthesized ATPA-7s could have molecular weights higher than the theoretical M_n value of ~900. However, handling of the crude ATPA-7 can dramatically affect the molecular weight of the final product. For example: (1) Low molecular weight fractions could easily be lost during rinsing or during the dissolution-reprecipitation work-up and doping steps. (2) A partial polymerization of some acetylene groups during synthesis could result

in increased molecular weight. (3) Finally, as is shown in Figure 71, a significant increase in lower molecular weight fractions between 1000 and 1200 occurred upon reduction with phenylhydrazine. This could be due to chain degradation resulting from carbon-nitrogen bond cleavage occurring during the reduction with phenylhydrazine (24 h at 115°C). Walls and Caballero [44] have reported the cleavage of N-benzylamines by hydrazine.

3.2.3 Conductivity Studies

A conductivity apparatus having an in-line 4-probe configuration was used. The two outer probes were connected to a floating (battery powered) current source, and the two inner probes were connected to a Keithley 610B electrometer. Conductivity values from ~1 to ~10^{-11} S/cm could be measured with this apparatus. Prior to conductivity measurement, samples weighing 100 to 150 mg were pressed (570 MPa; 82 ksi) into pellets having a thickness of ~0.8 mm and a diameter of 1.0 cm.

Conductivity Studies of ATPA(MHW), ATPA(MK), and COA(MK) Doped With HCl: Samples of ATPA and COA were subjected to the same doping procedures prior to the measurement of their conductivity. The samples were first brought to initial undoped states by grinding them into fine powders, followed by treating with a 10% ethanol/90% 0.1 M NH_4OH or NaOH solution for several hours and drying by suction filtration. These powders were then doped using either of two different methods. In the first method, they were dissolved in NMP, filtered, and reprecipitated by pouring into an equal volume of 0.1 to 1.0 HCl solution. The resulting suspension was then centrifuged or filtered using a glass frit, and the polymer was washed several times with HCl solution and allowed to dry. In the second doping method, an undoped powdered sample was triturated in a mortar with 0.1 to 1.0 M HCl in 10% ethanol/90%

water. It was then allowed to stand several hours, filtered, and dried. The powder, generally emerald-green, obtained from either method was then pulverized and pressed into pellets for conductivity measurements.

Table 4 summarizes the conductivity data obtained for several HCl-doped samples of ATPA and COA. The following points should be noted: (i) the highest conductivity observed was $2x10^{-2}$ S/cm, (ii) the COA and ATPA samples had similar conductivity values, (iii) treatment of a typical sample (a COA sample in particular) with O_2 increased its conductivity by a factor of 50.

Table 4. Conductivity of Doped Uncured Oligomers.

Sample#	Treatment*	Conductivity (S/cm) (Doped with HCl)	Conductivity (S/cm) (Doped with Tosylate)
ATPA-3(MK)	Unspecified	$2x10^{-3}$	$5x10^{-4}$
ATPA-3(MK)	m&p	-	$5x10^{-3}$
ATPA-7(MK)	m&p	-	$2x10^{-4}$
ATPA-7(MK)	ppt.	$4x10^{-3}$	$3x10^{-4}$
ATPA-7(MK)	0.1 M HCl-ppt.	10^{-2}	-
COA-7(MK)	0.1 M HCl-ppt.	$4x10^{-4}$	-
COA-7(MK)	Bubbled with O_2 0.1 M HCl-ppt.	$2x10^{-2}$	-

*Samples were doped either by reprecipitation from NMP or DMF solution (ppt) or samples were ground in a mortar while covered with the doping solution (m/p).
#MK refers to Manassen Khalif synthesis procedure.

The above conductivity values are ~50 times lower than were anticipated. For example, Wudl, et al. [37,39], obtained a conductivity as high as 1.0 S/cm from monodisperse octameric COA in the emeraldine oxidation state. Possible reasons for the low conductivity values of the present samples include the following: (1) Low molecular weight oligomers resulted from the

'one pot' synthesis used. Calculations show that over 20% by weight of the as-synthesized (not-extracted) material is attributable to oligomers shorter than octamers. According to Javadi et al. [45], tetramers are poorly conducting. (2) The samples were incompletely aromatized, as implied by NMR characterization data. (3) The samples were incompletely oxidized, as implied by UV-VIS and FTIR data. (4) Other impurities may have been present.

Conductivity of HCl-Doped Samples Having Modified Backbone Structures: Samples of m,p-polyphenyleneamineimine (m,p-PPAI; m,p-polyaniline), methoxy-substituted polyaniline (MeO-PPAI; poly(aniline-co-anisidine)), and m,p-ATPA-7 were doped with HCl using either of the following two approaches used for ATPAs and COA: (1) reprecipitation from NMP or DMF solution into aqueous HCl, or (2) trituration of powdered sample with 0.1 to 1.0 HCl in ethanol/water. The results are discussed below:

m,p-PPAI Doped With 0.1 M HCl in 5% Ethanol/95% Water: Conductivity values were significantly less than those from PPAI (i.e., para-polyaniline) prepared using the same MK approach. As is shown in Table 5 the highest conductivity obtained was 10^{-8} S/cm.

m,-ATPA-7 Doped By Pouring DMF Solution Into 1 M HCl: A dark green solid precipitate resulted. As is shown in Table 3, its conductivity was $2x10^{-8}$ S/cm.

MeO-PPAI Doped With 0.1 M HCl in 5% Ethanol/95% Water: The conductivity of this sample was 10^{-9} S/cm, much lower than observed for unsubstituted PPAI or ATPA-7. (See Table 5.) According to Pandy et al. [46], a random copolymer of aniline and anisidine has a conductivity of ~10^{-4} S/cm.

In summary, all of the modified-backbone samples had lower conductivity than the corresponding unmodified PPAI or ATPA-7. This lower conductivity may be intrinsic to these

Table 5. Doping and Conductivity of Polyaniline Derivatives and Uncured Oligomers.

Sample*	Doping#	Conductivity (S/cm)
Polymers:		
PPAI (MK)	1.0 M HCl-ppt	10^{-2}
(m,p-PPAI) (MK)	0.1 M HCl-m/p	$3x10^{-7}$
(MeO-PPAI) (MK)	0.1 M HCl-m/p	10^{-9}
Oligomers:		
ATPA-7 (MK)	1.0 M HCl-ppt	$1.3x10^{-2}$
m,p-ATPA-7 (MK)	0.1 M HCl-m/p	$2x10^{-8}$
MeO-ATPA-7 (MK)	0.1 M HCl-m/p	$<10^{-11}$

*MK refers to Manassen Khalif synthesis procedure.
#Samples were doped either by reprecipitation from NMP or DMF solution (ppt) or samples were ground in a mortar while covered with the doping solution (m/p).

modified structures, or may be a result of the modified materials being in non-emeraldine-like oxidation states under ambient conditions. Pandy et al., maintain that PPAIs having some methoxy substitution remain conductive, but the conductivity is reduced [46].

Doping ATPAs With Alternative Dopants for Improved Processability and Thermal Stability: Even though HCl is a good dopant for polyaniline, it was not a good dopant for the acetylene-terminated polyaniline oligomers. Our attempts to dope cured ATPAs with HCl failed, apparently because of its inability to penetrate the cured matrix. In addition, the high melting point of ATPAs made it difficult for them to cure without first being plasticized with appropriate curing agents. Therefore an alternative doping approach was required. Oligomers had to be doped prior to curing. Several dopants having a much lower volatility than HCl were investigated. These included tosylic acid, camphorsulfonic acid (CSA), dodecylbenzenesulfonic acid (DBSA), and benzenedisulfonic acid (BDSA). The results of these doping studies are described below.

Doping of ATPAs With Tosylic Acid: The conductivity of the samples doped with tosylic acid are shown in Table 4. Two doping approaches were used: First, a tosylic acid solution was used to precipitate ATPA out of NMP/H_2O solution. Second, solid ATPA was covered with a solution of dopant having pH = 2 to 3, then dried by suction filtration. The ATPAs had initial conductivity's as high as $4x10^{-3}$ S/cm.

The thermal stability of an ATPA-3 sample having an initial conductivity of approximately 10^{-3} S/cm, is shown in Figure 73. Over a period of 17 h at 150°C the conductivity decreased 2 orders of magnitude. The sample showed evidence of being cured following this procedure in that it became hard, and when ground up it was only slightly soluble in NMP, showing a fainter blue solution than the uncured material.

Doping of ATPAs With CSA: Two ATPA-7 samples were doped with camphorsulfonic acid (CSA). In one case, a powdered sample was exposed to a 0.2 M solution of CSA in 5% ethanol/95% water solution, and in the second case an ATPA-7 sample was dissolved in NMP, then precipitated by pouring this solution into 0.2 M CSA. The sample that was doped as a powder was hard and had lower conductivity. The sample doped by precipitation was soft and had higher conductivity. Following heating to 150°C and cooling to room temperature it became soft enough for the spring loaded conductivity probes to penetrate the surface, particularly when humidity was high. Conductivity as a function of exposure time at 150°C is shown in Table 6. These curing studies of the CSA-doped sample indicate that the conductivity drops rapidly within the first hours of cure.

Doping with DBSA: According to Wang and MacDiarmid [47], it is possible to dope polyaniline with dodecylbenzenesulfonic acid (DBSA) and cast these samples from xylene to

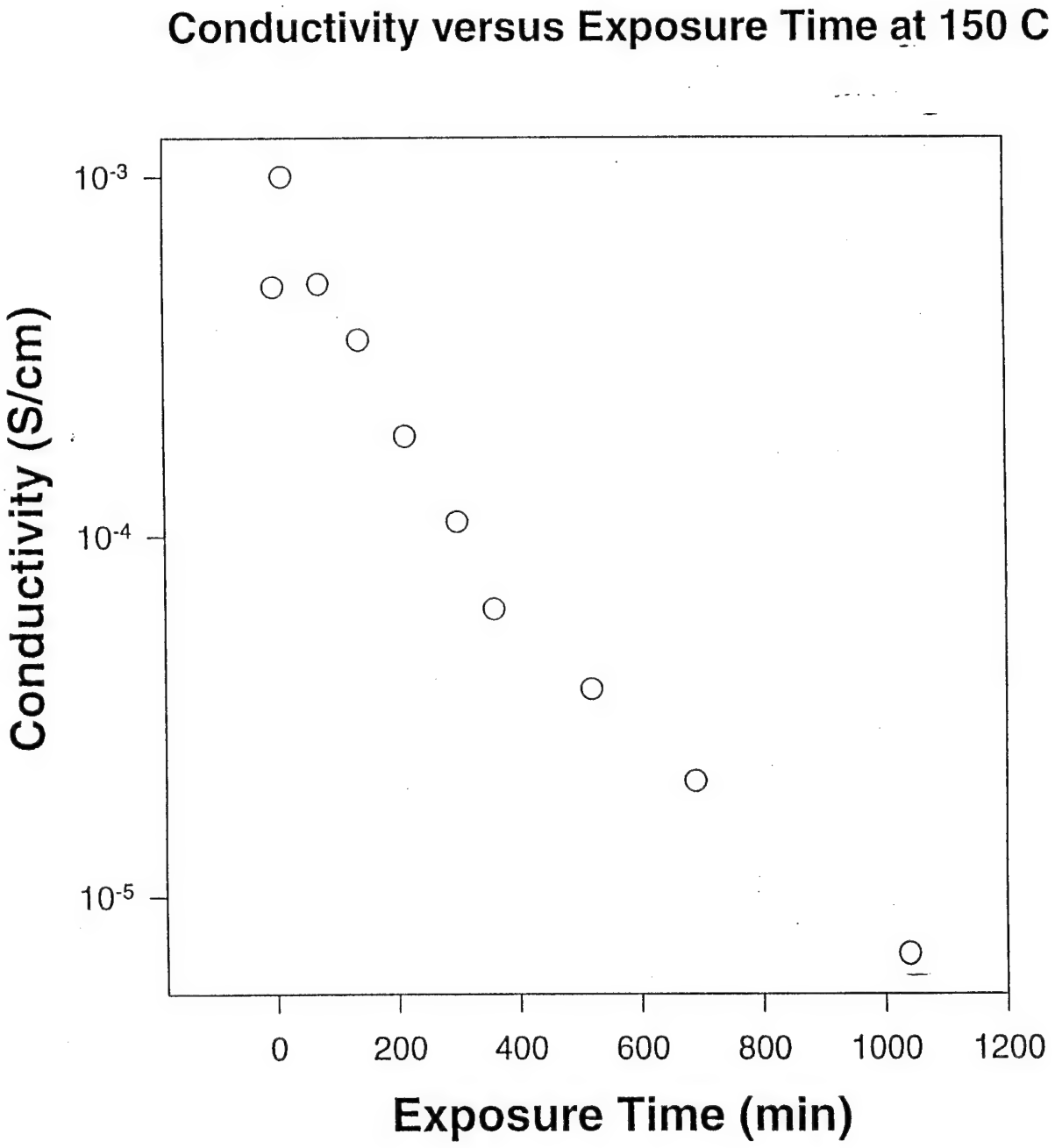

Figure 73. Conductivity (4-point probe) of tosylic acid-doped ATPA-3(MK) measured as a function of time at 150°C.

Table 6. Conductivity of ATPA-7 (MK)[$] Doped with 0.2 M Camphorsulfonic Acid versus Cure Time.

Type of Doping[+]	Time at 150°C (min.)	Conductivity (S/cm)
ppt.	0	na - sample too soft
	25	$1.2x10^{-5}$ -
	54	$4.5x10^{-8}$
	129	$9x10^{-7}$ to 10^{-3*} –
	1200	$6x10^{-9\#}$
m/p	0	na - sample too soft
	25	$1.2x10^{-6}$
	54	$6x10^{-7}$
	129	-
	1200	$<10^{-9}$

*Conductivity increased with room temperature humidity and probe penetration.
[#]Sample became harder, possibly from reduced humidity.
[+]Samples were doped either by reprecipitation from NMP or DMF solution (ppt) or samples were ground in a mortar while covered with doping solution (m/p).
[$]Mk refers to Manassen Khalif synthesis procedure

obtain a conductivity as high as 20 S/cm. Therefore highly conductive samples were expected using this approach. The doping procedure involved dissolving a sample in xylene containing 40% DBSA, followed by heating to 100°C for one day to drive off xylene. This left a gelatinous material which was subsequently triturated with water to leave a filterable solid. The solid was finally rinsed with 0.2 N DBSA and dried. A pellet of DBSA-doped PPAI that had been previously oxidized with $(NH_4)_2S_2O_8$ (see below) had a conductivity of only 2×10^{-4} S/cm, compared with 10^{-3} S/cm from HCl-doped PPAI.

Doping With Benzenedisulfonic Acid (BDSA): According to the patent literature, polyaniline doped with this dopant remains stable at 150°C for over 48 h [48]. Therefore a 0.1 M

solution of BDSA, acquired as its disodium salt (80%; the material also contained 20% sodium sulfate) and converted to free acid using an ion exchange column, was used to dope a sample of conventional polyaniline and a sample of ATPA-7. Following this procedure, the conductivity was monitored as a function of time at 150°C. The results are shown Figure 74. The polyaniline sample had an initial conductivity of ~1 S/cm, which gradually decreased to 0.1 S/cm after 48 h at

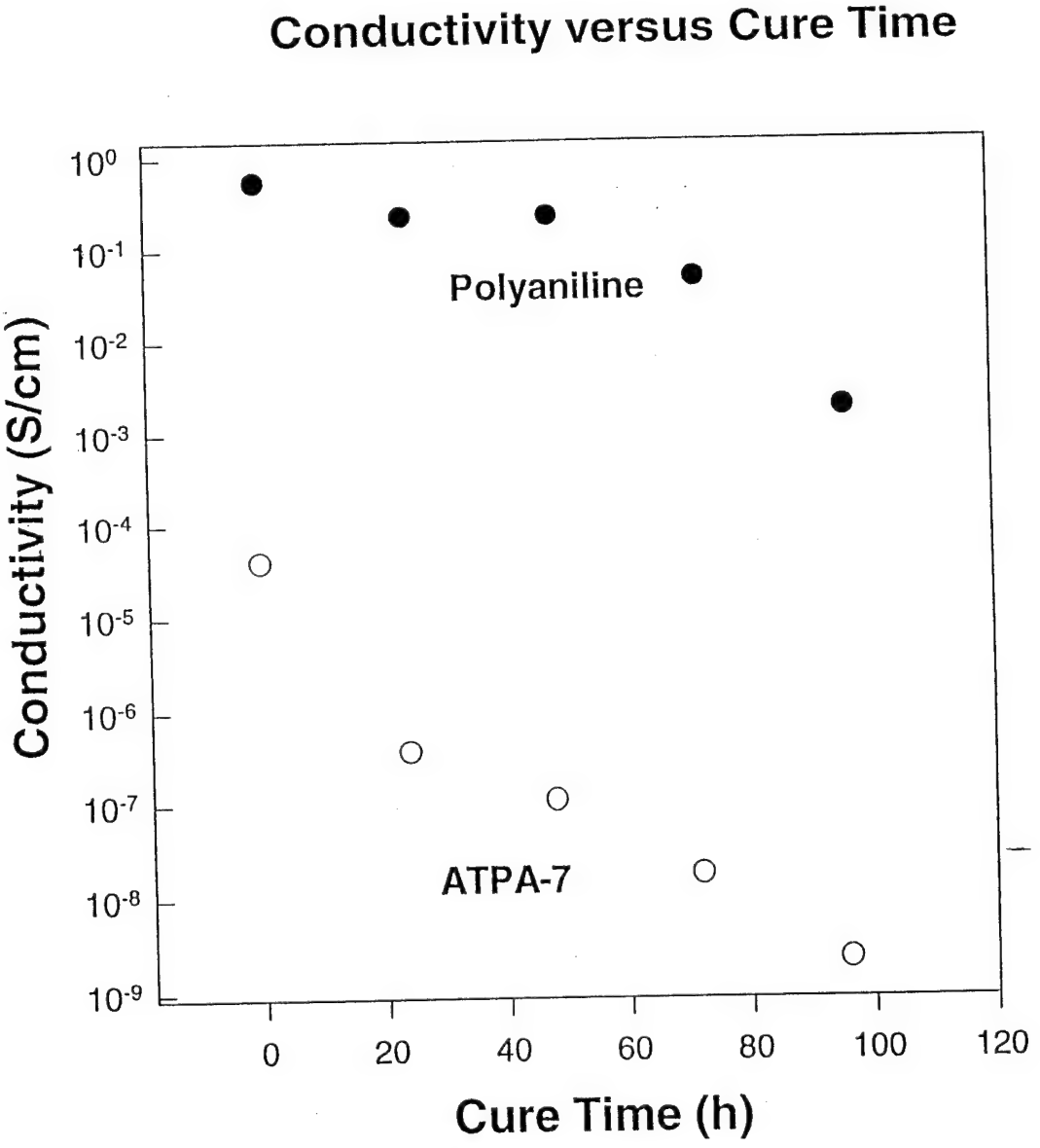

Figure 74. Conductivity of BDSA-doped polyaniline and BDSA-doped ATPA-7(MK) as a function of time at 150°C.

150°C. On the other hand, the ATPA-7 sample had an initial conductivity of only $6x10^{-5}$ S/cm, which gradually dropped to 10^{-6} S/cm after 20 h at 150°C. Thus, both BDSA-doped samples gradually decreased in conductivity with exposure to 150°C, but to a much lesser extent than conventional HCl-doped samples.

Despite its low conductivity, the BDSA-doped ATP-7 sample showed encouraging behavior in that: (1) Its conductivity dropped only to half after 2 h at 150°C and (2) prior to curing, the material was a highly processable gel, whereas following curing at 150°C for 2 h, the sample became a very hard solid. Small pieces of the cured material were so hard that they were extremely difficult to pulverize with a mortar and pestle. This behavior was in contrast to the relative ease with which typical uncured powders could be pulverized.

In summary, the sulfonic acid dopants appeared to lower the melting point of ATPA-7 below 150°C, and in the case of benzenedisulfonic acid (BDSA) the resulting cured ATPA-7 became a hard solid. The good stability of BDSA-doped polyaniline and ATPA-7 after 2 hours at 150°C shown in Figure 74, suggest that if ATPA-7 had high enough initial conductivity (e.g., 0.1 to 1 S/cm) it could be thermally processed into a useable conducting thermoset. Thus conducting thermosets from ATPA-7s should be feasible practical materials..

3.2.4 Additional Curing Studies

In addition to the curing observed when monitoring the thermal stability of conductivity in doped samples, other studies were performed focused on curing itself. Results are given below:

Curing of ATPA: ATPAs did not have visible melting points, nor did they show melting endotherms in their DSC plots. However, the effects of curing was observed in these samples. In a typical experiment, undoped powder was first pressed into a pellet and then the pellet was cured

at temperatures between 150 and 180°C for several hours. Following this procedure, pellets changed from soft powders to hard solids that were insoluble or slightly soluble in the case of 150°C cures, in NMP. Following curing of a pellet of ATPA-7, it was not possible to dope it with 1 M HCl even after days of exposure. This led to the alternative dopant studies described above.

As is shown in Figure 75, IR spectra from KBr pellets containing a few percent ATPA-7

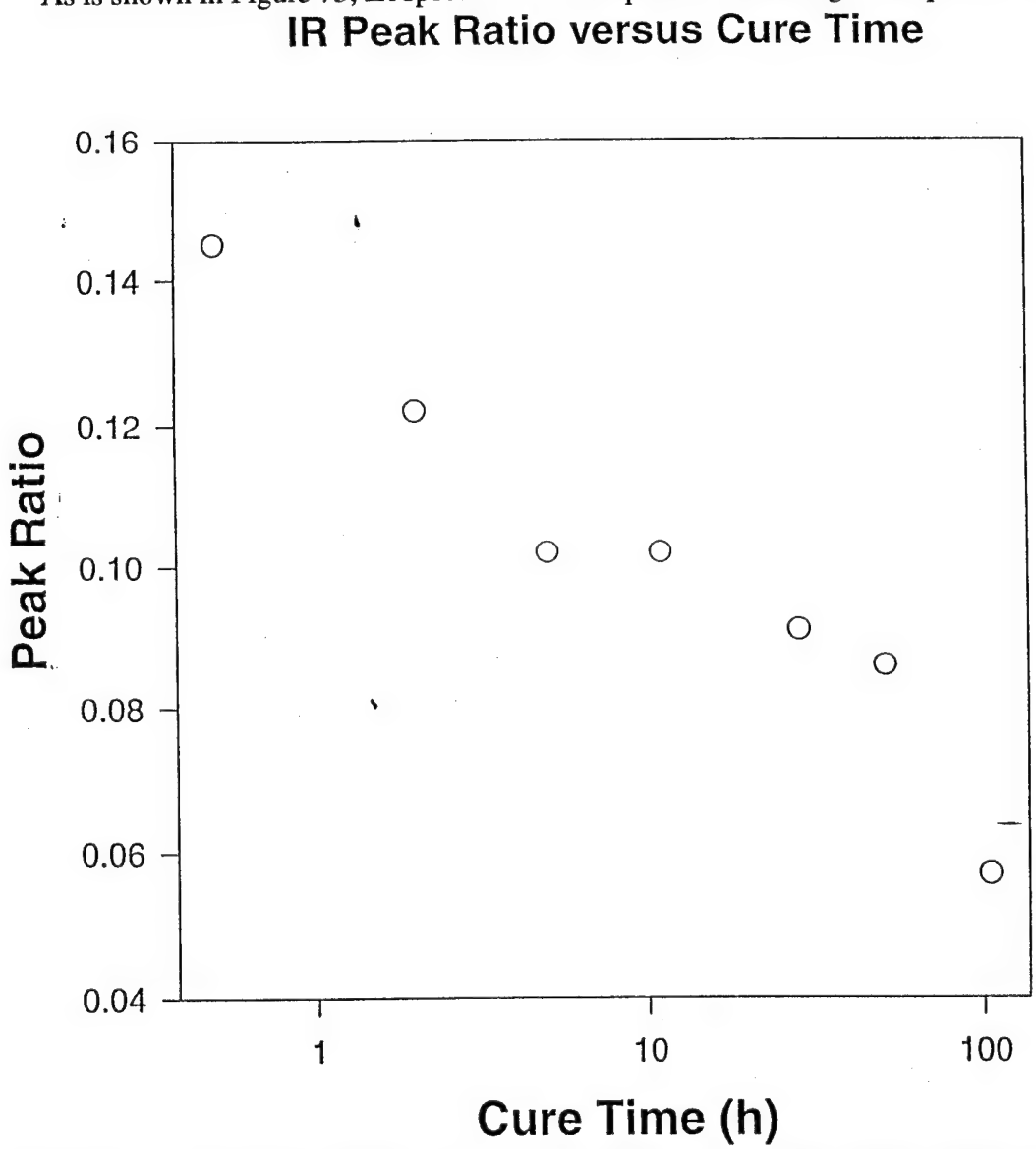

Figure 75. Curing of ATPA-7 (MK) at 150°C, as monitored by the ratio of the 3290 cm^{-1} (acetylene peak) to the 830 cm^{-1} IR peaks.

showed a decrease in the acetylene peak (3290 cm^{-1}) as a function of time at 150°C. The intensity of the C-H acetylene stretching peak at 3290 cm^{-1} was monitored relative to a peak with fairly constant intensity at 830 cm^{-1}. The intensity ratio decreased 33% after 10 h at 150°C and 60% after 100 h at 150°C. These results suggest that a significant number of the acetylene groups react at 150°C.

Blends of ATPA With Low Melting AT-Schiff Base: 1:1 w/w blends of ATPA-7 with the AT-Schiff base Thermcon 2000 (mp = 90°C) were prepared. The goal was to give ATPA a depressed melting point so that it could be more easily cured. First, ATPA-7 and Thermcon 2000 were dissolved in NMP, then the solvent was evaporated for 4 h at 90°C to leave a (visually) uniform thin film of polymer blend. The sample had a DSC endotherm at 175°C, followed by an apparent curing exotherm at 225°C (lower than observed for ATPA). When doped with HCl, the sample turned green and produced a narrow ESR line (0.24 mT), which is significant because a narrow ESR line correlates with polyaniline being conductive. However, since polyaniline generally loses its ESR spectrum in solution, the presence of an ESR spectrum in this sample may also indicate an aggregation of the ATPA instead of dispersion at the molecular level.

3.2.5 Oxidation of Samples for Improved Conductivity

One reason for reduced conductivity in ATPA and COA Oligomers is incomplete oxidation. Comparison of Figures 57 and 59 with Figure 60 indicates that samples were in lower oxidation states than the highest-conducting emeraldine state. According to Manassen and Khalif [38] oxidized forms of polyaniline are capable of dehydrogenating/aromatizing partially saturated cycloalkanes. Therefore, it is possible to both aromatize and oxidize polyaniline oligomers at

once using suitable oxidation procedures. Several samples were oxidized with O_2 gas. Details are given below:

COA(MK): A solution of COA in NMP held at 50°C was oxidized by bubbling with O_2 for 2-3 days. As shown in Table 7, prior to oxidation the sample had a conductivity of $4x10^{-4}$ S/cm, whereas following this procedure its conductivity had increased to $2x10^{-2}$ S/cm. UV-VIS

Table 7. Effect of Oxidation with O_2 on Conductivity of Polyaniline Derivatives and Uncured Oligomers.

Sample[+]	Doping*	Conductivity (S/cm)
PPAI(MK)-no O_2 exposure	1.0 M HCl--ppt	10^{-2}
PPAI(MK)-after O_2 exposure	1.0 M HCl--ppt	$2x10^{-2}$
ATPA-7(MK) (sample #1) --no O_2 exposure	0.1 M HCl--ppt	$4x10^{-3}$
ATPA-7(MK) (sample #1) --after O_2 exposure	0.1 M HCl--ppt	$2x10^{-3}$
ATPA-7(MK) (sample #2) --no O_2 exposure	0.1 M HCl--m/p	$9x10^{-5}$
ATPA-7(MK) (sample #2) --after O_2 exposure	0.1 M HCl--m/p	10^{-3}
COA(MK) --no O_2 exposure	0.1 M HCl--ppt	$3.9x10^{-4}$
COA(MK)--after O_2 exposure	0.1 M HCl--ppt	$2.1x10^{-2}$

*Samples were doped either by reprecipitation fromNMP or DMF solution (ppt) or samples were ground in a mortar while covered with the doping solution (m/p).
[+]MK refers to Manassen Khalif synthesis procedure.

spectra shown in Figure 76 were recorded from this sample as well as from an untreated sample. The spectrum for the former sample showed a significant increase in the 600 nm band, which indicated an increase in the fraction of quinoid groups. A third sample, untreated other than having been handled in solution under ambient atmospheric conditions, produced a 600 nm peak

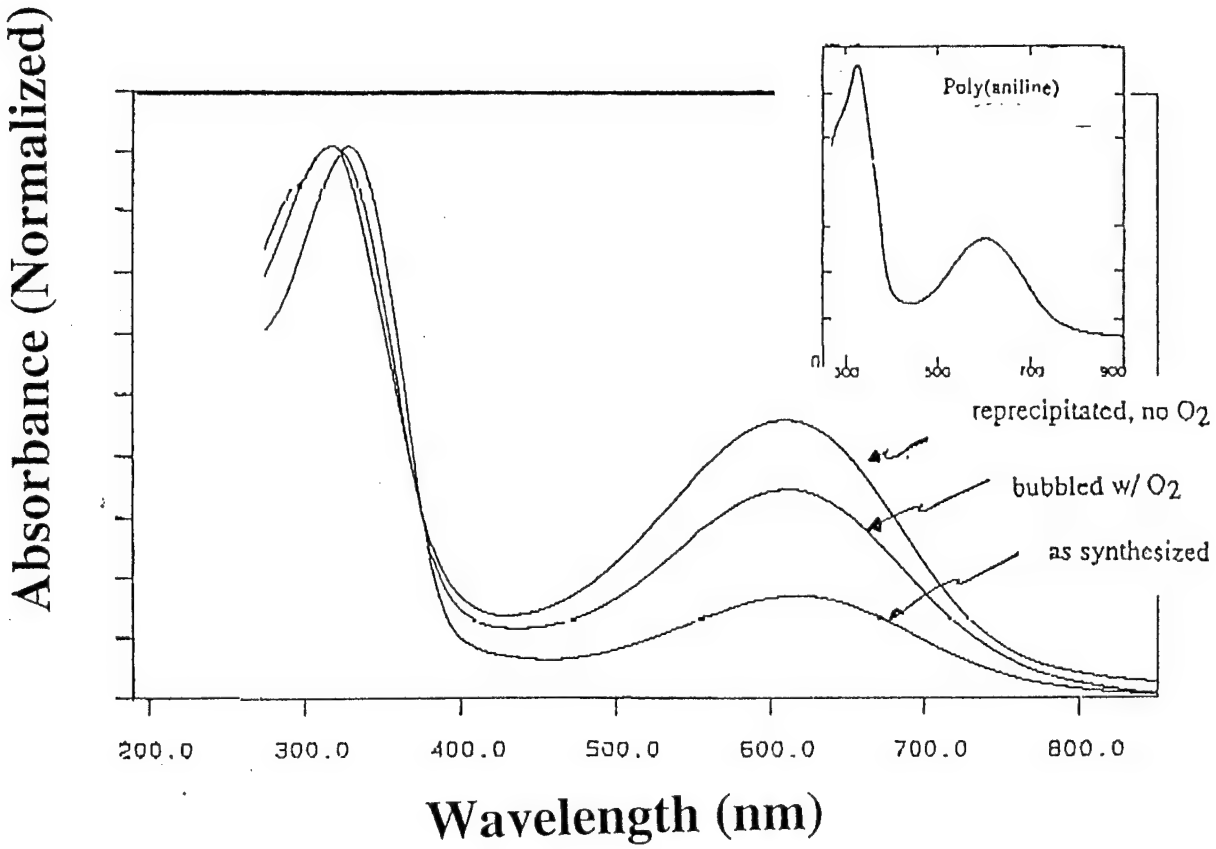

Figure 76. UV-VIS spectra of COA (MK) exposed to different treatments.

that was even more intense that of the O_2-bubbled sample. These results indicate that exposure of solutions of COA or ATPA oligomers to the atmosphere for long enough periods will result in significant (but perhaps not optimized) oxidation.

ATPA-7 (MK): When molecular oxygen was bubbled into DMF solutions of samples of ATPA-7 at room temperature for 6 to 22 hours, there was an increase in blue color and a dramatic increase in the intensity of the absorption at about 600 nm. The dark blue solid obtained

after work-up and drying gave an IR spectrum with an quinoid (1597 cm^{-1}) to benzenoid (1505 cm^{-1}) peak ratio of 1:2. As is shown in Figure 61(b), the UV-VIS spectrum had absorptions at 322 and 610 nm, with an intensity ratio of 3:1. As is shown in Table 7, after oxidation the electrical conductivity of the HCl doped samples increased from $9x10^{-5}$ to 10^{-3} S/cm.

For comparison, a dilute DMF solution of ATPA-7 reduced with phenylhydrazine is colorless and gives the UV-VIS spectrum shown in Figure 61(c) with an absorption at 332 nm only. After 17 hours treatment with O_2 the solution turns blue and the UV-VIS spectrum showed absorptions at 325 nm and 615 nm with an intensity ratio of 3:1. There was no quinoid absorption at 1597 cm^{-1} in the IR spectrum of the reduced material, only a benzene ring absorption at 1601 cm^{-1}.

GPC data from THF solutions of samples of ATPA-7 before and after treatment with oxygen indicated that there was no change in molecular weight distribution as a result of oxidation.

PPAI(MK): O_2 was bubbled into a stirred DMF solution of PPAI-MK for 22 h at room temperature and the reaction mixture worked-up as above. The FTIR spectrum showed an quinoid (1593 cm^{-1}) to benzenoid (1497 cm^{-1}) absorption ratio of 1:2. The UV-VIS spectrum in DMF had absorptions at 327 and 617 nm with a ratio of 2.6:1, indicating significant quinoid content. As is shown in Table 7 the electrical conductivity of an HCl doped sample was 2×10^{-2} S/cm.

Methoxy-ATPA-7 (MeO-ATPA-7)(MK): A sample of this material was oxidized by bubbling O_2 into a DMF solution maintained at 65-70°C for 19 hours. Precipitation from 1 M

HCl solution afforded a black powder that was soluble in methanol. A dilute DMF solution was light purple with maximum absorption at 283 and 496 nm. Acidification resulted in formation of a pale green-black color and a bathochromic shift to 595 nm. The long-wavelength absorption at 513 nm before oxidation and at 496 nm after oxidation, suggests that the MeO-ATPA-7 has significant pernigraniline structure. For MeO-ATPA-7 this is not surprising, since the 2-methoxy-1,4-diaminobenzene is expected to be more easily oxidized than unsubstituted p-phenylenediamine. The conductivity from the unoxidized sample was extremely low ($< 10^{-7}$ S/cm).

Dianisidine ATPA-7 (DA-ATPA-7)(MK): An attempt was made to oxidize this material by treating a DMF solution with O_2 at 70°C for 18 hours. It was isolated by precipitation from 1 M HCl solution. A dilute solution in DMF was colorless, and the UV-VIS spectrum was identical to the original material. A stronger oxidizing agent such as ammonium persulfate may be able to convert this to the emeraldine base form.

Oxidation Using Oxidants other than O_2: Oxidation of PPAI(MK) with a solution of ammonium persulfate in 1 M HCl resulted in a sample whose FTIR and UV-VIS spectra were essentially identical to the spectra produced by PPAI(MK) oxidized with molecular oxygen.

Oxidation of ATPA-7(MK) with o-chloranil resulted in a sample whose UV-VIS spectrum showed increased intensity in the 620 nm band, indicating a higher oxidation state. However, the sample may have been over-oxidized, because the conductivity actually decreased upon oxidation from a value of $9x10^{-5}$ S/cm to a value of $5x10^{-6}$ S/cm.

Summary of Oxidation Studies: COA, ATPA-7, and PPAI prepared by the MK synthesis can be effectively oxidized with O_2 under mild conditions. The HCl-doped samples have

increased conductivity but do not reach the expected optimum of ~1 S/cm. Preliminary studies using other oxidizing agents such as o-chloranil indicate no advantage over simple O_2 oxidation.

4.0 CONCLUSIONS AND ACCOMPLISHMENTS

It is appropriate here to speculate on some of the reasons for the relatively low conductivity exhibited by both the iodine-doped and the acid-doped thermoset polymers described in this report.

In particular, we expected the conductivity for the aniline oligomers to be of the order of 0.1 to 1.0 S/cm, which has been reported for monodispersed COA [39]. However, the best oligomeric samples synthesized in the present study had a conductivity of only $2x10^{-2}$ S/cm. The observed lower conductivity may be the result of (i) the presence of low molecular weight oligomers resulting from the 'one pot' synthetic procedures, (ii) incomplete aromatization of the samples, as suggested by NMR spectra that exhibit appreciable intensities in the aliphatic regions, (iii) incomplete oxidation , as implied by UV-VIS, IR, and electrochemical data, or (iv) the presence of other impurities, for example, Wudl [37] reported that premature exposure of the reaction mixture to ambient oxygen resulted in poorly conducting samples.

More generally, we conclude that the limiting factor determining the conductivity in doped thermoset polymers made from acetylene-terminated monomers may be the nature of the crosslink and that a conjugated crosslink may be a necessary but not sufficient condition for 'easy' charge transport (i.e., high mobility and high conductivity). Although there is evidence to suggest that the crosslink can have a polyene structure [6], there is also good reason to believe that several types of intramolecular cyclization reactions can take place which lead to the crosslink structures

shown in Figure 77 [7,8,11,12]. The substituted benzene structure is the result of a trimerization of acetylenic end-groups [12]. The enyne structure forms as the result of a Straus coupling [9,10] and can be the precursor to the formation of the substituted naphthalene structure [8].

Although all the structures shown as (a), (b), (c), and (d) in Figure 77 are conjugated, the

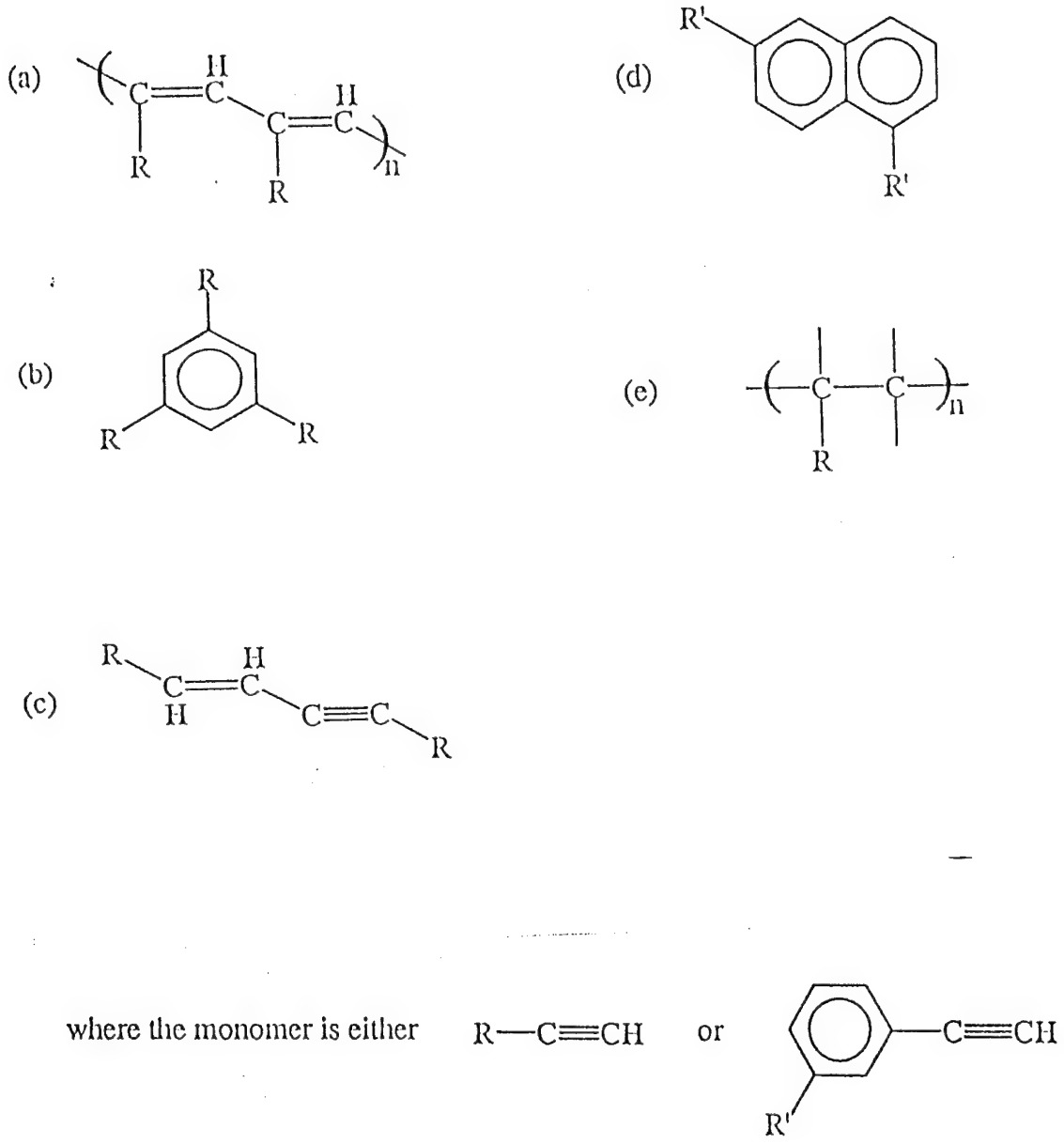

Figure 77. Possible structures of crosslinks in thermosets formed from acetylene-terminated monomers and oligomers: (a) the polyene, (b) the substituted benzene, (c) the enyne, (d) the substituted naphthalene, and (e) the non-conjugated linkage.

π-electron overlap in the polymer network may be reduced from the optimum values necessary for extensive delocalization and high mobility, for the following three reasons: (i) Para substitution of the acetylenic groups on the aromatic ring will provide the greatest overlap of the π-electrons on the crosslink with those in the main chain, whereas in both Thermcon 1000 and Thermcon 2000 the acetylenic end-groups are meta substituted. Yet, the measured conductivity values in 3T-2Ac and 3T-2AcPh, where the end-groups were para substituted, showed no marked improvement over those measured in Thermcon 1000 and Thermcon 2000. (ii) The overlap between the π-electrons on the main chain and those in the crosslink may be reduced if the aromatic ring attached to the acetylene end-groups, is rotated out of the plane of either the polyene chain, or the aromatic rings in the crosslink and (iii) The polyene chain may not lie in a plane but is twisted out of the plane because of steric effects arising from substituents (e.g., the R and R' groups in Figure 77).

On the other hand, the presence of a sufficient number of non-conjugated crosslinks with the structure shown in Figure 77(f), could also explain the low conductivity. These would form as a result of free radical branching reactions [7,10].

A summary of the accomplishments and conclusions drawn from all the results described above follows:

- Two types of conducting AT thermosets have been developed,viz., AT-Schiff base and AT-polythiophene thermosets, where the monomers were first cured then doped with iodine and secondly, AT-polyanilines, where the oligomers were first doped with protonic acids then cured.

- The mechanical properties of the thermoset are important since, to avoid fracture, it has to accommodate the internal strains that arise from the swelling caused by the absorbed redox dopant .
- AT-Schiff base and AT-polythiophene monomers were identified which showed a wide window for cure, i.e., a large temperature difference(> 30°C) between themelting temperature for the monomer and the maximum in the exotherm, so as toensure uniform curing and the required mechanical properties
- The linescan profiles obtained using Energy Dispersive Spectroscopy (EDX) indicated that the iodine dopant concentration was constant behind a steep front.
- The iodine uptake was linearly dependent on the exposure time to the iodine vapor.
- The presence of the steep fronts and the linear dependence of the iodine uptake indicated that the iodine entered the thermoset in a non-Fickian manner, and exhibitedCase II type diffusion.
- The rate of iodine uptake depended on the crosslink density in the thermoset.
- The iodine penetration depths could be measured by using scanning electron microscopy of the sample cross sections.
- The iodine penetration depths were linearly dependent on the amount of iodine in the sample. This was additional evidence that the iodine concentration behind the front was constant.
- Thermosets made from phenylacetylene-terminated monomer (3T-2AcPh) absorbed three times more iodine than that formed from the AT-monomer, Thermcon 1000, without fracturing.

- Bulk conductivity depended on the nature of the crosslink. Conductivity in iodine-doped thermoset made from AT monomers which have conjugated crosslinks was ten times larger than epoxy- or vinyl-terminated monomers having non-conjugated crosslinks.
- Bulk conductivity in iodine-doped thermosets made from AT monomers depended on the nature of the backbone. Conductivity in iodine-doped CDEB was over ten times lower than that in Thermcon 1000.
- Bulk conductivity measurements in iodine-doped thermosets made from Thermcon 1000, Thermcon 2000 and phenyleneacetylene-terminated terthiophene (3T-2AcPh) all showed the same value at the same iodine content ($\sigma = 2.7 \times 10^{-4}$ S/cm).
- Microcracks in the thermosets reduced the bulk conductivity at low iodine contents.
- The spin susceptibility measured by ESR provided evidence for the existence of polarons and bipolarons in iodine-doped thermosets.
- The effective g-value and the ESR lineshape parameters exhibited effects attributable to the presence of iodine counter ions because of the large spin-orbit interactions associated with iodine.
- The spin susceptibility, the effective g-value and the lineshape parameters measured in thermosets showed both reversible and irreversible effects as a function of iodine content.
- These reversible effects could be explained in terms of a model involving equilibrium between polymeric radical cation complexes (i.e., polarons) containing different stoichiometric amounts of iodine.
- The temperature dependence of the ESR lineshape parameters indicated localized motions were associated with polarons in the iodine-doped thermosets

- Infrared spectra indicated that crosslinking takes place in acetylene-terminated oligomers.
- Optical spectra measured in iodine doped acetylene terminated thermosets showed an absorbance peak below the band edge which suggests polaron formation.
- Photoluminescence measurements indicated that polarons become trapped on the polymer chains, resulting in increased nonradiative recombination.
- Photoconductivity measurements suggested that the charge carrier mobility was low in acetylene-terminated thermosets.
- Two different methods were used to synthesize AT-polyaniline oligomers (identified as the MHW method and the MK method).
- Demonstrated that MK method, a more convenient method for synthesis, was as effective as the MHW for the synthesis of acetylene-terminated octamers.
- Demonstrated that a one-pot synthesis using the MK approach produced aniline oligomers having a conductivity 10^{-2} S/cm
- Synthesized ATPA oligomers with methoxy-substituted aniline and meta-phenylenediamine units and showed that these samples had low conductivity compared with non-substituted ATPA.
- Measured the degree of oxidation of ATPAs using UV-VIS and IR spectroscopies.
- Verified by IR spectroscopy that ATPAs contained acetylene, benzenoid and quinoid groups.
- Used NMR to identify incomplete aromatization as a possible cause of low conductivity in ATPAs.
- Found that ATPAs have similar ESR properties to polyaniline in that both showed a large increase (over two orders of magnitude) in spin concentrations on doping with protonic acids.

- Determined by mass spectrometry that ATPAs have a polyaniline type backbone structure.
- Determined by coulometry that after synthesis ATPAs were in low oxidation states.
- Inferred from gel-permeation chromatography that a broad distribution of molecular weights was a possible cause for low conductivity.
- Determined that elemental oxygen was the most effective oxidation reagent for increasing the conductivity of ATPAs.
- Demonstrated that the conductivity of as-synthesized ATPA could be increased a factor of 50 by mild oxidation.
- Verified by IR spectroscopy that acetylene end-groups of ATPAs reacted at a cure temperature of 150°C.
- Demonstrated that blends of ATPAs with Thermcon 2000 could be cured to form hard solids.
- Demonstrated that ATPAs could be made processible by doping with plasticizing dopants such as camphorsulfonic acid.
- The stability of BDSA-doped ATPA-7 after 2 h at 150°C, suggested that conducting thermosets will be useable materials if the conductivities of the uncured monomers can be increased to ~1 S/cm.
- One of the possible reasons for the relatively low conductivity exhibited by the doped thermosets was the presence of nonconjugated crosslinks in the polymer network.
- Another possible reason for the low conductivity was the reduced overlap between the π-electrons in the crosslink and the π-electrons in the backbone.

5.0 REFERENCES

1. T. Itoh, H. Shirakawa, and S. Ikeda, J. Polym. Sci., Polym. Chem. Ed., 12, 11 (1974).
2. H. Shirakawa, E.J. Louis, A. G. Macdiarmid, C. K. Chiang, and A. J. Heeger, J.Chem. Soc. Chem. Comm., 578 (1977).
3. J. I. Kroschwitz (Ed.), *Electrical and Electronic Properties of Polymers: A State-of-the-Art Compendium,* Wiley, New York 1988.
4. T. A. Skotheim (Ed.), *Handbook of Conducting Polymers, Vols. 1 and 2*, Marcel Dekker, New York, 1986.
5. H. H. S. Javadi, K. R.. Cromack, A. G. MacDiarmid, and A. J. Epstein, Phys. Rev. B, 39, 3579 (1989).
6. J. M. Pickard, E. G. Jones, and I. J. Goldfarb, Macromolecules 12, 895 (1979).
7. R. F. Kovar, G. F. L. Ehlers, and F. E. Arnold, J. Polym.Sci., Chem. Ed., 15, 108 (1977).
8. B. A. Reinhardt, and F. E. Arnold, Polymer Preprints, 20, 211, (1979).
9. F. Straus, Ann. 342, 190 (1905).
10. H. G. Viehe (Ed.), *Chemistry of Acetylenes*, Dekker, New York, 1969.
11. A. C. Lind, C. G. Fry, R. L. Levy, and T. C. Sandreczki, AFWAL-TR-86-4049, Materials Laboratory, Wright-Patterson Air Force Base,OH 45433-6533.
12. A. L. Landis, N. Bilow, R. H. Boschan, R. E. Lawrence, and T. J. Aponyi, Polymer Preprints, 15, 533 (1974).
13. A. H. Windle, in J. Comyn (Ed.), *Polymer Permeability*, Elsevier Applied Science, Barking, U.K., 1985, Chapter 3.
14. R. D. Rossi, and S. P Fenelli, U.S. Patent No. 4,730,032.
15. R. G. Bryant, B. J. Jensen, and P. M. Hergenrother, Polym. Prepr. 34, 566, 1993.
16. G. M. Jayaraman, G. Meyer , R. Srinivarsan, and J. E. McGrath, Polym. Prepr. 34, 513, 1993.
17. B. Wasserman, M S. Dressellhaus, M. Wolf, G. Wnek, and J. D. Woodhouse, J. Appl. Phys. 60, 668, (1990).
18. F. H. Ruddy, J. Bartko, and K. F. Schoch, J. Mater. Res. 3, 1253 (1993).
19. C. J. Bedell, C. J. Sofield, L. B. Bridwell, and I. M. Brown, J. Appl. Phys. 67, 1736 (1990).
20. W. B. Austin, N. Bilow, W. J. Kelleghan, and K. S. Y. Lau, J. Org.Chem., 46, 2280 (1981).

21. H. Ringsdorf, and G. Greber, Makromol. Chem., 31, 50 (1950).
22. A. Blumstein, Mol. Cryst. Liq. Cryst., 33, 35 (1976).
23. J. A. Mikroyannidis, Makromol. Chem. 190, 1867 (1989).
24. T. C. Sandreczki, and C. Y.-C Lee, Polymer Preprints 23, (2) 185 (1982).
25. G. Odian, *Principles of Polymerization*, McGraw-Hill New York, 1970, page 454.
26. J. C. Scott, P. Pfluger, M. Krounbi, and G.B. Street, Phys. Rev.B, 28, 2140 (1983).
27. E. Boesman and D.J. Schoemaker, J. Chem. Phys. 37, 671 (1962).
28. R. Kubo and K. J. Tomita, J. Phys. Soc. Jpn., 9, 888 (1954).
29. D. Bloor, R. J. Kennedy, and D. N. Batchelder, J. Polym. Sci. Phys. 17, 1355 (1979).
30. T. R. Walton, J. Appl. Polym. Sci. 33, 971 (1987).
31. T. R. Walton, J. Appl. Polym. Sci. 37, 1921 (1989).
32. Y. Wei, R. Hariharan, and J. K. Ray, J. Polym. Sci. Chem. 29, 749 (1991).
33. R. H. Friend, D. D. C. Bradley, and P. D. Townsend, J. Phys. D: Appl. Phys. 20, 1367 (1987).
34. K. Fesser, A. R. Bishop, and D. K. Campbell, Phys. Rev. B27, 4804 (1983).
35. A. O. Patil, A. J. Heeger, and F. Wudl, Chem. Rev. 88, 183 (1988).
36. J. Honzl, and M. Tlustakova, J. Polym Sci., Part C. 22, 451 (1968).
37. F. Wudl, R. O. Angus, Jr., F. L. Lu, P. M. Allemand, D. J. Vachon, M. Nowak, Z.X. Liu, and A. J. Heeger, J. Am. Chem. Soc. 109, 3677 (1987).
38. J. Manassen. and Sh. Khalif, J. Am. Chem. Soc. 88, 1943 (1966).
39. F. L. Lu, F. Wudl, M. Nowak, and A J. Heeger, J. Am. Chem. Soc. 108, 8311 (1986).
40. Y. Sun, A. G. McDiarmid, and A. J. Epstein, J. Chem. Soc., Chem Commun., 529, (1990).
41. A. G. McDiarmid, J. C. Chang, A. F. Richter, and N. L. D. Somasiri, in L. Alcacer (Ed.), *Conducting Polymers*, Reidel Publishing, New York, 1987, page105.
42. P. P. Fu and R G. Harvey, Chem. Rev., 78, 317, (1978).
43. Y. Wei, K. Hsueh, X. Tang, and Y. Sun, Polym. Prepr., 30(1), 226, (1989).
44. F. Walls and J. Caballero, Bol. Inst. Quim. Univ.Nacl. Auton. Mex. 15, 74 (1963).
45. H. H. S. Javadi, S. P. Treat, J. M. Ginder, J. F. Wolfe, and A. J. Epstein, J. Phys. Chem. Solids 51, 107 (1990).
46. S. S. Pandey, S. Annapoorni, and B. D. Malhotra, Macromolecules, 26, 3190, (1993).

47. H.-L. Wang, and A. G. MacDiarmid, Bull. Am. Phys. Soc., 39, 426, (1994).

48. R. E. Cameron, International Patent Application Number PCT/US 89/03131, International Publication Number WO 90/01775, 22 February 1990, Lockheed Corporation, USA.

6.0 EXECUTIVE SUMMARY

6.1 Personnel

The following personnel contributed to the research described in this report:

Professor I. M. Brown, Department of Physics and Chemistry, University of Missouri-St. Louis, St. Louis, Missouri 63121.

Professor D. J. Leopold, Department of Physics, Washington University, St. Louis, Missouri 63130.

Professor T. C. Sandreczki, Department of Chemistry, University of Missouri-Kansas City, Missouri 64110.

Professor S. Mohite, Department of Chemistry, SouthWest Missouri State University, Springfield, Missouri 65804.

Professor J. Wilbur, Department of Chemistry, SouthWest Missouri State University, Springfield, Missouri 65804.

6.2 Publications

1. I. M. Brown, D. J. Leopold, S. Mohite, and T. C. Sandreczki, "Conducting Thermoset Polymers: A Comparative Study of Schiff Base Precursors with Different End-Groups," Synthetic Metals 72, 269 (1995).
2. I. M. Brown, D. J. Leopold, S. Mohite, J. Wilbur, T. C. Sandreczki, J. Park, and Z. Zhong, "Conducting Thermosets from Reactive Schiff-Base and Polyaniline Oligomers," Polymeric Materials: Science and Engineering, 72, 280 (1995).